Modelling phytoplankton across many scales: transient dynamics, human interactions, and niche differentiation in the light spectrum

by

Christopher M. Heggerud

A thesis submitted in partial fulfillment of the requirements for the degree of

Doctor of Philosophy

in

Applied Mathematics

Department of Mathematical and Statistical Sciences
University of Alberta

Abstract

In recent decades freshwater lakes have seen an increase in human presence. A common byproduct of this human presence is anthropogenic nutrient pollution resulting in eutrophication, a term that is becoming all too synonymous with harmful algal blooms. It is well known that phytoplankton require both light and nutrients for growth but their dynamics are ecologically complex with dependencies on lake characteristics and resource dynamics. In this thesis I take a holistic approach towards understanding the complexities of phytoplankton dynamics and their dependencies on resource dynamics, niches, and human interactions.

I first introduce concepts relevant to the study of phytoplankton dynamics including a background on phytoplankton and lake characteristics, ecological stoichiometry, human environmental systems and a brief overview of singular perturbation theory, stability and bifurcation theory, and monotone dynamical systems theory. In the second part I gain insight towards the transient dynamics of phytoplankton. I study a stoichiometrically derived model for cyanobacteria dependent on phosphorus and light availability. There is natural separation of time scales between the internal nutrient dynamics and growth dynamics. The internal nutrient dynamics are much faster allowing for the utilization of multi-scale analysis to gain an in-depth mechanistic understanding of the transient dynamics.

In the third part I couple a well studied stoichiometric cyanobacteria model to a socio-economic model for describing human-ecosystem interactions. The socio-economic model considers two strategies humans assume, to be environmentally friendly by lowering anthropogenic nutrient inputs into a lake, or the opposite. Various costs related to social ostracism, social norms, financial burden, and environmental concern of cyanobacteria influence how the population behaves. The coupled model exhibits bistable dynamics in the case of a single lake, with one stable state corresponding to the environmentally friendly state with low cyanobacteria abundance, and the other to high pollution rates and high cyanobacteria abundance. Furthermore, I consider a network of lakes connected via social interactions and show tristability of three network regimes corresponding to high cooperation, low cooperation, and mixed levels of cooperation throughout the network. In each case I show the potential for regime shifts between levels of cooperation and cyanobacteria abundance based on costs associated with social ostracism, social pressure and concern for cyanobacteria.

In the fourth part I offer support for the hypothesis that niche differentiation in the light spectrum is an explanation of the paradox of the plankton. The paradox of the plankton highlights the contradiction between the competitive exclusion principle and the observed diversity of phytoplankton. By explicitly considering the visible light spectrum I can treat light as a continuum of resources rather than a single resource. I propose a spatially explicit reaction-diffusion-advection model to explore under what circumstances coexistence is possible from mathematical, numerical and biological perspectives with a focus of niche differentiation. Furthermore I consider realistic scenarios of phytoplankton competition and water turbidity and show how the model

helps to explain the paradox of the plankton.

Finally, I summarize key results and discuss their implications in the literature. I discuss some limitations of the modelling efforts and provide suggestions for areas of future work based on the current state of knowledge.

Preface

This thesis has been structured as paper based where Chapters 2-4 are the three main components of original work. Some of the research included in this thesis was conducted as part of collaborations detailed below. Mark A. Lewis and Hao Wang are supervisory authors in Chapters 2 and 3 and Hao Wang is the supervisory author of Chapter 4.

Chapter 2 of this thesis is an original work that has been published as Christopher M. Heggerud, Hao Wang, and Mark A. Lewis (2020). "Transient dynamics of a stoichiometric cyanobacteria model via multiple-scale analysis". *SIAM Journal on Applied Mathematics* 80.3, pp. 1223–1246. C.M. Heggerud was responsible for the model development, analysis, and manuscript composition. H. Wang and M.A. Lewis were the supervisory authors and assisted in the model analysis and contributed to manuscript edits.

Chapter 3 of this thesis is an original work that will soon be submitted for publication as Christopher M. Heggerud, Hao Wang, and Mark A. Lewis. "Coupling the socio-economic and ecological dynamics of cyanobacteria: single lake and network dynamics". C.M. Heggerud was responsible for the model development, analysis, and manuscript composition. H.Wang and M.A. Lewis were the supervisory authors and assisted in the model analysis and contributed to manuscript edits.

Chapter 4 of this thesis is an original work that will soon be submitted

for publication as Christopher M. Heggerud, King-Yeung Lam and Hao Wang. "Niche differentiation in the light spectrum promotes coexistence of phytoplankton species: a spatial modelling approach". C.M. Heggerud was responsible for the model development, numerical simulations, manuscript composition and analysis. K.-Y. Lam was responsible for analysis and model development and manuscript composition. H. Wang was the supervisory author and assisted in the conceptualization, model development, and contributed to manuscript edits.

"Secrets must be exposed when found. Detours must be taken when encountered. And if you are the one who stands at the crossroads or the place of concealment, you must never leave it to another to act in your place."

-Qui-Gon Jinn

Acknowledgements

I would like to start by thanking my supervisors, Mark Lewis and Hao Wang for giving me the chance to work with them over the past 6 years. Hao has been encouraging and patient, allowing me to challenge myself. His helpful feedback and confidence in me are all invaluable to me and have allowed me to learn and advance. Mark has given me the opportunity to grow as an academic. His support, guidance and the environment he has cultivated in his lab have made it possible for me to succeed.

Both Mark and Hao have opened up many doors for me through encouragement to speak at conferences, invitations to workshops and in general always looking out for my best interests both career wise and with my family. Both have created amazing lab environments allowing for friendships to be made and research to be enhanced simultaneously. I am truly grateful to have had the opportunity to be a member of both your labs and to have been under your guidance.

Thanks to Rolf Vinebrooke, my committee member, for his enthusiasm in my projects from a biological perspective and the stimulating discussions we have had. I would also like to thank King-Yeung (Adrian) Lam for the opportunity to collaborate. I have learned a great deal from you.

I would also like to thank the University of Alberta for the Alberta Graduate Excellence Scholarship, NSERC for the Canadian Graduate Scholarship

(Masters), and Alberta Innovates for the Graduate Student Scholarship for all of the financial support I have received over the years.

I would like to thank past and present members of the Lewis Research Group and the Hao Wang Research Group for the feedback, support, and general friendships that have been made. Special thanks to Kim Wilke-Budinski for her laughter and help with so very many things and to Peter Harrington for his comradery in classes, research and life.

Finally, I would like to thank my friends and family for putting up with me through the trying times of my PhD. To Beckett and Elsie for the continuous joy they bring to me, and to my wife, Charlotte, thank you for all that you do, no words can describe my appreciation.

Table of Contents

List of Tables

List of Figures

Chapter 1

Introduction

1.1 Motivation

Harmful algal blooms are an increasingly prevalent global concern that reduce aquatic ecosystem health, lower recreational value of lakes, and increase water treatment and other economical costs (Paerl and Otten, 2013). Unfortunately, a driving factor in the formation of harmful algal blooms is human in nature. Human presence often leads to an excess amount of nutrients in the ecosystem than what is required for life, resulting in eutrophic conditions and thus, promoting algal growth. For example, a popular lake in central Alberta, Pigeon Lake, has seen an increase in urban, rural and agricultural development in the last several decades, now having several municipalities within its watershed. This increased human presence has resulted in nutrient pollution and an increased frequency of harmful algal blooms raising health concerns for humans and the environment. However, management strategies, based on human behaviour and natural processes, have since been implemented to mitigate the occurrence of blooms and slight improvements have been noted (Teichreb, 2012; Pigeon Lake Watershed Management Plan Steering Committee, 2018). Even at the base of the issue, the growth kinetics of phytoplankton is complex

and depends on several components, such as light, nutrient resources, water characteristics, and climate. The addition of human interaction even increases this complexity, but is an important aspect to consider for full understanding of phytoplankton dynamics and to create effective mitigation strategies. To my best knowledge no such connections between the various aspects of complex phytoplankton dynamics and human behaviour have been made. Thus, the goal of this thesis is to gain understanding of the ecological complexities involved in phytoplankton dynamics by studying detailed cellular level aspects of lake ecology and human interactions involved in phytoplankton dynamics.

Below I give a brief introduction to the concepts comprising this thesis including a background on phytoplankton, lake characteristics, ecological stoichiometry, human environmental systems, and the mathematical theories of singular perturbations, stability and bifurcations, and monotone dynamical systems. Lastly, I give an overview of the thesis structure.

1.2 Lake characteristics and phytoplankton

There are many characteristics to consider when modelling lake systems that include depth, surface area, water colour and stratification. Of most concern in this thesis is the characteristics pertaining to water colour and stratification. A stratified lake can be thermally separated into two distinct vertical layers, called the epilimnion and the hypolimnion (Kalff, 2002). The epilimnion is the top warmer layer and is typically well mixed, seeing homogeneous distributions of nutrient concentrations and particulate matter. Because of the homogeneous nature of the epilimnion models that are not spatially explicit, such as ordinary differential equations, can be successful in studying dynamics in the epilimnion, (e.g., Wang et al. (2007), Berger et al. (2006), Stomp et al.

(2007b), and Zhang et al. (2021)). However, the colder hypolimnion and non-stratified lakes are typically not well mixed and are thus non-homogeneous with respect to phytoplankton distribution and nutrient concentrations. For this reason, unmixed water requires spatially explicit modelling to effectively be studied. One such case is the use of partial differential equation models to study phytoplankton growth and competition as in Jiang et al. (2019), Jiang, Lam, and Lou (2021), Hsu, Shi, and Wang (2014), Zhang et al. (2021), and Du and Mei (2011). In this thesis I consider dynamics under the well mixed assumption in Chapters 2 and 3, and consider the unmixed case in Chapter 4.

Phytoplankton are referred to as any planktonic species that use sunlight as a form of energy. For example, cyanobacteria are a type of prokaryotic phytoplankton that play a key role in oxygenating the atmosphere and require both nutrients and light for their growth. Nutrient requirements of phytoplankton can be approximated by the Redfield ratio (Redfield, 1934) and primarily consider carbon, nitrogen and phosphorus. However, other elements such as iron and magnesium are also essential for phytoplankton growth and cellular structure, but with a lower requirement (Whitton, 2012; Reynolds, 2006; Cunningham and John, 2017). Furthermore, phytoplankton are typically non-homeostatic with respect to their internal nutrient content, meaning the amount of internal nutrients can fluctuate significantly. This leads to a commonly observed phenomena called luxury consumption, where storage of excess nutrient occurs intracellularly (Whitton, 2012; Droop, 1968). Although nitrogen is a crucial element in lake ecology, throughout this thesis I assume it is available in abundance and do not consider its dynamics. Instead I turn my focus towards phosphorus, which is often the most limiting nutrient (Whitton, 2012). Although lake nutrient dynamics are complex, involving sedimentation,

erosion, and atmospheric processes, a large factor contributing to lake nutrient concentrations can be anthropogenic. Run-off from agricultural fertilizers and urban waste are a cause of modern lake eutrophication (Paerl, 2014; Watson et al., 2015) and often result in overabundance of phytoplankton species. For these reasons it is important to explicitly consider the dynamics of phytoplankton and their dependence on anthropogenic nutrient inputs.

Water colour is influenced by the dissolved and floating particulates and the respective light attenuation. Light attenuation occurs when incident photons are absorbed by materials, while the remaining photons are either reflected or scattered. This attenuation results in an overall loss of light at large water depths and is modelled by the exponential Lambert-Beer law. However, depending on the particulates, certain colours, or wavelengths, of light are absorbed deferentially resulting in non-uniform absorption across the light spectrum. This non-uniformity gives rise to colour differences amongst lakes (Burson et al., 2019; Stomp et al., 2007b) and materials in general. Furthermore, each phytoplankton species absorbs light in a unique non-uniform way giving rise to niche differentiation in the light spectrum. This allows for species diversity by limiting interspecies competition for light, which is the main topic of Chapter 4. Since phytoplankton require light for growth, light limitation readily occurs under two main scenarios. First, since light is attenuated throughout the water column, light limitation occurs if a species is unable to maintain close proximity to the water surface due to strong mixing or sinking. Second, since phytoplankton themselves attenuate light, light limitation occurs when there is a large abundance of phytoplankton, this phenomenon is often referred to as self-shading and is studied in many mathematical models (Berger et al., 2006; Huisman and Weissing, 1994; Wang et al., 2007; Shigesada and Okubo, 1981;

Reynolds, 2006).

1.3 Ecological stoichiometry

Ecological stoichiometry is defined as the study of the balance of energy and elemental resources in ecological processes (Sterner and Elser, 2002). It is a powerful framework that allows for the consideration of microscopic phenomena, such as nutrient uptake and cell division, to make macro-scale conclusions such as algal bloom formation and species persistence. In the context of phytoplankton, ecological stoichiometry is a useful tool as it allows for the non-homeostatic nutrient assumption to be explicitly considered. That is, resource explicit models that assume homeostasis often use the Monod equation for growth (Monod, 1949) with the growth rate μ given as

$$\mu = \mu_{max} \frac{R}{h + R}, \tag{1.1}$$

where R is the nutrient concentration in the media, μ_{max} is the maximum growth rate, and h is the half saturation constant for growth. Because of the homeostatic assumption, the Monod form assumes that growth and nutrient uptake occur as simultaneous processes, which is only reasonable in distinct cases of very large uptake rates (Darvehei, Bahri, and Moheimani, 2018). However, in general, phytoplankton have variable internal stoichiometry contradicting the homeostatic assumption and implying that nutrient uptake and growth are relatively decoupled (Sterner and Elser, 2002; Whitton, 2012; Reynolds, 2006). This is where ecological stoichiometry and the Droop equation become cogent for phytoplankton modelling. The Droop model (Droop, 1968) assumes that phytoplankton growth is a function of internal nutrient as opposed to the Monod assumption of growth dependence on nutrient concen-

tration in the media and is given by

$$\mu = \mu_{max}(1 - \frac{q}{Q}), \tag{1.2}$$

where Q is the internal nutrient cell quota (mg of nutrient per cell), and q tsis the minimum cell quota requirement of the cell for cellular structure and metabolic processes. Without careful consideration of the chemical heterogeneity of phytoplankton, modelling efforts and predictions may be unreliable. Empirical evidence of such inconsistencies has been shown. For example, Urabe et al. (2002) empirically showed that competition outcomes of a producer-grazer system depended heavily on the internal nutrient content of the producer and their interactions could not be accurately modelled outside of the ecological stoichiometric framework. More recent studies have shown the importance of ecological stoichiometry as a modelling framework to accurately predict and understand biological phenomenon pertaining to toxicant stress (Peace et al., 2021; Huang, Wang, and Lewis, 2015; Peace, Poteat, and Wang, 2016), organic matter decomposition (Wang, Jiang, and Weitz, 2009; Chang, Shi, and Wang, 2021; Kong et al., 2019) and resource limitation (Wang et al., 2007; Andersen, Elser, and Hessen, 2004; Sterner and Elser, 2002).

In Chapters 2 and 3 of this thesis I consider phytoplankton dynamics and explicitly consider nutrient dynamics. Due to the non-homeostatic nature of most phytoplankton I deem the framework of ecological stoichiometry necessary for meaningful results.

1.4 Human environmental systems

In the current modern era human interaction with ecosystems is irrefutable. From fisheries to forestries, and scales ranging from a single lake to the atmosphere, humans undeniably influence their surrounding environments. Some

examples of these influences include nutrient pollution resulting in eutrophication, carbon emissions contributing to the climate crisis, over exploitation of resources, or in a positive light, culling species or materials to maintain biodiversity. However, all of these influences involve a series of decisions humans make that are influenced by factors such as monetary costs, ostracism, social norms, and the intrinsic value of the ecosystem.

Typically speaking, an individual will make the most economical decision, but complexity arises when the decisions are based on psychological aspects like social pressures and intrinsic nature value. For example, an individual may feel that a clean lake is more important to them than spending money on an environmentally friendly septic system, and thus choose the environmentally favourable strategy in the absence of other pressures. However, if the individual is the only person amongst their peers to choose such a strategy they may feel their efforts are meaningless and assume the status quo (Fransson and Gärling, 1999). Conversely, if the individual is one of the last to assume the environmentally favourable strategy they may feel added pressure from social norms and potential ostracism, increasing the probability of adopting that strategy (Tavoni, Schlüter, and Levin, 2012). These types of social dilemmas are often considered in problems often referred to as the common-goods game (Hofbauer and Sigmund, 2003; Kinzig et al., 2013) and is observed in the case study of Pigeon lake described in Section 1.1.

Additionally, the state of the environment plays a critical role in human decisions. That is, if there is no environmental concern then the pressure to assume an environmentally friendly strategy is minimal. On the other hand, when the environment is in a critical state, an individual is more likely to respond favourably and more so if a large portion of the population is already

responding favourably. These additional pressures stemming from communal dynamics give rise to frequency dependence (Iwasa, Uchida, and Yokomizo, 2007) where the magnitude of the pressure is proportional to the number of individuals of each strategy. However, in many cases these human responses are futile, or seemingly have no effect as the timescale differences between human response and ecological rebound can vary drastically (Hastings, 2016).

1.5 Mathematical theory

To study the dynamics of phytoplankton and their dependencies on nutrients, human interaction, and the light spectrum, I utilize some main mathematical theories: singular perturbation theory, stability and bifurcation theory, and monotone dynamical systems theory.

1.5.1 Stability and bifurcation theory

Throughout this thesis I discuss the stability of equilibria and their respective bifurcations. The stability of an equilibrium helps to describe the potential long-term dynamics of a system. For example, a locally stable equilibrium will eventually attract all solutions within its neighbourhood. Moreover, globally stable equilibria eventually attract all solutions regardless of their initial conditions. In addition, each stable equilibrium acts as an attractor in the sense that all solutions within its basin of attraction will eventually tend towards it. In the case of a globally stable equilibrium its basin of attraction is the entire state space, whereas in the case of a bistable system two disjoint basins of attraction exist corresponding to the two locally stable equilibria. Several classical techniques in mathematics are used to study attracting basins and stability of equilibrium including linearization for local stability and monotone

dynamical systems for global stability (Perko, 2001; Smith, 1995).

A bifurcation occurs when a smooth change in model parameters cause a qualitative change in a dynamical systems behaviour, that could correspond to either a different number of equilibria, or a change in stability of equilibria (Perko, 2001). The study of equilibria and their stability allows one to make conclusions regarding the long-term dynamics of a system. Moreover, the study of bifurcations help to understand how model parameters affect the range of possible long-term outcomes. A classic example of the study of stability and bifurcations is the phenomena of hysteresis in which a bistable system transitions from one state to another after a parameter change but fails to return to original state under the reversal of said parameter change (Carpenter, 2005; Ludwig, Jones, and Holling, 1978). Typically, hysteresis in ecological systems occurs as the result of a saddle-node bifurcation. A saddle-node bifurcation occurs when two equilibria collide and annihilate each other as a model parameter is changed. In the context of ecological hysteresis, the transition from one state to another is often the result of passing the saddle-node bifurcation point. In Chapter 3 I use such bifurcation theory to understand transitions between environmentally favourable and unfavourable outcomes and in Chapter 4 I use stability to understand the competitive outcomes between phytoplankton communities and numerically consider their bifurcations.

1.5.2 Singular perturbation theory

In Chapters 2 and 3 I utilize the mathematical theory of singular perturbations to simplify the complex ecological models. This simplification allows one to draw conclusions about the transient and long term behaviours of the ecological study system without studying the complex system directly.

I define a singular perturbation as a perturbation to a system that qualitatively changes its solution, as opposed to a regular perturbation that only quantitatively changes its solution. For example, consider two algebraic equations $\epsilon x^2 + x = 0$ and $x + \epsilon = 0$ where ϵ is a small parameter. Both equations are perturbations of the equation $x = 0$, but the addition of ϵx^2 introduces the possibility of a second solution to the problem whereas the addition of just ϵ only quantitatively changes the solution. Thus, the first equation is a singularly perturbed problem, which is more challenging to deal with than the regularly perturbed second equation.

Singular perturbation theory is an incredibly powerful mathematical tool to study ecological systems with clear separation of timescales. When timescales can be separated the dynamics of the entire system can be studied via subsystems, in which each subsystem operates on its own timescale. For example, consider the system

$$\begin{cases} \dot{u} = f(u, v; \epsilon), \\ \dot{v} = \epsilon g(u, v; \epsilon), \end{cases} \tag{1.3}$$

where ϵ is a small positive parameter. In this case two timescales arise, the fast scale given by t and the slow scale given by $\tau = \epsilon t$. Thus, system (1.3) can be reduced to two subsystems. By letting $\epsilon \to 0$ I arrive at the fast subsystem:

$$\begin{cases} \dot{u} = f(u, v; 0), \\ \dot{v} = 0. \end{cases} \tag{1.4}$$

By performing the change of variables $\tau = \epsilon t$ and letting $\epsilon \to 0$ the arrive at the slow subsystem:

$$\begin{cases} 0 = f(u, v; 0), \\ v' = g(u, v; 0). \end{cases} \tag{1.5}$$

The variable u is considered the fast variable and v the slow variable. This reduction now allows for the study of two simpler systems given by (1.4) and (1.5) as opposed to one complicated system (1.3). The study of the fast

system is often related to transient dynamics in which the interest lies in short term behaviour of the system. Whereas the study of the slow system is a simplification of the long term asymptotic behaviour of the system. The study of the slow system makes what is often referred to as the quasi steady state approximation, in which it is assumed the fast variables are in a quasi steady state given by $0 = f(u, v)$.

The two subsystems can be linked through asymptotic methods such as the method of matched asymptotic expansion which yields a single approximate solution to the full system (Kuehn, 2015). The results of the study of the subsystems are easily connected to the full system via the results of Fenichel (1979). That is, typically the dynamics of the full system are merely a perturbation of $\mathcal{O}(\epsilon)$ of the subsystem dynamics. By denoting the critical manifold as $\mathcal{M}_0$ where $\mathcal{M}_0$ is a subset of fixed points given by $f(u, v; 0) = 0$ the two results of Fenichel, applied to system (1.3), are given in the following two theorems.

Theorem 1.1 (Fenichel's first theorem (Hek, 2010))**.** *Suppose* $\mathcal{M}_0 \subset \{f(u, v; 0) = 0\}$ *is compact, possibly with boundary, and normally hyperbolic. Suppose f and g are smooth. Then for* $\epsilon > 0$ *and sufficiently small, there exists a manifold* $\mathcal{M}_\epsilon$, $\mathcal{O}(\epsilon)$ *close and diffeomorphic to* $\mathcal{M}_0$*, that is locally invariant under the flow of the full problem* (1.3)*.*

Theorem 1.2 (Fenichel's second theorem (Hek, 2010))**.** *Suppose* $\mathcal{M}_0 \subset \{f(u, v; 0) = 0\}$ *is compact, possibly with boundary, and normally hyperbolic. Suppose f and g are smooth. Then for* $\epsilon > 0$ *and sufficiently small, there exist manifolds* $W^s(\mathcal{M}_\epsilon)$ *and* $W^u(\mathcal{M}_\epsilon)$ *that are* $\mathcal{O}(\epsilon)$ *close and diffeomorphic to* $W^s(\mathcal{M}_0)$ *and* $W^s(\mathcal{M}_0)$*, respectively, and that are locally invariant under the flow of* (1.3)

Fenichel's first theorem, Theorem 1.1, can be summarized by saying that the flow of system (1.5), which is inherently restricted to $\mathcal{M}_0$, is close to the flow of the full system (1.3) when restricted to its slow manifold $\mathcal{M}_\epsilon$. Note that a systems slow manifold denotes the subset of state space in which the dynamics quickly tend towards and remain for all time (or perhaps leave through its boundary). Furthermore, the stable and unstable manifolds $W^s(\mathcal{M}_0)$ and $W^u(\mathcal{M}_0)$ are subsets of state space such that the flow will tend to $\mathcal{M}_0$ in forward time if it is in $W^s(\mathcal{M}_0)$ and in backward time if it is in $W^u(\mathcal{M}_0)$. Fenichel's second theorem, Theorem 1.2, gives the striking result that even the flow of the full system (1.3) near the stable or unstable manifolds of $\mathcal{M}_\epsilon$ is close to flow of the reduced system near the stable or unstable manifolds of $\mathcal{M}_0$, respectively (Hek, 2010; Kuehn, 2015).

Singular perturbation theory has been utilized in several seminal papers throughout the course of mathematical biology history including the Van der Pol oscillator (van der Pol, 1926) and the classical Michaelis Menton enzyme kinetics (Keener and Sneyd, 1998) and is further applied in Chapters 2 and 3.

1.5.3 Monotone dynamical systems

In Chapter 4 I utilize the theory of monotone dynamical systems to understand the long term coexistence of competing phytoplankton species. Monotone dynamical systems theory was popularized by Smith (1995) and is a powerful theory in studying global dynamics of competitive dynamical systems. The use of monotone dynamical systems theory has become common in biological modelling applications for several reasons. First, the conditions for monotonicity of a system are easily deduced by observing the ordering of solutions to a dynamical system. Simplistically, a system is monotone if its solutions pre-

serve the ordering of the initial conditions for all time. Second, monotonicity of a system limits the possible dynamical outcomes allowing for deduction of global stability results. That is, a monotone system with bounded solutions will converge to an equilibrium. In essence the conditions for monotonicity and its implications seem trivial, however application of this theory is often complex and difficult to argue. For example, solutions to complex systems are typically only given numerically thus the confirmation of the monotone condition can be nontrivial making. Nonetheless, this theory has been used for the study of many systems in biology including the study of competitive outcomes amongst phytoplankton species (Jiang et al., 2019; Jiang, Lam, and Lou, 2021; Hsu, Shi, and Wang, 2014).

1.6 Thesis overview

The main chapters of this thesis answer questions that are interconnected in an ecological and mathematical way. That being said, each chapter can be understood individually and is either published or soon to be submitted for publication. The overarching theme of this thesis is the ecological complexity involved in phytoplankton dynamics. I break down the large-scale problem by individually studying transient dynamics of phytoplankton, niche differentiation in the light spectrum, and the coupling between phytoplankton and human interactions. The synthesis of the three main components of this thesis provide insight towards a general understanding of phytoplankton and its complexities.

In Chapter 2, I model the transient cyanobacteria dynamics via the explicit application of singular perturbation theory to a mechanistically derived stoichiometric model. The model dynamics occur in distinct phases that can

be interpreted as occurring near critical manifolds corresponding to light or nutrient limitation. The transition between manifolds corresponds to bloom collapse, and an approximation for bloom longevity is given.

In Chapter 3, I explore the regime outcomes of a coupled socio-economic-cyanobacteria model. Singular perturbation theory allows for the separation of timescales between the ecological and human dynamics. Bistability and tristability are observed for the various systems resulting in regime shifts between favourable, or less favourable environmental outcomes dependent on socio-economic parameter values.

In Chapter 4, I explore coexistence of competing phytoplankton species. The specific allowance of niche differentiation in the light spectrum gives rise to robust coexistence regions shown both analytically and numerically. I offer a realistic competition scenario and explain how my results contribute to the explanation of the paradox of the plankton.

This thesis is concluded with a discussion of the results and their significance in Chapter 5.

Chapter 2

Transient dynamics of a stoichiometric cyanobacteria model via multi-scale analysis

2.1 Introduction

Ecological systems are intricate and require key molecules and elements to function in an integrative nonlinear way. We can attempt to mechanistically model ecological systems in terms of these key molecules and elements. Ecological stoichiometry, the study of the balance of energy (such as light and carbon) and elemental resources (such as phosphorus and nitrogen) in ecological interactions and processes (Sterner and Elser, 2002), is a powerful tool for studying and interpreting macroscopic phenomena via microscopic building blocks associated with nutrients and energy in an ecological system. Ecological stoichiometry has become increasingly popular in theoretical ecology (Sterner and Elser, 2002; Hessen et al., 2013) and its predictions have been supported by an array of empirical studies (Sterner and Elser, 2002; Elser et al., 1998; Paerl and Otten, 2013; Berger et al., 2006; Van De Waal et al., 2009). While classical mathematical models cannot explain many observed ecological phenomena, due to the lack of mechanistic modelling of limiting nutrients or

energy, ecological stoichiometry allows us to mechanistically model the effects of limiting resources on ecological dynamics and trophic interactions (Wang et al., 2007; Andersen, Elser, and Hessen, 2004; Sterner and Elser, 2002; Berger et al., 2006; Grover, 2003; Loladze, Kuang, and Elser, 2000). Some such models include producer-grazer interactions (Wang, Kuang, and Loladze, 2008; Loladze, Kuang, and Elser, 2000), algae-bacteria interactions (Wang et al., 2007), organic matter decomposition (Kong, Salceanu, and Wang, 2017) and toxin stress on various trophic interactions (Huang et al., 2013; Huang, Wang, and Lewis, 2015; Peace, Poteat, and Wang, 2016). These studies show the crucial role that ecological stoichiometry has to play in the mechanistic modelling of biological dynamics and the successful interpretation of many existing paradoxes.

Harmful algal blooms (HABs) have become an issue of global concern in aquatic ecosystems (Paerl and Otten, 2013). HABs occur for a variety of reasons, but most commonly are the result of eutrophication (Paerl, 2014). Eutrophication is described as an excess of nutrients required for organismal growth in a body of water. In North America, eutrophication is commonly caused by industrial, agricultural and urban nutrient runoff (Paerl, 2014). In temperate regions these anthropogenic sources of nutrient promote the growth of algae and, perhaps more importantly, the growth of cyanobacteria (CB) (Paerl and Otten, 2013). Many genera of cyanobacteria produce toxins, called cyanotoxins, which are harmful to humans, agriculture, and the aquatic dynamics within lakes and water-bodies. A cyanobacterial bloom can be detrimental to the aquatic ecosystem causing toxification and anoxia. This results in low productivity of the ecosystem (Paerl and Otten, 2013). For these reasons it is important to understand how anthropogenic nutrient inputs and

eutrophication influence HAB longevity and severity.

The majority of temperate lakes are stratified, meaning they are separated into two distinct thermal layers by a thermocline. The hypolimnion is the cold and stagnant layer, with little to no solar energy, which lies underneath the thermocline. Above the thermocline is the warmer, well mixed, and more active layer called the epilimnion. Availability of sunlight in the epilimnion allows phytoplankton to grow, provided there are sufficient nutrients available. Phosphorus is most commonly the limiting nutrient in temperate lakes, followed by nitrogen. Nutrients can be added to the water column through several distinct mechanisms such as a slow mixing between stratified layers, inputs from rivers, rain or snow melt runoff, and industrial or agricultural runoff (Paerl, 2014). Since phytoplankton growth depends on both light and available nutrients, we must also consider the stoichiometry of the phytoplankton when formulating models. Furthermore, the transient dynamics of the phytoplankton depend heavily on the initial nutrient concentration. Several models only consider the stratified water column when investigating phytoplankton dynamics (Huisman and Weissing, 1994; Melina Celeste et al., 2017; Yoshiyama et al., 2009). Other models consider light limitation (Martínez, Mairet, and Bernard, 2018; Huisman and Weissing, 1994). Few have considered both stratification, light limitation and the stoichiometry of phytoplankton (Wang et al., 2007; Berger et al., 2006).

Often, asymptotic dynamics, such as stability of equilibria or limit cycles, are the main focus of mathematical model analysis. However, the asymptotic dynamics can be misleading or uninformative when asking management questions pertaining to shorter time scales. For this reason transient dynamics, dynamics that occur on a smaller time scale, should not be over looked (Hast-

ings et al., 2018). A slight change in initial conditions or a perturbation can drastically alter the transient dynamics of an ecosystem. Understanding the transient dynamics and their sensitivity to changes may be crucial to management strategies aimed at short term predictions of ecosystem behaviour (Hastings et al., 2018).

The dynamics of cyanobacteria occur on multiple time-scales. It is not uncommon for cyanobacteria to persist at a low concentration of biomass for long periods. Once conditions are right, a fast increase in CB biomass occurs, often resulting in HABs. The blooms can persist for varied periods of time but often senesce quickly. Furthermore, cyanobacteria have very small, although varying, nutrient to carbon ratios. Hence, the measures of internal nutrient and biomass are different orders of magnitude (Whitton, 2012). All of these factors inspire a multiple time-scale analysis. Fortunately, the multiple time-scale analysis allows us to study the driving mechanisms behind the transient dynamics of cyanobacteria.

Singular perturbation theory boasts a broad range of biological applications. This theory is based on the limiting behaviour of multi-scale dynamics, a common biological feature. The theory from singular perturbations used for multiple time-scales typically employs asymptotic techniques such as matching and series expansions (Kuehn, 2015). Perhaps most relevant to our study is the theory developed by Neil Fenichel that gives a geometric interpretation of phase spaces of perturbed systems with relation to the simpler unperturbed system (Fenichel, 1979). This theory allows applied mathematicians to perform analysis on simplified versions of complex systems and draw conclusions about the complex system. Furthermore, this theory allows the in-depth study of the transient dynamics of a system, which is of great importance

to ecosystem management and ecological predictions (Hastings et al., 2018). Singular perturbation theory is by no means new and has been utilized in several milestone models in biology such as the Van der Pol oscillator (van der Pol, 1926; Bertram and Rubin, 2017), Hodgkin Huxley model (Hodgkin and Huxley, 1952; Rubin and Wechselberger, 2007), Michaelis Menton enzyme kinetics (Keener and Sneyd, 1998), and more recently in predator-prey dynamics (Rinaldi and Muratori, 1992; Hek, 2010) as well as in numerous applications outside biology. *To our best knowledge, no rigorous application of the theory has yet been applied to stoichiometric models in ecology. In this chapter we provide a rigorous application of multi-scale methods to understand the transient dynamics of a stoichiometric cyanobacteria model.* The mathematical analysis also yields an interesting type of dynamics at the fold curve (Hek, 2010; Kuehn, 2015). That is, the transient dynamics transition from one slow sub-manifold to another, as discussed in Section 2.5.

We extend the stoichiometric model of Wang et al. (2007) to consider the dynamics under various initial levels and anthropogenic inputs of dissolved mineral phosphorus and analyze the resultant transient dynamics. The various levels of dissolved mineral phosphorous are representative of the level of eutrophication. We notice from the numerical simulation, shown in Section 2.3, that interesting transient dynamics arise, inspiring a multiple time-scale analysis. In Section 2.4 we perform the multiple time-scale analysis and mathematically describe the dynamics presented in Section 2.3. In Section 2.4 we show that, for certain initial conditions, a "switch" in the dynamics from being light limited to phosphorus limited, must occur. In Section 2.6 we approximate the longevity of blooms with regard to the initial eutrophication level, initial conditions, and model parameters. Finally, we discuss how these results

create a deeper biological understanding of transient cyanobacteria dynamics and discuss the mathematical implications in Section 2.8. The results presented in this chapter show the unique application of multi-scale methods to stoichiometric models and how useful they can be in applying the results to real-world systems.

2.2 Model formulation

In this section we discuss the biological background, mechanisms and assumptions used to construct our model. The model consists of three interconnected variables, B, Q, and P that represent the concentration of carbon biomass of cyanobacteria, phosphorus cell quota, and concentration of mineral phosphorus, respectively. To track the rates of change of each variable we use a system of three interconnected nonlinear differential equations. The derivation of the model follows that of Berger et al. (2006) and Wang et al. (2007).

We assume the dynamics occur in a well-mixed epilimnion with depth z_m. We assume that water exchange, with respect to the epilimnion, occurs via two mechanisms. First, we assume that water is exchanged between the epilimnion and the hypolimnion. Second, we assume that water is exchanged between the epilimnion and the inflow/outflow of rivers, rain run-off and springs. We assume that both water exchange mechanisms occur at rate D. Furthermore, we assume that the concentration of phosphorus is constant and equal in both the hypolimnion and inflow, denoted with p_{in}. The rate of concentration change of CB and phosphorus due to the water exchange is proportional to the volume of the epilimnion. That is, the amount of particulates exchanged is related to the proportion of particulates located near the boundaries. In a larger volume, a smaller proportion of total substrate lies near the epilimnion boundaries. On

the other hand, in a smaller volume a larger proportion of substrates in the epilimnion will be exchanged. Hence, the particulate exchange rate, in and out, is inversely proportional to the depth of the well-mixed epilimnion.

Cyanobacteria lose carbon through respiration resulting in a decrease of carbon biomass (Whitton, 2012). Assuming sufficient nutrient the cyanobacterial photosynthesis, and thereby growth, depends on light availability throughout the epilimnion. The light intensity along the water column is attenuated by cyanobacteria and other suspended particles. Following Lambert-Beer's law (Huisman and Weissing, 1994), we model the light intensity at a given water depth, s, and cyanobacterial biomass concentration, B, by

$$L(s, B) = I_{in} \exp\left[-(K_{bg} + kB)s\right]. \tag{2.1}$$

The parameters I_{in}, K_{bg} and k_b are described in Table 2.1. The light-dependent cyanobacterial growth is modeled with the Monod equation, $\frac{L(s,B)}{L(s,B)+H}$, which is empirically supported (Kirk, 2010). However, this function is depth-dependent. Thus, applying the well mixed assumption we average the carbon/energy production function over the depth of the epilimnion. The light-dependent cyanobacterial growth function is

$$h(B) \equiv \frac{1}{z_m} \int_0^{z_m} \frac{L(s, B)}{L(s, B) + H} ds. \tag{2.2}$$

This integral is easily evaluated and used in later analysis. The internal phosphorus-dependent growth function follows the empirically well-tested Droop form, $1 - \frac{Q_m}{Q}$, where Q_m is the minimum cell quota. The product of the light and phosphorus-dependent cyanobacterial growth functions scales the maximum cyanobacterial reproduction rate, r, as $rB(1 - \frac{Q_m}{Q})h(B)$.

Nutrient uptake is a decreasing function of cyanobacterial cell quota. Uptake is maximal when the cell quota is at its minimum, Q_m, but should cease

when cell quota is at its maximum, Q_M. Nutrient uptake follows the empirically supported Monod form (Morel, 1987), which is a saturating function of dissolved mineral phosphorous. These assumptions yield the nutrient uptake function:

$$\rho(Q,P) = \rho_m\Big(\frac{Q_M - Q}{Q_M - Q_m}\Big)\frac{P}{P+M}. \tag{2.3}$$

Where ρ_m and M are the maximum phosphorus uptake rate and the half saturation coefficient for CB phosphorus uptake, respectively.

The combination of the above assumptions yields the following stoichiometric cyanobacteria model:

$$\begin{cases} \dfrac{dB}{dt} = \underbrace{rB\Big(1-\dfrac{Q_m}{Q}\Big)h(B)}_{\text{growth limited by P and light}} - \underbrace{\nu_r B}_{\text{respiration}} - \underbrace{\dfrac{D}{z_m}B}_{\text{exchange}}, \\ \dfrac{dQ}{dt} = \underbrace{\rho(Q,P)}_{\text{replenishment}} - \underbrace{rQ\Big(1-\dfrac{Q_m}{Q}\Big)h(B)}_{\text{cell quota dilution due to cell division}}, \\ \dfrac{dP}{dt} = \underbrace{\dfrac{D}{z_m}(p_{in}-P)}_{\text{P input and exchange}} - \underbrace{B\rho(P,Q).}_{\text{P consumption}} \end{cases} \tag{2.4}$$

We also denote the total phosphorus concentration in the system by $R = BQ+P$. All parameter definitions and values used throughout this chapter are found in Table 2.1. The parameter values listed are representative of realistic phytoplankton traits. Global qualitative analysis and bifurcation plots of the model (2.4) were discussed by Wang et al. (2007) and will not be restated here. For the purpose of this chapter we are interested in the transient dynamics for various initial conditions. In particular we study how the dynamics depend on the initial phosphorus concentration as it is a descriptor of how eutrophic the environment is initially.

Table 2.1: Definitions and values for parameters of system (2.4). Parameter values are obtained from Diehl, Berger, and Wöhrl (2005), Kalff (2002), Whitton (2012), and Berger et al. (2006).

Par.	Meaning	Value	Biological Values
r	Maximum CB specific production rate	1	1 $/day$
Q_m	CB cell quota at which growth ceases (minimum)	0.004	0.004 gP/gC
Q_M	CB cell quota at which nutrient uptake ceases (maximum)	0.04	0.04 gP/gC
z_m	Depth of epilimnion	7	$> 0 - 10m$
ν_r	CB respiration loss rate	0.35	0.05-0.6 $/day$
D	Water exchange rate	0.02	m/day
H	Half saturation coefficient of light-dependent CB production	120	120 $\mu mol/(m^2 \cdot s)$
ρ_m	Maximum CB Phosphorus uptake rate	1	0.2-1 $gP/gC/day$
M	Half saturation coefficient for CB nutrient uptake	1.5	1.5 mgP/m^3
p_{in}	Concentration of dissolved inorganic phosphorus in the hypolimnion and inflow	5	0-150 mgP/m^3
K_{bg}	Background light attenuation	0.3	0.3-0.9 $/m$
k	Algal specific light attenuation	0.0004	0.0003-0.0004 m^2/mgC
I_{in}	Light intensity at water surface	300	300 $\mu mol/(m^2 \cdot s)$

2.3 Model simulation

In this section we simulate model (2.4) for one year to illustrate the unique qualitative nature of the dynamics. To motivate the analysis of future sections, we notice abrupt transition layers in B and Q, as seen in Figure 2.1, that are

now understood to be triggered by a slow change in phosphorus concentration. We seek to compute the times at which the abrupt transitions will occur. This provides important insight towards understanding bloom longevity. One could easily compute this time duration numerically, but we show in Section 2.6 we can approximate the longevity of the bloom as a function of model parameters and initial conditions.

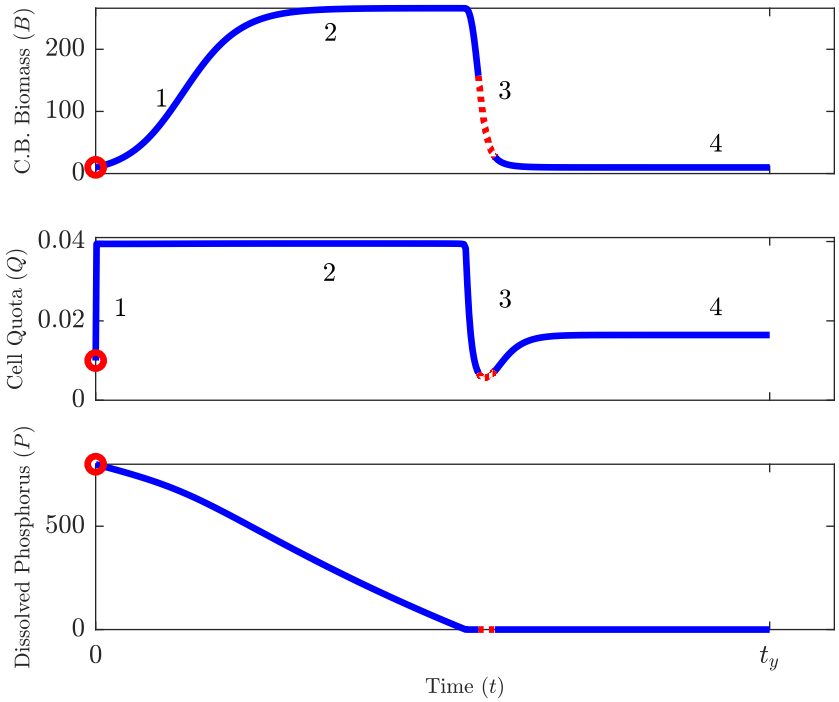

Figure 2.1: Dynamics of model (2.4) with parameter values listed in table 2.1. The dynamics involve four main phases; 1) the abrupt increase of cell quota and CB biomass, 2) the apparent bloom phase, 3) the sudden crash of the cell quota and CB biomass, and 4) the low constant phase. $t_y = 365$ days and the solid blue portions of the curves represent when light is limiting growth. The red dotted portions represent when phosphorous is limiting.

Figure 2.1 illustrates the model dynamics simulated over one year. The dynamics can be described as four separate phases. First, the sudden growth, or onset of the cyanobacterial bloom. This phase is encouraged by rapid up-

take of phosphorus, as we discuss in Section 2.4.2, allowing the CB to grow at a rate near its maximum. Second, is the extended period of time where the bloom is not growing but remains at a high level. Here, the cyanobacterial phosphorus uptake is constant resulting in a slow decrease in available phosphorus. Also, the CB reach a biomass level where self-shading occurs causing their growth to be light limited (Whitton, 2012). The third phase involves the abrupt decrease in both cell-quota and cyanobacteria. In this phase, the phosphorus concentration has become essentially depleted. This results in the fourth phase, where all variables tend to a low equilibrium. We discuss each phase in greater detail in following sections.

2.4 Multiple time-scale dynamics

In this section we explain mathematically the mechanisms responsible for the phases, and transitions between them, discussed in Section 2.3. We begin with a nondimensionalization of model (2.4) given by (2.5) and determine that the system contains small perturbation parameters. We proceed by deriving fast and slow subsystems of (2.5). The fast subsystem explains the abrupt uptake of phosphorus. The slow subsystem allows us to understand the transition layers by looking at the unique characteristics of the critical manifold. This analysis finally allows us to approximate the longevity of the bloom.

2.4.1 Nondimensionalization

We re-scale system (2.4) to achieve dimensionless variables and parameters. The dimensionless system is given below:

$$\frac{du}{d\tau} = u\Big(1 - \frac{1}{\gamma v}\Big)\frac{1}{u + k_1}\log\Big(\frac{1+I}{1 + I\exp(-u - k_1)}\Big) - (\alpha + \beta)u \tag{2.5a}$$
$$= ug(u, v; \beta),$$
$$\delta\frac{dv}{d\tau} = (1 - v)\frac{w - \sigma uv}{w - \sigma uv + \mu} + \delta\Big(\frac{1}{\gamma} - v\Big)\frac{1}{u + k_1}\log\Big(\frac{1+I}{1 + I\exp(-u - k_1)}\Big) \tag{2.5b}$$
$$= f(u, v, w; \delta),$$
$$\frac{dw}{d\tau} = -\alpha\sigma uv - \beta(w - 1) = h(u, v, w; \beta), \tag{2.5c}$$

with $u = kz_mB$, $v = \frac{Q}{Q_M}$, $w = \frac{R}{p_{in}} = \frac{P+BQ}{p_{in}}$, and $\tau = rt$. The parameters and their respective dimensionless quantities are given in table 2.2.

Table 2.2: Dimensionless parameters for system (2.5)

Parameter	Definition	Value
α	ν_r/r	0.35
β	$\frac{D}{rz_m}$	0.0029
δ	$\frac{r(Q_M - Q_m)}{\rho_m}$	0.036
μ	M/p_{in}	0.3
γ	$\frac{Q_M}{Q_m}$	10
σ	$\frac{Q_M}{p_{in}z_mk}$	2.9
k_1	z_mK_{bg}	2.1
I	I_{in}/H	2.5

This scaling allows all state variables to be of order one. However, β and δ are smaller than other parameters and will be treated as small independent perturbation parameters, each of which is biologically motivated. The parameter β is directly proportional to the exchange rate between the hypolimnion, or inflows and outflows, and the epilimnion. In stagnant or deep stratified lakes β is small. The parameter δ is proportional to $Q_M - Q_m$, the difference

between maximum and minimum cell quota. The cell quotas are considered small as the phosphorus to carbon ratio of a single cell is naturally small, even at the maximum (Diehl, Berger, and Wöhrl, 2005; Whitton, 2012). Note that when $\beta = 0$ the structure of the system is qualitatively the same as when β is nonzero, thus β acts as a regular perturbation. When $\delta = 0$ the system is reduced to an algebraic-differential system, for this reason we say δ causes a singular perturbation.

2.4.2 Fast time-scale dynamics

In this section we study the fast system. We show that the abrupt uptake of phosphorus that motivates the bloom occurs on the fast time-scale and use this to understand the first phase of the dynamics shown in Figure 2.1. Furthermore, we obtain the first order approximation of the system on the fast time-scale, which will then be used to form the uniform first order approximation.

We introduce the intermediate variable $\xi(\beta, \delta)$ so that the fast time-scale is $t_1 = \tau/\xi(\beta, \delta)$, where ξ is to be determined. Let $U(t_1) = u(\xi t_1)$, $V(t_1) = v(\xi t_1)$ and $W(t_1) = w(\xi t_1)$. Then U, V and W are functions of the fast time variable and are referred to as the fast variables. The fast system dynamics are then given by the following system of equations:

$$\begin{aligned}
\frac{1}{\xi(\beta,\delta)}\frac{dU}{dt_1} &= U\Big(1-\frac{1}{\gamma V}\Big)\frac{1}{U+k_1}\log\Big(\frac{1+I}{1+I\exp(-U-k_1)}\Big)-(\alpha+\beta)U,\\
\frac{1}{\xi(\beta,\delta)}\delta\frac{dV}{dt_1} &= (1-V)\frac{W-\sigma UV}{W-\sigma UV+\mu}+\\
&\qquad \delta(1/\gamma - V)\frac{1}{U+k_1}\log\Big(\frac{1+I}{1+I\exp(-U-k_1)}\Big),\\
\frac{1}{\xi(\beta,\delta)}\frac{dW}{dt_1} &= -\alpha\sigma UV-\beta(W-1).
\end{aligned} \tag{2.6}$$

We choose $\xi(\beta, \delta) = \delta$ in order to retain the term involving $\frac{dV}{dt}$. A two param-

eter asymptotic expansion in β and δ for $U(t_1)$ is given by

$$U(t_1) = \sum_{i,j\geq 0} \beta^i \delta^j U_{i,j}(t_1) = U_{0,0} + \beta U_{1,0} + \delta U_{0,1} + \beta\delta U_{1,1} + \cdots, \tag{2.7}$$

and is defined similarly for all functions. After applying the two parameter asymptotic expansion in β and δ for each of the fast variables and letting $\beta, \delta \to 0$, we obtain the subsystem that describes the first order approximation of the fast time variables:

$$\begin{aligned} \frac{dU_{0,0}}{dt_1} &= 0, \\ \frac{dV_{0,0}}{dt_1} &= (1 - V_{0,0})\frac{W_{0,0} - \sigma U_{0,0}V_{0,0}}{W_{0,0} - \sigma U_{0,0}V_{0,0} + \mu}, \\ \frac{dW_{0,0}}{dt_1} &= 0. \end{aligned} \tag{2.8}$$

We let $U_{00}(t_1) = u(0)$ and $W_{00}(t_1) = w(0)$ in order to satisfy the initial conditions. There are two possible equilibrium values, $V_{0,0} = 1$ and $V_{0,0} = W_{00}/\sigma U_{00}$. Note that

$$w(\tau) - \sigma u(\tau)v(\tau) \geq 0 \tag{2.9}$$

and

$$1/\gamma \leq v(\tau) \leq 1 \tag{2.10}$$

are biological restrictions representing the dissolved mineral phosphorus and the cell quota restrictions respectively. Of course, these biological restrictions apply to the fast variables as well. Thus, depending on the initial conditions at least one of the equilibria is biologically unfeasible.

Since U_{00} and W_{00} are constant the differential equation for V_{00} in (2.8) is separable and easily solved. The implicit solution is given by

$$\frac{b-1}{1-a}\log(1-V) - \frac{a-b}{1-a}\log(a-V) = t + C, \tag{2.11}$$

where $a = \frac{W}{\sigma U}$, $b = \frac{\mu}{\sigma U} + a$, and C is determined by the initial conditions. Note that the biological restrictions on the initial conditions and flow ensure that $(1 - V), (a - V) \geq 0$. The solution to the fast system can only be given implicitly, however we are still able to determine several more characteristics of the solution.

If we assume that $a > 1$, then as $t \to \infty$ the LHS of equation (2.11) tends to ∞. Since $V(0) < 1$ and $\frac{dV}{dt_1}$ is positive it is clear that $V(t_1)$ is monotone increasing with a horizontal asymptote $V = 1$.

We now assume that $a < 1$. Then as $t \to \infty$ the LHS of equation (2.11) tends to ∞. Since $V(0) < a$ and $\frac{dV}{dt_1}$ is positive it is clear that $V(t_1)$ is monotone increasing with a horizontal asymptote $V = a$.

We now conclude that

$$\lim_{t_1 \to \infty} V_{00} = \min\{1, a\} = \min\{1, \frac{w(0)}{\sigma u(0)}\}, \tag{2.12}$$

which satisfies the biological restriction (2.9).

To determine concavity we compute

$$\frac{d^2V}{dt^2} = -\frac{dV}{dt}(b - V)^{-2}[V^2 - 2bV + ab + b - a]. \tag{2.13}$$

By Descartes' rule of sign, the quadratic term has either 2 or 0 positive roots. Hence $\frac{d^2V}{dt^2}$ can change signs either twice or never, this number depends on the discriminant $4b^2 - 4(ab + b - a)$. The zeros occur at

$$V = b \pm \sqrt{b^2 - ab - b + a} \tag{2.14}$$

$$= b \pm \sqrt{(b - a)(b - 1)} \tag{2.15}$$

and at equilibria. Thus, if $b < 1$ then there are no real roots. Furthermore, if $b \geq 1$ then two positive roots appear. However, it is easily verified that $b \pm \sqrt{(b - a)(b - 1)} > \min\{1, a\}$ and recalling that $1/\gamma \leq V \leq \min\{1, a\}$ we

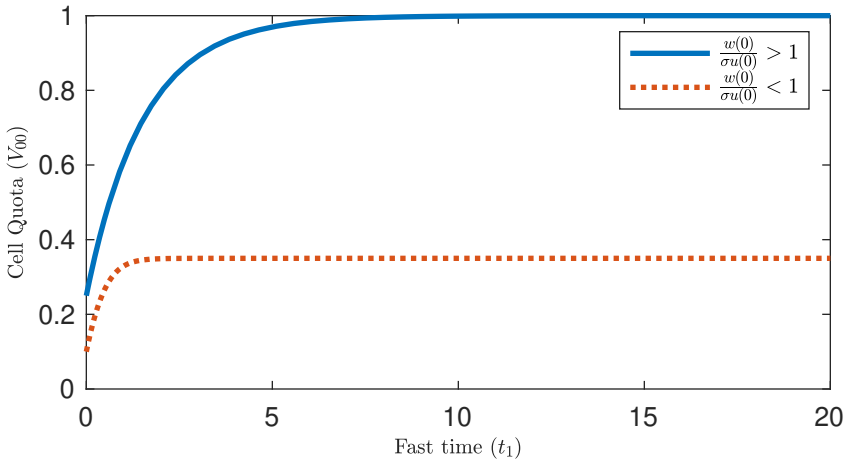

Figure 2.2: First order approximation of cell quota (V_{00}) dynamics on the fast time-scale for two different sets of initial conditions with parameter values given in table 2.2. The dotted curve shows the dynamics for $\frac{w(0)}{\sigma u(0)} < 1$, and the solid curve for $\frac{w(0)}{\sigma u(0)} > 1$. On the fast time-scale, the CB biomass (U_{00}) and total phosphorus (W_{00}) remain constant at their initial values.

conclude that there are no inflection points in the domain. Furthermore it is easy to see that $\frac{d^2V}{dt^2} < 0$ for $1/\gamma < V < \min\{1, a\}$. Hence, $V(t)$ is concave down in its domain. The dynamics of V_{00} for each case are shown in Figure 2.2.

2.4.3 Slow time-scale dynamics

In this section we study the slow system. We show that the growth of cyanobacteria is motivated by its fast P uptake and is dependent on the available P to sustain its growth. We show that once the P concentration becomes too low, the bloom can no longer be sustained. This is mathematically described as a transition from one sub-manifold of the critical manifold to another. Furthermore, we obtain the first order approximation of the system on the slow time-scale and will later use this to obtain a uniform first order approximation.

We assume that the slow time-scale is given by $t_2 = \tau$. Again, applying the

asymptotic expansion in β and δ as in (2.7) to the slow variables and letting $\beta, \delta \to 0$ we arrive at the following slow system:

$$\begin{aligned}
\frac{du_{00}}{dt_2} &= u_{00}\Big(1 - \frac{1}{\gamma v_{00}}\Big)\frac{1}{u_{00}+k_1}\log\Big(\frac{1+I}{1+I\exp(-u_{00}-k_1)}\Big) - \alpha u_{00} \\
0 &= (1-v_{00})\frac{w_{00}-\sigma u_{00}v_{00}}{w_{00}-\sigma u_{00}v_{00}+\mu}, \\
\frac{dw_{00}}{dt_2} &= -\alpha\sigma u_{00}v_{00}.
\end{aligned} \tag{2.16}$$

The slow system becomes an algebraic-differential system constrained by the set satisfying

$$0 = (1-v_{00})\frac{w_{00}-\sigma u_{00}v_{00}}{w_{00}-\sigma u_{00}v_{00}+\mu}. \tag{2.17}$$

The critical manifold, M_0, is a subset of the set given by (2.17). The set (2.17) can be divided into two sub-manifolds. Furthermore, the variables are only defined within the biological domain $\mathcal{D} = \{(u,v,w) | w - \sigma uv \geq 0, \frac{1}{\gamma} \leq v \leq 1, u, w \geq 0\}$. Thus, relevant manifolds and sub-manifolds are within $\mathcal{D}$. We define the sub-manifolds as:

$$M_0^0 = \{(u,v,w) : v_{00} = 1\} \cap \mathcal{D}, \tag{2.18}$$

$$M_0^1 = \{(u,v,w) : w_{00} - \sigma u_{00}v_{00} = 0\} \cap \mathcal{D}. \tag{2.19}$$

Furthermore, let $\mathcal{C} = M_0^0 \cap M_0^1 = \{(u,v,w) : w = \sigma u, v = 1\}$. Note that $M_0^0 \cup M_0^1 = \{(u,v,w) : 0 = (1-v_{00})\frac{w_{00}-\sigma u_{00}v_{00}}{w_{00}-\sigma u_{00}v_{00}+\mu}\} \cap \mathcal{D}$. Also, on M_0^0 the restriction (2.9) is equivalent to $\frac{w_{00}}{\sigma u_{00}} \geq 1$. We initially study the dynamics on each sub-manifold separately.

Dynamics on M_0^0

Here, we examine the dynamics of system (2.16) restricted to the sub-manifold M_0^0. On M_0^0, $v_{00} = 1$ and we write system (2.16) as

$$\begin{aligned}
\frac{du_{00}}{dt_2} &= u_{00}\Big(1 - \frac{1}{\gamma}\Big)\frac{1}{u_{00}+k_1}\log\Big(\frac{1+I}{1+I\exp(-u_{00}-k_1)}\Big) - \alpha u_{00}, \\
\frac{dw_{00}}{dt_2} &= -\alpha\sigma u_{00}.
\end{aligned} \tag{2.20}$$

The trivial equilibrium, $u_{00} = 0$, is unstable when $(1-\frac{1}{\gamma})\frac{1}{k_1}\log\frac{1+I}{1+I\exp(-k_1)} > \alpha$, which is true for the parameter values considered. That is, u_{00} will remain positive for all time forcing w_{00} to diverge to negative infinity. Figure 2.3 shows the dynamics of this case for appropriate initial conditions. For appropriate

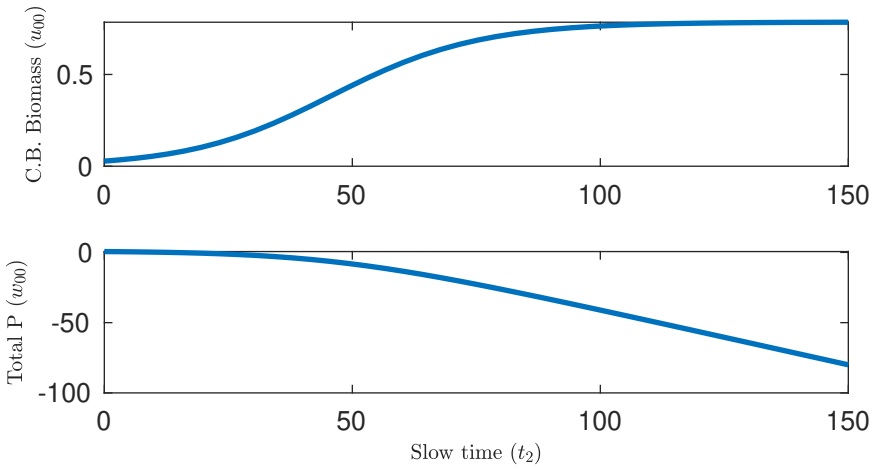

Figure 2.3: Slow scale dynamics of equation (2.20) with parameter values given in table 2.2 and initial conditions such that $w_{00}/\sigma u_{00} > 1$. In this case $v_{00} = 1$ and the dynamics occur on M_0^0.

initial conditions these dynamics will eventually violate the biological restriction (2.9). However, we show in later sections how this violation is avoided by allowing the dynamics to switch to the sub-manifold M_0^1.

Dynamics on M_0^1

Here we examine the dynamics of system (2.16) restricted to the sub-manifold M_0^1. On M_0^1, $w_{00} = \sigma u_{00} v_{00}$ and we write system (2.16) as

$$\begin{aligned}\frac{du_{00}}{dt_2} &= u_{00}\Big(1 - \frac{1}{\gamma w_{00}/\sigma u_{00}}\Big)\frac{1}{u_{00}+k_1}\log\Big(\frac{1+I}{1+I\exp(-u_{00}-k_1)}\Big) - \alpha u_{00},\\ \frac{dw_{00}}{dt_2} &= -\alpha w_{00}.\end{aligned} \tag{2.21}$$

In this case w_{00} will decay to zero. The term $(1 - \frac{1}{\gamma w_{00}/\sigma u_{00}})$ is always positive, however as w_{00} decays $(1 - \frac{1}{\gamma w_{00}/\sigma u_{00}})$ will become increasingly small. Eventually $-\alpha u_{00}$ will dominate forcing u_{00} to also tend to zero. Note that we are not concerned with any singularity as we focus on M_0^1 with the restriction (2.10). Numerically this can be seen in Figure 2.4.

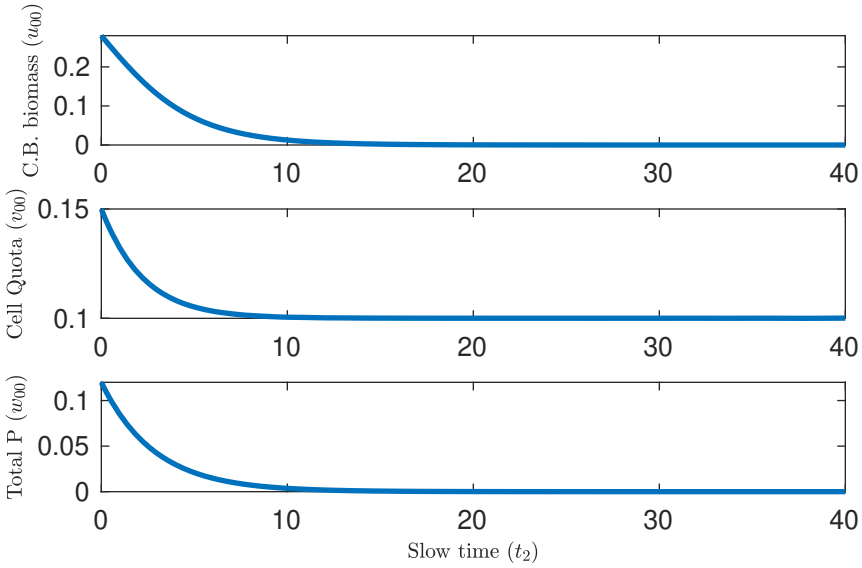

Figure 2.4: Slow scale dynamics given by system (2.21) with parameter values given by table 2.2 and initial conditions such that $w_{00}/\sigma u_{00} < 1$. Here, $v_{00} = w_{00}/\sigma u_{00}$ and the dynamics occur on M_0^1.

2.4.4 Asymptotic matching

We now satisfy the asymptotic matching conditions that are required to "glue" the fast and slow dynamics together. By satisfying the matching conditions we generate the first order uniform approximation of system (2.5). We additionally show that for a given initial condition only one of the cases discussed in Section 2.4.3 can satisfy the matching conditions. To obtain a first order uniform approximation the following asymptotic matching conditions must be

satisfied (Kuehn, 2015):

$$\lim_{t_1\to\infty} U_{00}(t_1) = \lim_{t_2\to 0} u_{00}(t_2) = u_m, \tag{2.22a}$$

$$\lim_{t_1\to\infty} V_{00}(t_1) = \lim_{t_2\to 0} v_{00}(t_2) = v_m, \tag{2.22b}$$

$$\lim_{t_1\to\infty} W_{00}(t_1) = \lim_{t_2\to 0} w_{00}(t_2) = w_m. \tag{2.22c}$$

The uniform approximations are then given by

$$u_{00}^{(u)}(t_2) = U_{00}(t_2/\delta) + u_{00}(t_2) - u_m, \tag{2.23a}$$

$$v_{00}^{(u)}(t_2) = V_{00}(t_2/\delta) + v_{00}(t_2) - v_m, \tag{2.23b}$$

$$w_{00}^{(u)}(t_2) = W_{00}(t_2/\delta) + w_{00}(t_2) - u_m. \tag{2.23c}$$

In section 2.4.2 we show that $\lim_{t_1\to\infty} V_{00}(t_1) = \min\{1, \frac{w(0)}{\sigma u(0)}\}$. Also, since U_{00} and V_{00} are constant, $\lim_{t_1\to\infty} U_{00}(t_1) = u(0)$ and $\lim_{t_1\to\infty} W_{00}(t_1) = w(0)$. Thus, in order to satisfy the matching conditions (2.22) we require $\lim_{t_2\to 0} u_{00}(t_2) = u(0) = u_m$, $\lim_{t_2\to 0} w_{00}(t_2) = w(0) = w_m$ and $\lim_{t_2\to 0} v_{00}(t_2) = \min\{1, \frac{w(0)}{\sigma u(0)}\} = v_m$. It is clear that conditions (2.22a) and (2.22c) can be easily satisfied by adjusting the initial conditions of the slow system.

Now, if $\frac{w(0)}{\sigma u(0)} > 1$ then $v_m = 1$. This means that as t_2 tends to zero, v_{00} must tend to one. Hence, for small t_2 the dynamics must be restricted to M_0^0. However, eventually condition (2.9) will be violated. We address this issue in the next section. Alternatively, if $\frac{w(0)}{\sigma u(0)} \leq 1$ then $v_m = \frac{w(0)}{\sigma u(0)}$. Thus, for small t_2 the dynamics must be restricted to M_0^1 to avoid violating (2.9). Unfortunately, the solution for u_{00} can only be given implicitly. However, we can still apply the matching conditions to obtain the first order approximation numerically.

2.4.5 The "Switch" from M_0^0 to M_0^1

In this section we address the issue that if the slow system dynamics are restricted to M_0^0 then eventually the condition (2.9) is violated. To maintain

the inequality (2.9) we allow the dynamics to switch from M_0^0 to M_0^1 at some point in time. The dynamics are shown in Figure 2.5.

We assume that $\frac{w(0)}{\sigma u(0)} > 1$, then the solution to system (2.16) is restricted to M_0^0 to match with the inner solution. However, it is clear that u_{00} will tend to the stable positive equilibrium resulting in w_{00} decreasing and eventually violating condition (2.9). Since w_{00} is decreasing to zero, v_{00} is held constant at one, and u_{00} tends towards a positive equilibrium, there must exist a time, t_s, when $w_{00} = \sigma u_{00} v_{00}$. If the slow dynamics, governed by system (2.16), remain on M_0^0 for $t > t_s$ then condition (2.9) is violated for all $t > t_s$.

However, at time t_s, $w_{00} = \sigma u_{00} v_{00}$, and this point is on the curve $\mathcal{C} = M_0^0 \cup M_0^1$. Thus, to ensure the biological conditions remain satisfied for all time we require the slow system to undergo a switch. In other words, the dynamics of the slow time-scale are governed by system (2.16) restricted to M_0^0 for time $t \leq t_s$ and restricted to M_0^1 for time $t > t_s$. For $t > t_s$ v_{00} is no longer restricted to be equal to one and the equilibrium equation for u_{00} changes. If $\frac{w(0)}{\sigma u(0)} \leq 1$, then the slow dynamics are restricted to M_0^1 and no conditions will be violated, hence no switch is necessary.

The approximation is now able to capture the sudden decrease found in the dynamics. We explain this biologically as a switch that occurs. The switch happens once the nutrient uptake is limited by the cell quota or by the available nutrient. The case in Section 2.4.3 assumes that the available nutrient is ample, thus the cell quota will be high. The case in Section 2.4.3 assumes that the available nutrient is limited, thus the cell quota and CB biomass will be low.

When allowing the switch we are able to define u_{00}, v_{00} and w_{00} such that no biological restrictions are broken. If the slow dynamics are restricted to M_0^0

for $t_2 \leq t_s$ and restricted to M_0^1 for $t_2 > t_s$ then (2.9) is not breached and we are able to form the uniform approximation discussed in Section 2.4.4. Figure 2.5 shows the first order approximation compared to the numerical solution.

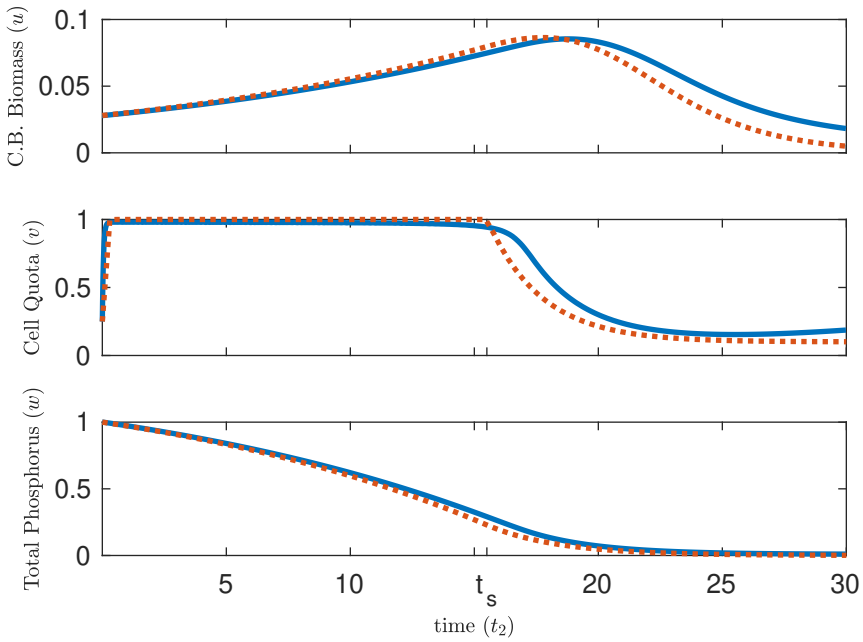

Figure 2.5: Dynamics of the uniform approximation and simulation of the full system for initial conditions such that $\frac{w(0)}{\sigma u} > 1$. Dotted line shows the first order uniform approximation of system (2.5) given by equations (2.23). Recall that the dynamics undergo a "switch" at time t_s. The solid line shows the dynamics of the full system (2.5).

If the initial conditions are such that $w(0)/\sigma u(0) \leq 1$ then by restricting the dynamics to M_0^0 on the slow time-scale we can not satisfy the matching conditions. Hence, the slow dynamics are governed by (2.21) and the system does not switch. Figure 2.6 shows the approximation in this case.

2.5 Geometry of the critical manifold

In this section we combine the above sections to understand analytically and visually the mechanisms that drive the dynamics discussed in Figure 2.1. We

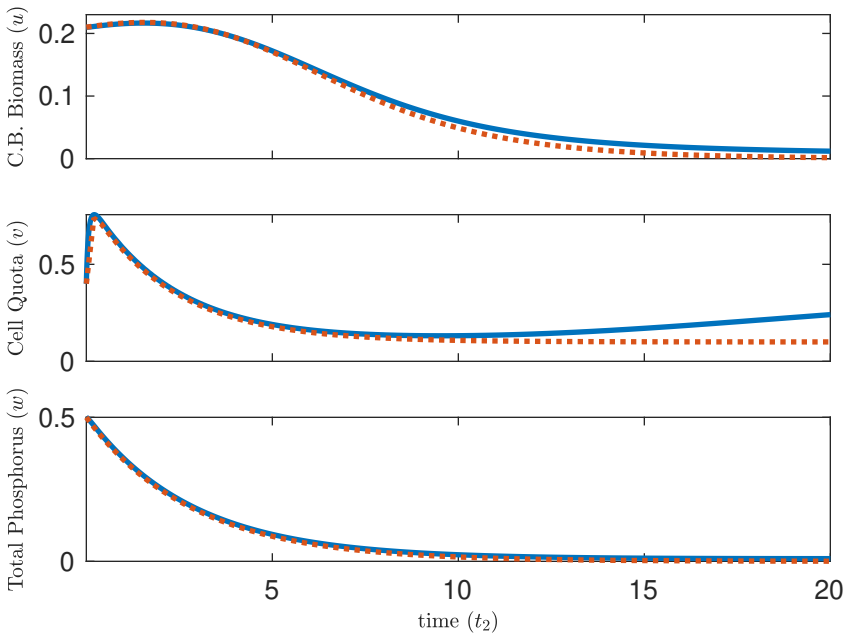

Figure 2.6: Dynamics of the first order uniform approximation and simulation of the full system for initial conditions such that $\frac{w(0)}{\sigma u} \leq 1$. Dotted line shows the first order uniform approximation of system (2.5) given by equations (2.23). Recall that the dynamics do not undergo a "switch" in this case. The solid line shows the dynamics of the full system (2.5).

show that the "switch" discussed in Section 2.4.5 is motivated by a loss of hyperbolicity of M_0^0 and M_0^1, both of which are subsets of the critical manifold M_0. Biologically, this is related to the gradual depletion of available phosphorus. Recall that the system (2.5) is defined on the domain $\mathcal{D} = \{(u, v, w) | u, w \geq 0, w - \sigma uv \geq 0, \frac{1}{\gamma} \leq v \leq 1\}$ and that functions g, f and h are defined in equations (2.5a),(4.6) and (2.5c), respectively.

2.5.1 Characteristics of the sub-manifolds

Here, we look at the reduced system given by (2.16). The variables, u, v, w are confined by the equation $(1 - v)\frac{w - \sigma uv}{w - \sigma uv + \mu} = 0$ as they flow on the slow time-scale. We show the hyperbolicity criterion of the two sets M_0^0 and M_0^1.

The critical manifold, M_0, is contained in the set $f(u, v, w; 0) = 0$.

Hyperbolicity of M_0^0

To determine the hyperbolicity of M_0^0 in the system's domain we examine the eigenvalues of

$$\frac{\partial f}{\partial v}(u, v, w; 0)|_{M_0^0} = \frac{\partial}{\partial v}(1 - v)\frac{w - \sigma uv}{w - \sigma uv + \mu}\Big|_{M_0^0} \tag{2.24}$$

$$= \frac{(\sigma u - w)}{(w - \sigma u + \mu)}. \tag{2.25}$$

It is convenient that the manifold M_0^0 is normally hyperbolic in the entire domain, except along the curve described by $\mathcal{C}$. Furthermore, we notice that the eigenvalues of $\frac{\partial f}{\partial v}(u, v, w; 0)|_{M_0^0 \cap \mathcal{D}}$ have negative real parts everywhere except on the curve $\mathcal{C}$. This implies that M_0^0 has a three dimensional stable manifold $W^s(M_0^0)$ (Hek, 2010), and a two dimensional unstable manifold $W^u(M_0^0)$ that we conjecture to be M_0^0 itself given the dynamics of the fast system.

Hyperbolicity of M_0^1

Likewise, we examine the hyperbolicity of the sub-manifold M_0^1 on $\mathcal{D}$ by determining the eigenvalues of $\frac{\partial f}{\partial v}(u, v, w; 0)|_{M_0^1}$. From previous calculations

$$\frac{\partial f}{\partial v}(u, v, w; 0)|_{M_0^1} = \frac{\partial}{\partial v}(1 - v)\frac{w - \sigma uv}{w - \sigma uv + \mu}\Big|_{M_0^1} \tag{2.26}$$

$$= \frac{(\sigma uv - w)(w - \sigma uv + \mu) + \sigma\mu u(v - 1)}{(w - \sigma uv + \mu)^2}\Big|_{M_0^1}$$

$$= \frac{\sigma\mu u(v - 1)}{\mu^2}. \tag{2.27}$$

Thus it is clear that the manifold M_0^1 is hyperbolic on the set defined by $\mathcal{D}\backslash(\{v = 1\} \cup \{u = 0\})$. Again the eigenvalues have negative real parts where M_0^1 is hyperbolic implying that M_0^1 has a three dimensional stable manifold

$W^s(M_0^1)$, and a two dimensional unstable manifold $W^u(M_0^1)$ (Hek, 2010) that we conjecture to be M_0^1 itself.

Figure 2.7 shows the visual representation of the manifolds and corresponding dynamics. First we note that the dynamics initially tend towards M_0^0. This is the fast time-scale dynamics discussed in Section 2.4.2. If the initial conditions are such that no switch needs to occur, the fast dynamics are "cut-off" by M_0^1 and approach M_0^1 instead. Lastly, we can see that the dynamics on M_0^0 transition to M_0^1 as it approaches the curve $\mathcal{C}$. This figure illustrates where the "switch" occurs geometrically and the role of the fast time-scale.

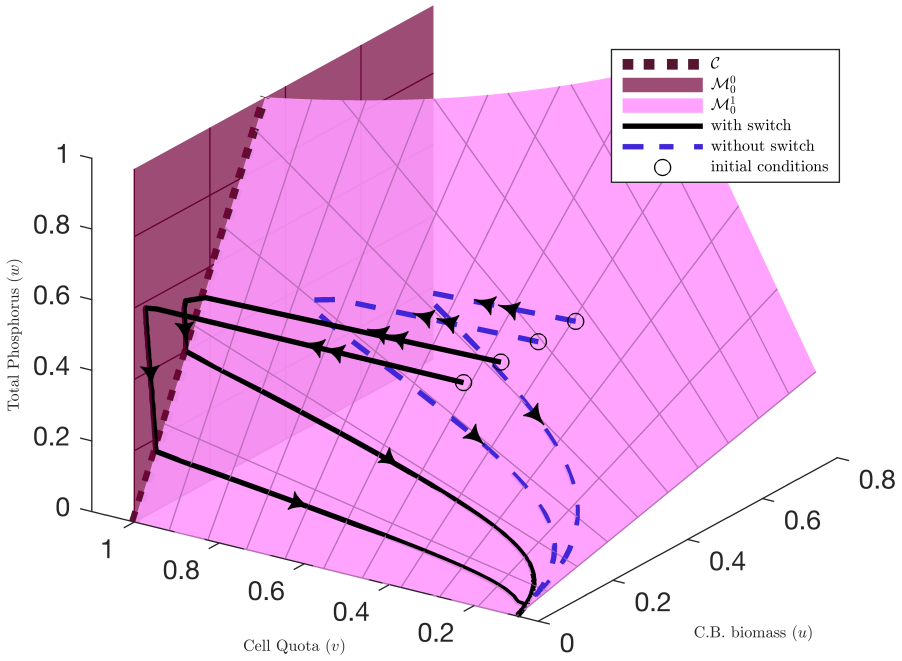

Figure 2.7: Shows the geometric orientation of M_0^0 in burgundy and M_0^1 in pink. Trajectories for various initial conditions are shown. Trajectories with initial conditions such that $\frac{w(0)}{\sigma u(0)} > 1$ are in black, and in blue (dashed) otherwise. All trajectories start away from M_0^0 and M_0^1. The double arrow indicates the fast dynamics (away from M_0^0 and M_0^1) and the single arrow the slow dynamics (on, or near M_0^0 or M_0^1). The curve $\mathcal{C}$ indicated in dark red (dotted) is the curve where hyperbolicity is lost on each manifold. When the trajectories approach $\mathcal{C}$ the dynamics switch from M_0^0 to M_0^1 as discussed in Section 2.4.5

2.6 Approximation of the switching time

Here, we re-examine the slow system (2.5). In particular we study the dynamics restricted to M_0^0 to better study the switching time, t_s. That is, we are interested in approximating the time it takes for the dynamics to intersect the curve $\mathcal{C}$. We can numerically compute t_s from the numerical solutions of system (2.20). Unfortunately it is impossible to write t_s as an explicit function of model parameters without making certain approximations.

By graphical inspection, we observe that the function $ug(u, 1; 0)$ resembles a quadratic polynomial. In the region we are concerned with, $v_{00} = 1$. Hence we can postulate that the approximation is of the form $au^2 + bu + c$. We further know that $u = 0$ satisfies $ug(u, 1, 0) = 0$ (Wang et al., 2007). Hence, in our approximation $c = 0$. Furthermore, as shown by Wang et al. (2007), $g(u, 1, 0) = 0$ has a positive unique solution. Thus, we can rewrite the approximation in the form:

$$ug(u, 1; 0, 0) \approx au(u^* - u), \tag{2.28}$$

where u^* is the mentioned positive solution, which also represents the biomass during a bloom, and a is to be determined. We determine a by equating the derivatives at $u = 0$. In other words, $au(u^* - u)'|_{u=0} = ((ug)'|_{u=0}$. Then we obtain

$$a = \Big[\big(1 - \frac{1}{\gamma}\big)\frac{1}{k_1}\log\Big(\frac{1+I}{1+I\exp(-k_1)}\Big) - \alpha\Big]\frac{1}{u^*}.$$

Figure 2.8 shows the comparison between $ug(u, 1; 0)$ and the approximation.

Now we can form an approximation of system (2.20) where $v_{00} = 1$. We denote with a tilde the approximation of the first order solution (i.e. $\tilde{u} \approx u_{00}$)).

$$\begin{aligned} \frac{d\tilde{u}}{dt_2} &= a\tilde{u}(u^* - \tilde{u}), \\ \frac{d\tilde{w}}{dt_2} &= -\alpha\sigma\tilde{u}. \end{aligned} \tag{2.29}$$

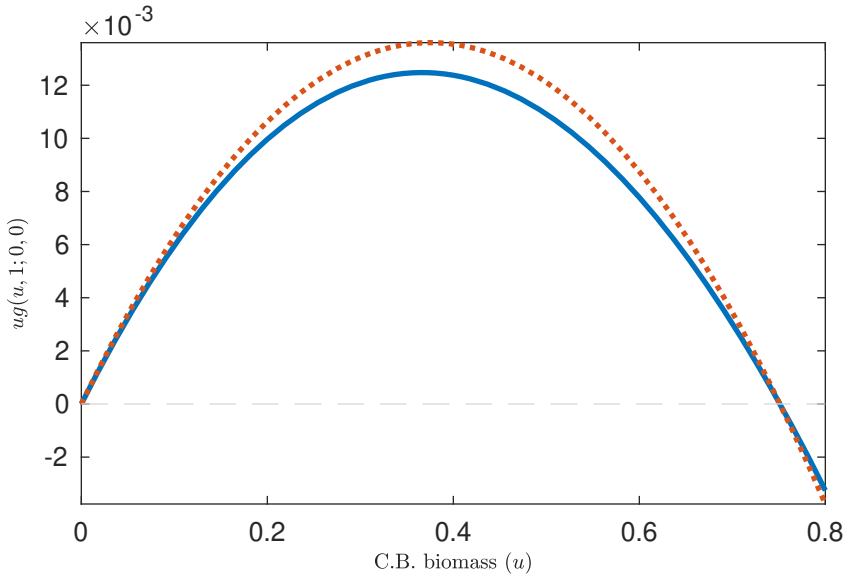

Figure 2.8: Comparison of the curves $ug(u, 1; 0)$ (dotted line) and its approximation $au(u - u^*)$ (solid line) given by (2.28).

We solve the first differential equation for $\tilde{u}$ as

$$\tilde{u} = \frac{Cu^* e^{au^* t_2}}{1 + Ce^{au^* t_2}}, \tag{2.30}$$

where $C = u(0)/(u^* - u(0))$. Then solving for $\tilde{w}$ from the second differential equation, we obtain

$$\frac{d\tilde{w}}{dt} = -\alpha\sigma \frac{Cu^* e^{au^* t}}{1 + Ce^{au^* t}} \tag{2.31}$$

$$\tilde{w} + B = \int -\alpha\sigma \frac{Cu^* e^{au^* t}}{1 + Ce^{au^* t}} dt \tag{2.32}$$

$$\tilde{w} + B = \frac{-\alpha\sigma}{a} \log(1 + Ce^{au^* t}), \tag{2.33}$$

where $B = \frac{-\alpha\sigma}{a} \log(1 + C) - w(0)$ in order to satisfy initial conditions. t_s is the time that satisfies the equation $\tilde{w} = \sigma\tilde{u}$ or

$$\frac{-\alpha\sigma}{a} \log(1 + Ce^{au^* t}) - B = \sigma \frac{Cu^* e^{au^* t}}{1 + Ce^{au^* t}}. \tag{2.34}$$

Now, recall that $C = \frac{u(0)}{u^* - u(0)}$. Hence, if our initial condition for CB is such that the ratio between u^* and $u(0)$ is small, which is generally true when the CB

biomass does not start in a bloom state, we can approximate $\log(1 + Ce^{u^*at})$ with Ce^{u^*at}. Of course, this is only valid if e^{u^*at} does not become large. However, the RHS of (2.34) is bounded and positive. The LHS of (2.34) is monotone decreasing with respect to t, and for large values of t is negative. Hence, the solution of (2.34), if it exists, remains bounded. Thus, the approximation remains valid. We approximate the time t_s by solving the equation (2.34). For simplicity let $x = Ce^{au^*t}$, then (2.34) becomes

$$\frac{-\alpha\sigma}{a}x - B = \sigma\frac{u^*x}{1+x} \tag{2.35}$$

$$\iff \quad 0 = x^2 + (1 + B\frac{a}{\alpha\sigma} + \frac{au^*}{\sigma})x + B\frac{a}{\alpha\sigma} \tag{2.36}$$

It is easily verified that $B\frac{a}{\alpha\sigma} < 0$, thus, following Descartes' rule of sign, there is one positive and one negative solution to the above equation. We are only interested in the positive solution expressed as

$$x_s = -\frac{1}{2}(1 + B\frac{a}{\alpha\sigma} + \frac{au^*}{\sigma}) + \sqrt{\frac{1}{4}(1 + B\frac{a}{\alpha\sigma} + \frac{au^*}{\sigma})^2 - B\frac{a}{\alpha\sigma}} > 0. \tag{2.37}$$

Thus,

$$t_s = \log(x_s/C)/au^*. \tag{2.38}$$

Figure 2.9 shows the value of t_s as a function of the initial condition for w. In this situation $w(0)$ is easily related to the level of eutrophication. We further note that t_s is non-negative for reasonable values of $w(0)$, mainly those satisfying condition (2.9). Furthermore, the values of t_s computed are reasonable when compared to real-life HAB times (Taranu et al., 2012; Whitton, 2012).

2.7 Fenichel's theorems applied

Here, we apply Fenichel's theorems to show that the flow of our singularly perturbed system, restricted to the slow manifold, is a small perturbation of

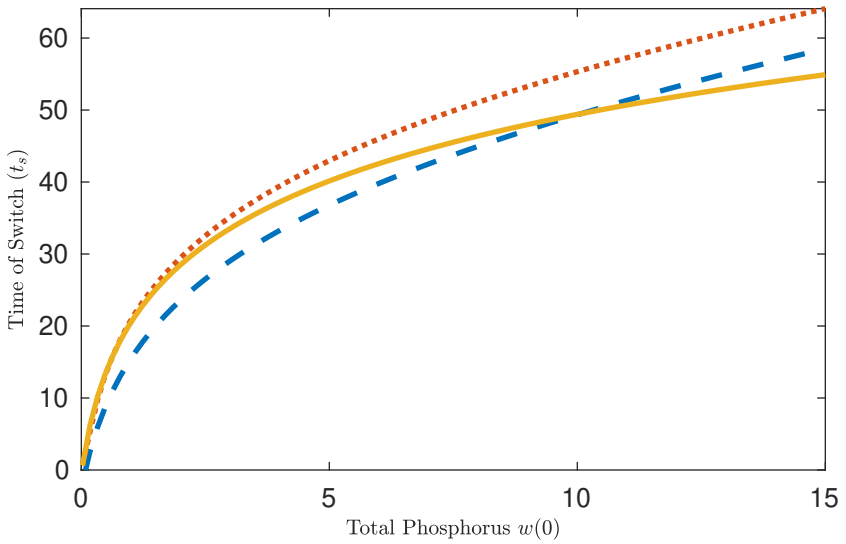

Figure 2.9: The switching time t_s as a function of $w(0)$. The initial condition $w(0)$ serves as a proxy for initial level of eutrophication. The solid curve gives t_s computed using the approximation given in (2.38). The dashed and dotted curves give t_s as the implicit solution of (2.34), and numerical value from simulations of system (2.5) for given values of $w(0)$, respectively.

the dynamics covered in the subsystem analysis of Section 2.4. Furthermore, the stable and unstable manifolds of the reduced system and the full system can be related by a small perturbation.

Recall that β acts as a regular perturbation parameter of system (2.5). Since the theory presented in this section is relevant to singular perturbations, we set, for simplicity, $\beta = 0$.

Consider the critical manifold $M_0 \subset M_0^0 \cup M_0^1 = \{f(u, v, w; 0, 0) = 0\} \cap \mathcal{D}$. We introduce an open epsilon neighbourhood of the curve $\mathcal{C}$ by $\mathcal{N}(\mathcal{C}; \epsilon) = \{x = (u, v, w) \in \mathcal{D} \mid d(x; \mathcal{C}) < \epsilon\}$ where $0 < \epsilon \ll 1$ and $d(x; A)$ is the least distance from a point x to a set A. We further denote the manifolds $M_0^{0h} = M_0^0 \backslash \mathcal{N}(\mathcal{C}; \epsilon)$ and $M_0^{1h} = M_0^1 \backslash \mathcal{N}(\mathcal{C}; \epsilon)$. Now, our critical manifold consists of two hyperbolic sets, and a small set near the non-hyperbolic set.

We can apply the results of Fenichel to obtain the following results.

Theorem 2.1 (Hek, 2010; Fenichel, 1979)**.** *For $\delta > 0$ and sufficiently small, there exists manifolds M_δ^0 and M_δ^1, $\mathcal{O}(\delta)$ close and diffeomorphic to M_0^{0h} and M_0^{1h} respectively, that are locally invariant under the flow of the system* (2.5) *with $\beta = 0$.*

In essence, theorem 2.1 implies that the system (2.5) with $\beta = 0$ has a flow that when restricted M_δ^0 or M_δ^1 is a small perturbation, of order δ, to system (2.16) flow on the respective sub-manifolds M_0^{0h} or M_0^{1h}. Furthermore, we can say the dynamics on M_δ will remain on M_δ except perhaps at the boundary of M_δ. We note that the sets M_δ^0 and M_δ^1 are, in general, not sets of fixed points and hence stability of these manifolds is thought of in a different manner. The following theorem alludes to the "stability" of our system.

Theorem 2.2 (Hek, 2010; Fenichel, 1979)**.** *For $\delta > 0$ and sufficiently small, there exists manifolds $W^s(M_\delta^0)$ $(W^s(M_\delta^1))$ and $W^u(M_\delta^0)$ $(W^u(M_\delta^1))$ that is $\mathcal{O}(\delta)$ close and diffeomorphic to $W^s(M_0^{0h})$ $(W^s(M_0^{1h}))$ and $W^u(M_0^{0h})$ $(W^u(M_0^{1h}))$, respectively, and that are locally invariant under the flow of the system* (2.5) *with $\beta = 0$.*

Since M_δ^0 and M_δ^1 are not sets of fixed points (unlike M_0^{0h} and M_0^{1h}) we discuss what the notation of stability means with respect to M_δ^0 and M_δ^1. The manifold $W^s(M_\delta^{0,1})$ $(W^u(M_\delta^{0,1}))$ is still referred to as the stable (unstable) manifold. Stability (or instability) here means that the flow in $W^s(M_\delta^{0,1})$ $(W^u(M_\delta^{0,1}))$ decays to $M_\delta^{0,1}$ in forward time (backward time) (Kuehn, 2015; Hek, 2010).

Theorems and 2.1 and 2.2 are direct results of Fenichel's first and second theorems given by Theorem 1.1 and Theorem 1.2, respectively. As a result, they allow us to draw the conclusion that the dynamics of the reduced system

are a small perturbation of the dynamics of the full system with $\beta = 0$. Hence, we conclude that the biological interpretation of the reduced system dynamics is also valid of the dynamics of the full system.

2.8 Biological interpretation

We now discuss how the analysis allows us to understand the biological mechanisms on a deeper level. In fact, we extend the results regarding the dynamics on the critical manifold to relate them back to the singularly perturbed system (2.5) with $\beta = 0$. In doing this we show that the flow of our singularly perturbed system, restricted to the slow manifold, is a small perturbation of the dynamics covered in the subsystem analysis. Also, the stable and unstable manifolds of the reduced system and the full system can be related by a small perturbation. We refer the reader to Section 2.7 for the details. As discussed in Section 2.7 we conclude that the biological interpretation of the reduced system is also applicable to the full system.

First, we assume $\frac{w(0)}{\sigma u(0)} > 1$ which implies that phosphorus is not limiting. The fast system (2.8) has V_{00} approaching 1. To satisfy the matching conditions we require the slow dynamics to be restricted to M_0^0, initially. M_0^0 is described as the surface where cell quota is maximal, which is biologically consistent with the assumption of sufficient phosphorus. Now, the slow scale dynamics are governed by (2.16) restricted to M_0^0. We have shown that u_{00} approaches a positive equilibrium while w_{00} decreases. Biologically, since there is sufficient phosphorus it is clear that the cyanobacteria will grow, until growth is limited by light. Also, we expect the total phosphorus to decline as it is being exchanged. Eventually, at time t_s, w_{00} will have decreased such that $w_{00} = \sigma u_{00} v_{00}$. This is also the point in time where the flow on M_0^0 intersects

M_0^1. Biologically, we describe this as the point where phosphorus becomes limiting. At t_s the slow dynamics switch and are now governed by (2.16) restricted to M_0^1. We describe manifold M_0^1 as being phosphorus limited, thus, we expect and observe the cyanobacteria collapse. Figure 2.7 shows these dynamics with respect to the manifolds. Figure 2.5 shows these dynamics with respect to time. In other words, Figure 2.5 shows the complete uniform approximation and its relation to the dynamics of the full system (2.5).

Now, if $\frac{w(0)}{\sigma u(0)} < 1$ the dynamics are simpler. This initial condition implies, biologically, that phosphorus will be limited. On the fast time-scale we see V_{00} approach $\frac{w(0)}{\sigma u(0)}$, which is less than the maximal cell quota. This implies nutrient is limiting. However cyanobacteria can still grow, depending on the nutrient limitation compared to the initial condition. To satisfy the matching condition the slow dynamics are restricted to M_0^1, the limited nutrient manifold. There is no switch on the slow time-scale and the cyanobacteria simply decline along with the total phosphorus. Figure 2.7 shows this dynamic with respect to the manifolds and Figure 2.6 compares the uniform approximation to the full system (2.5).

The details in Appendix 2.7 allow us to draw the conclusion that the dynamics of the reduced system are a small perturbation of the dynamics of the full system with $\beta = 0$. Hence, we conclude that the biological interpretation of the reduced system dynamics, described above, is also valid for the dynamics of the full system. Furthermore, we are able to interpret the geometry of the system biologically, leading to a deeper knowledge of cyanobacterial systems.

2.9 Discussion

Cyanobacteria are incredibly common in freshwater ecosystems. In fact, it is rare to encounter a freshwater environment where cyanobacteria are absent. The prevalence of cyanobacteria often has a negative impact on water treatment costs, recreation, and aquatic health. The potential socio-economical impact of cyanobacteria motivates the complete understanding of their dynamics, in particular their short term dynamics. Several papers have successfully gained further insight into algae and cyanobacteria dynamics, (Melina Celeste et al., 2017; Wang et al., 2007; Huisman and Weissing, 1994; Berger et al., 2006; Diehl, Berger, and Wöhrl, 2005), but there is still much more that can be understood. In this chapter we attempt to understand the transient cyanobacteria dynamics for various eutrophic initial states.

We study the previously established and well studied stoichiometric models of Wang et al. (2007) and Berger et al. (2006). The mechanistic structure of the model, as well as the dynamics, lead to a multiple time-scale analysis. We find that δ is a small parameter that acts as a singular perturbation. This is not surprising as δ is proportional to the difference between the maximum and minimum cell quota. The cell quota, Q, measures the phosphorus to carbon ratio inside of a single cell. This ratio is naturally small for almost all living organisms but varies significantly for cyanobacteria (Whitton, 2012). The other two variables, B and R, measure concentrations of cyanobacterial carbon biomass and total phosphorus respectively, which are large compared to the phosphorus to carbon ratio of a single cell. Due to the difference of magnitude between our state variables it is intuitive that the system yields a multi-scale dynamic. Also, we observe in Figure 2.1 abrupt transition layers that were not fully understood. For these reasons an analysis of multiple time

scales is performed.

We have shown that the fast system behaves as follows: both the CB biomass and dissolved phosphorus concentrations are constant, and the cell quota will increase monotonically towards $\min\{1, \frac{w(0)}{\sigma u(0)}\}$. This implies that the P uptake occurs on the fast time-scale, whereas CB growth and nutrient depletion are slower processes.

The slow scale analysis yields an interesting structure of the critical manifolds for system (2.16). The critical manifold can be broken down into to two sub-manifolds, M_0^0 and M_0^1. We interpret M_0^0 as representing the dynamics when nutrient is sufficient, alternatively M_0^1 describes the dynamics when nutrient is insufficient. The two sub-manifolds are hyperbolic everywhere except near their intersection, which is denoted as the curve $\mathcal{C}$. If the initial condition has sufficient nutrient the dynamics will quickly approach M_0^0. On the other hand, when the initial condition has insufficient available phosphorus the dynamics quickly approach M_0^1. When nutrient is sufficient the cell quota is maximal, and the cyanobacteria biomass is high and the CB can grow until phosphorus is depleted or when the dynamics leave M_0^0 by approaching $\mathcal{C}$. When the dynamics, initially with sufficient nutrient, approach $\mathcal{C}$ an abrupt transition must occur to avoid biological violations. This transition is described as a switch in the dynamics from sufficient nutrient to insufficient. This switch is analogous to jump points, or fold points described in the literature (Kuehn, 2015; Hek, 2010). On M_0^1 available phosphorus is insufficient to support a high cyanobacteria biomass forcing a crash of the bloom. This insight is consistent with what is believed to drive cyanobacteria dynamics. That is, it is commonly believed that a more eutrophic state will yield larger CB biomass. Furthermore, light is also crucial in bloom formation, but often

not the limiting resource (Paerl and Otten, 2013; Whitton, 2012; Merel et al., 2013). Biologically, the concept of "sufficient" nutrient for a population has not yet been adequately described. This work can help suggest as to what "sufficient" nutrient means from a mathematical perspective.

Furthermore, the analysis described in Sections 2.4 and 2.5 make it possible to compute an approximation for the biologically relevant switching time discussed in Section 2.6. We describe the switching time, t_s, approximated by (2.38), as the time it takes for the flow to transition from the sufficient phosphorus manifold (M_0^0) to the insufficient phosphorus manifold (M_0^1). Given the interpretation of the sub-manifolds, the computation of t_s allows us to approximate the longevity of a bloom with respect to reasonable model parameter values. In particular, t_s depends on the initial condition for total phosphorus (Figure 2.9), which serves as a proxy for the eutrophic state. Our approximation of bloom longevity is of similar scale to what is observed in real aquatic ecosystems (Taranu et al., 2012).

Finally, we applied the classical results of Neil Fenichel to relate the dynamics of the reduced system (2.16) to the dynamics of the full model (2.5)(See Appendix 2.7) (Hek, 2010; Fenichel, 1979). The reduced system allows us provide a meaningful biological interpretation of the driving mechanisms and Fenichel's theorems show the interpretation is applicable to the full system.

Our model assumes that the input nutrient from the hypolimnion, rivers and runoff is constant. Realistically, the concentrations of inputs are varying and large amounts of phosphorus are suddenly added after rainfall events or spring run off (Paerl and Otten, 2013; Taranu et al., 2012). Interestingly, our model can easily be extended to account for impulsively added phosphorus. Figure 2.10 shows the three year dynamics when considering large, but varying, annual

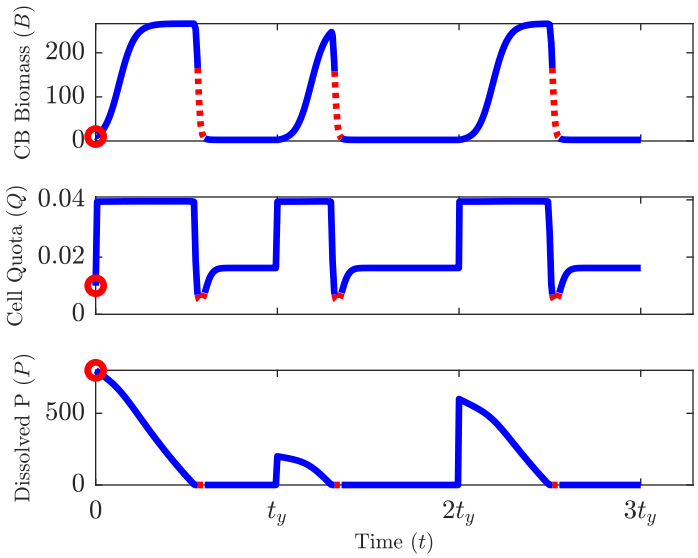

Figure 2.10: Shows the three year dynamics of System (2.4) with varying phosphorus impulses each year (t_y).

inputs of phosphorus. The impulsive model can make for a more realistic long term understanding of the dynamics with respect to the within year transient dynamics. Also, it has been shown that for large values of z_m, CB will not persist (Wang et al., 2007). This illustrates the importance of epilimnion depth in CB dynamics, however we do not consider variations of z_m in this analysis. While our model assumes a stratified lake, many temperate lakes are dimictic or polymictic, meaning stratification is broken occasionally throughout the year (Kalff, 2002), causing complex changes in the CB density and nutrient distribution (Griffith et al., 1973). The factors listed above are important to CB dynamics and should be considered in future work. Although slight changes of our results will occur upon consideration of these factors, we expect that the main driving mechanisms shown here are robust. That is, additional mechanisms will enhance the reality of our model but would still likely act as perturbations of the reduced models (2.8) and (2.16), in which the driving

mechanisms were established.

Our analysis has shed light on the mechanisms driving certain aspects of cyanobacteria dynamics. However, certain aspects are still left to be mathematically explained, namely the non-zero low CB biomass phase seen in Figure 2.1. Our analysis suggests that the CB biomass will tend to zero, which is not true of the full model and generally not true biologically. We suspect that considering the perturbation parameter, β, to be non-zero will allow us to understand this phase of the dynamics. However, analysis of the higher order approximations is not considered here and should be considered in the future.

Cyanobacteria are considered primary producers, thus organisms in higher trophic levels depend directly on CB dynamics. This study helps build a framework to study transient aquatic dynamics in eutrophic conditions. Future work could include the study of symbiotic, predator-prey, and competitive interactions that depend on the cyanobacteria transient dynamics. Furthermore, cyanotoxins are a large global concern that affect agriculture, recreation, water treatment and aquatic organisms. This model can be extended to consider cyanotoxin production and its influences on aquatic interactions.

To our knowledge, analysis of the form in this chapter has not been performed on any stoichiometric model in ecology. These results are important for future work in studying the transient dynamics of cyanobacteria, as well as building a framework to study transient dynamics in other ecological stoichiometry models. Specifically, they are useful to determining the mechanisms that motivate each aspect of the transient dynamics.

Chapter 3

Coupling the social and ecological dynamics of cyanobacteria: single lake and network dynamics

3.1 Introduction

Cyanobacterial harmful algal blooms (CHABs) are an ever present global concern in aquatic environments. The presence of CHABs often leads to several adverse outcomes both ecologically and economically. For example, CHABs can decrease ecosystem productivity by creating anoxic conditions and producing toxins as metabolic byproducts (Orr and Jones, 1998; Kaebernick and Neilan, 2001). Economically, CHABs add costs to water treatment, lower recreational and tourism value, and add risks when using freshwater for agricultural purposes. Although CHABs occur for a variety of reasons they are most commonly a result of eutrophication. Eutrophic conditions occur when an excess amount of nutrients required for organismal growth is in an aquatic ecosystem. Furthermore, eutrophication often occurs as a result of anthropogenic nutrient pollution from agriculture, industrial and urban run-off (Paerl, 2014). In this sense there is a noteworthy connection between anthropogenic nutrient

pollution and economic costs due to CHABs.

The study of systems where human and environmental dynamics are intertwined is beginning to receive more attention in the literature. For example, the importance of linking human and social dynamics to climate models to understand climate trajectories has been addressed (Beckage et al., 2020; Bury, Bauch, and Anand, 2019). Other researchers have used social processes to better understand disease outbreaks (Pedro et al., 2020; Fair et al., 2021). Ecologically, social dynamics have been coupled to forestry, fishery and other common-pool resource models to gain insight towards the balance between sustainable resource use and profit seekers (Satake et al., 2007; Farahbakhsh, Bauch, and Anand, 2021; Lee and Iwasa, 2011; Wang et al., 2016). Socio-ecological mechanisms to support persistent of native species of grasses that are under stress from anthropogenic nitrogen sources and invasive species have also been studied (Thampi, Bauch, and Anand, 2019). Finally, coupled socio-economic and ecosystem models for lake eutrophication have been considered by Iwasa, Uchida, and Yokomizo (2007) and Iwasa, Suzuki-Ohno, and Yokomizo (2010), but do not consider phytoplankton dynamics. In essence, human activities often result in changes in the ecological system, however changes in the ecological system will, in-turn, have an impact on the human behaviours thus creating a feedback loop. These types of systems are thought of as an integration between an ecological system and socio-economic system. Mathematical modelling of such systems typically involves the coupling of an ecological model that has terms dependent on human decisions to a human socio-economic model with outputs dependent on the state of the ecology (Iwasa, Uchida, and Yokomizo, 2007; Satake et al., 2007).

Socio-economic models can be derived by considering social norms and

pressures, monetary costs and psychology associated with the ecological system (Fransson and Gärling, 1999). As is the case in many current environmental issues, social ostracism can occur when an individual does not behave in a way that is environmentally favourable (Poon et al., 2015). Social ostracism occurs when a group or individual excludes or slanders another group or individual based on an action, opinion or response. Psychologically, being ostracised is harmful as humans have a basic want of being accepted (Williams, 2007). As a response to ostracism humans often change behaviour to further avoid ostracism (Williams and Nida, 2011). In the context of environmental issues, such as lake pollution, groups who assume non-environmentally favourable roles are often ostracised more than those that do (Poon et al., 2015; Iwasa, Uchida, and Yokomizo, 2007; Sun and Hilker, 2020) adding costs to the defection role. This means that modelling of socio-economic systems should include factors that account for social pressures. In addition, social norms often influence a person to assume a strategy regardless of its environmental impacts (Kinzig et al., 2013). Social norms are described as the set of rules and behaviours a society deems appropriate and are often established based upon the behaviour of the majority, regardless of any implications. Intrinsically, there exists pressure to adhere to these social norms although it is indirect. Socioeconomic dynamics may be dependent on the frequency of each strategy, and not on the costs alone. Furthermore, the direct social costs due to ostracism and indirect costs due adherence to norms can be non-local and come from distanced social connections. Costs associated with pro-environmental roles often exceed the non-environmentally favourable role. These costs are often monetary and involve the investment in infrastructure to filter or treat urban water run-off. Additionally, lakes with low water quality and persistent

HABs face additional costs associated with decreased land value, recreation, and tourism based on the presence of toxins, and visual and olfactorily unpleasant nature of HABs (Nicholls and Crompton, 2018; Wolf and Klaiber, 2017).

In many cases socio-economic models often have a game-theoretic component in which players choose one of several strategies based on the associated utility differences to the other strategies (Iwasa, Uchida, and Yokomizo, 2007; Farahbakhsh, Bauch, and Anand, 2021; Suzuki and Iwasa, 2009; Iwasa, Suzuki-Ohno, and Yokomizo, 2010; Sun and Hilker, 2020). Each strategy then has an associated disturbance of the ecological system, i.e. high vs. low pollution or deforestation rates. Individuals assume strategies at rates that are dependent on the perceived costs of each strategy, or fitness in game theory literature, and can be modelled in many different forms. For example, the logit best-response dynamics assumes there is a probability an individual assumes a strategy based on associated costs, where as the replicator dynamics assumes that the individual chooses a strategy based on learning it from other individuals and allows for strong conformity (Sun and Hilker, 2021; Farahbakhsh, Bauch, and Anand, 2021; Bury, Bauch, and Anand, 2019; Iwasa, Uchida, and Yokomizo, 2007). By explicitly considering distinct strategies and their associated costs ecosystem managers can use these models to gain insight towards policy implementation to obtain a favourable outcome.

Many phytoplankton models have been used for the study of algal dynamics and take various forms including discrete time models, ODEs and PDES. In this study we extend a stoichiometric model that has been well established in the literature (Heggerud, Wang, and Lewis, 2020; Wang et al., 2007; Berger et al., 2006). Ecological stoichiometry is defined as the study of the balance

of energy and resources in ecological systems (Sterner and Elser, 2002). This is a powerful tool as it allows the study of large scale phenomena, like CB abundance, by considering small scale components like internal energy and nutrients. The use of ecological stoichiometry has become increasingly common because of its ability to mechanistically capture the effects of resource limitations on ecological systems. For example, ecological stoichiometry has been used to study predator prey systems (Mitra and Flynn, 2005; Branco et al., 2018), producer-grazer systems (Wang, Kuang, and Loladze, 2008; Loladze, Kuang, and Elser, 2000), phytoplankton dynamics (Klausmeier, Litchman, and Levin, 2004; Wang et al., 2007), toxicology (Peace et al., 2021) and plant-disease dynamics (Lacroix, Seabloom, and Borer, 2017) with great success. Ecological stoichiometry has been used to discuss the timescale separation between nutrient uptake and both algal growth and available nutrient depletion in Heggerud, Wang, and Lewis (2020). Separation of timescales allowed for the in-depth study of algal transient dynamics and driving mechanisms. This, along with many other studies, has established a solid modelling framework for phytoplankton dynamics (Wang et al., 2007; Berger et al., 2006; Huisman and Weissing, 1994). Additional complexity arises when coupling such ecological models to socio-economic models, both mathematically and in terms of timescales (Hastings, 2016; Hastings, 2010). Human behaviour may change slower than the ecological dynamics and furthermore, the response of the ecological systems to human management strategies may be delayed (Carpenter, 2005; Hastings, 2016).

Phosphorus is commonly considered to be a nutrient of interest in aquatic systems (Carpenter, 2005; Whitton, 2012). Furthermore, the Redfield ratio (C:N:P=106:16:1) (Redfield, 1934) implies that CB demands phosphorus

more than other elements, except perhaps nitrogen (Sterner and Elser, 2002; Whitton, 2012). However, since the demand for phosphorus is high the uptake rates and cell quotas for phosphorus will also be larger than other elements, expect perhaps nitrogen, and thus the corresponding phosphorus dynamics in the media occur on similar timescales to other ecological processes (Whitton, 2012; Heggerud, Wang, and Lewis, 2020). Other nutrients, such as iron, can limit phytoplankton growth in a significant way by limiting photosynthesis, such as the case of peat lakes in the Netherlands (Smolders and Roelofs, 1993) and regions of the Antarctic (Koch et al., 2019). The extended Redfield ratio implies the requirement of iron is much less than phosphorus and as a result cell quota values are small compared to those for phosphorus (Cunningham and John, 2017). This means that the iron dynamics in the media may occur on a different timescale than the remaining ecological dynamics (Wurtsbaugh and Horne, 1983). Thus, the timescale of the ecological dynamics depends on the study species and the nutrient being considered as uptake and growth rates can vary among species and nutrient (Whitton, 2012).

In this chapter we couple the ecological dynamics of cyanobacteria (CB) with the socio-economic dynamics of humans at each lake. We consider a network of lakes which are connected via social interactions only, allowing for presence of social norms and ostracism to influence human decision making. The ecological dynamics are given by extending the well established stoichiometric CB model of (Heggerud, Wang, and Lewis, 2020; Wang et al., 2007). The socio-economic model is an extension of the models discussed in (Iwasa, Uchida, and Yokomizo, 2007; Suzuki and Iwasa, 2009; Iwasa, Suzuki-Ohno, and Yokomizo, 2010; Sun and Hilker, 2020) in which individuals in a population choose to either cooperate by lowering pollution rates, or defect, by

continuing to pollute at higher rates. The individuals choose their strategy based on costs associated with social pressure, concern for CB, tourism and recreation value, and infrastructure investment (Iwasa, Uchida, and Yokomizo, 2007). We fully derive the network model and offer several useful simplifications in Section 4.2. Our analysis begins in Section 3.3 where we consider the coupled dynamics at a single lake. The analysis of the single lake case is done by utilizing the separation in time scales in several different ways, including a phase line analysis for when phosphorus is the polluting nutrient in Section 3.3.1 and phase plane analysis when iron is the polluting nutrient in Section 3.3.2. In each case we observe bistable behaviour and gain insight towards the socio-economic parameter regions that lead to favourable outcomes. Lastly, in Section 3.4, we revisit the network model. We simplify the network model to allow the system to be studied in the restricted phase plane showing three possible equilibria corresponding the low, high, and mixed levels of cooperation regimes throughout the network. Finally, discuss several two-parameter bifurcation plots which highlight under which parameter regions each regime occurs.

3.2 A coupled cyanobacteria-socio-economic network model

In this section we extend a well established CB model (Wang et al., 2007; Heggerud, Wang, and Lewis, 2020; Berger et al., 2006) to account for socio-economic dynamics that alter the amount of anthropogenic nutrient input. The CB model considers three state variables: CB abundance, cell quota, and available nutrient. The socio-economic component tracks the proportion of co-operators given by the best-response dynamics (Iwasa, Uchida, and Yokomizo,

2007). We separately consider phosphorus and iron as the limiting nutrient and introduce the phosphorus in this section. Several approximations of certain mechanistic modelling components are provided to aid in later analysis. We assume that several distinct lakes are connected via social connections, due the presence of social communication. Each individual in the network assumes one of two strategies, cooperation or defection denoted with $\mathcal{C}$ and $\mathcal{D}$, respectively. Locally, each strategy will face costs associated with the abundance of CB but only defectors will face a cost associated with social ostracism. In addition, we assume that each strategy faces a societal cost from the lake network that is proportional to the frequency of players of opposing strategies, this is referred to as a network social norm cost.

We now couple a socio-economic model (Iwasa, Uchida, and Yokomizo, 2007; Iwasa, Suzuki-Ohno, and Yokomizo, 2010) a stoichiometric phytoplankton model (Wang et al., 2007; Heggerud, Wang, and Lewis, 2020; Berger et al., 2006) yielding

$$\begin{cases} \dfrac{dB_i}{dt} = rB_i(1-\dfrac{Q_m}{Q_i})h(B_i) - \nu_r B_i - \dfrac{D}{z_e}B_i, \\ \dfrac{dQ_i}{dt} = \rho(Q_i,P_i) - rQ_i(1-\dfrac{Q_m}{Q_i})h(B_i), \\ \dfrac{dP_i}{dt} = \dfrac{D}{z_e}(I(F_i(t)) - P_i) - B_i\rho(P_i,Q_i), \\ \dfrac{dF_i}{dt} = r_{i,\mathcal{DC}}(F_i,B_i)(1-F_i) - r_{i,\mathcal{CD}}(F_i,B_i)F_i, \end{cases} \tag{3.1}$$

where B_i, Q_i, P_i and F_i represent the concentration of CB carbon biomass, the internal phosphorus to carbon nutrient ratio (cell quota), dissolved mineral phosphorus and the frequency of cooperators, respectively at lake i. The functions $h(B)$ and $\rho(Q,P)$ represent the light dependent growth of CB and phosphorus uptake, respectively. Both functions follow the form of (Heggerud,

Wang, and Lewis, 2020; Wang et al., 2007) with

$$h(B) = \frac{1}{z_m}\int_0^{z_m} \frac{I_{in}\exp[-(K_{bg}+kB)s]}{H + I_{in}\exp[-(K_{bg}+kB)s]}ds$$
$$= \frac{1}{z_m(K_{bg}+kB)}\ln\left(\frac{H+I_{in}}{H+I_{in}\exp[-(K_{bg}+kB)z_m]}\right), \quad (3.2)$$

and

$$\rho(Q,P) = \rho_m \frac{Q_M - Q}{Q_M - Q_m}\frac{P}{M+P}. \quad (3.3)$$

The anthropogenic phosphorus addition is given as

$$I(F_i(t)) = p_{i,\mathcal{D}}(1 - F_i(t)) + p_{i,\mathcal{C}}F_i(t), \quad (3.4)$$

where $p_{i,\mathcal{C}}$ and $p_{i,\mathcal{D}}$ are the phosphorus input concentrations of the cooperators and defectors, respectively, with $p_{i,\mathcal{C}} \leq p_{i,\mathcal{D}}$.

The derivation of $h(B)$ is based on sound principles and assumptions of algal growth rates and light attenuation via the Lambert-Beer law. However, as with many other mathematical models, approximations of complex but meaningful functions can prove useful in analysis. We note that the key features of $h(B)$ are that it is monotone decreasing and that $\lim_{B\to\infty} h(B) = 0$. Thus, we assume that $h(B)$ is sufficiently approximated as follows:

$$h(B) \approx h_{app}(B) = \frac{1}{\tilde{a}B + \tilde{b}}, \quad (3.5)$$

where $\tilde{a}$ and $\tilde{b}$ are values such that $h(B) = h_{app}(B)$ for $B = 0$ and $B = 1/kz_m$ and are given as $\tilde{b} = 1/h(0)$ and $\tilde{a} = \frac{kz_m}{h(1/kz_m)} - \frac{kz_m}{h(0)}$. The comparison of $h(B)$ and $h_{app}(B)$ is given in Figure 3.1

Many previous studies have established socio-economic dynamics based upon cost functions (Iwasa, Uchida, and Yokomizo, 2007; Iwasa, Suzuki-Ohno, and Yokomizo, 2010; Sun and Hilker, 2021; Farahbakhsh, Bauch, and Anand, 2021; Satake et al., 2007). We extend these results to suit our model in the

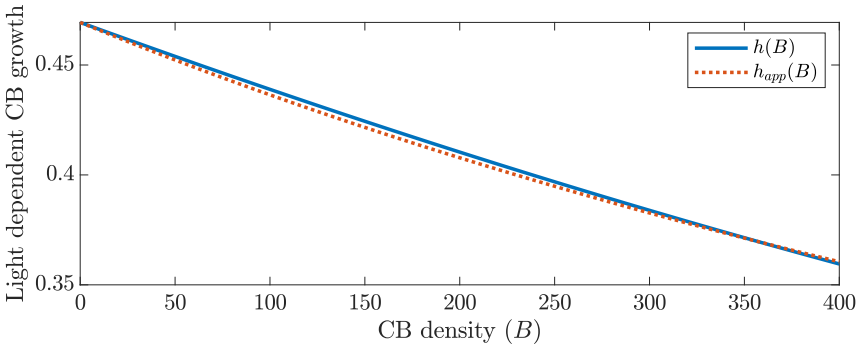

Figure 3.1: Light dependent growth function, $h(B)$, and its approximation, $h_{app}(B)$ given by (3.5).

following fashion. Let $C_{i,\mathcal{C}}(B_i)$ and $C_{i,\mathcal{D}}(F_i, B_i)$ denote the cost associated with each strategy at lake i. Each strategy has an associated baseline cost, $c_{i,\mathcal{C}}$ and $c_{i,\mathcal{D}}$ with $c_{i,\mathcal{C}} > c_{i,\mathcal{D}}$. Both strategies also face a 'recreational' cost associated with the abundance of CB. Defectors face an additional cost of social ostracism that increases with CB abundance and the frequency of cooperators. Additionally, each strategy faces a network social norm cost that is proportional to the connectivity to each lake in the network and frequency of players of opposing strategy at that lake. The costs faced by the defector and cooperator are given respectively by

$$C_{i,\mathcal{D}}(F_i, B_i) = \underbrace{c_{i,\mathcal{D}}}_{\text{baseline cost}} + \alpha \underbrace{(1 + \xi F_i)}_{\text{ostracism}} \underbrace{\psi B_i}_{\text{concern for CB}} + \underbrace{\phi B_i}_{\text{cost of CB}} + \underbrace{d_{\mathcal{D}} \bar{F}}_{\text{social norm pressure}}, \tag{3.6}$$

$$C_{i,\mathcal{C}}(B_i) = c_{i,\mathcal{C}} + \phi B_i + \underbrace{d_{\mathcal{C}}(1 - \bar{F})}_{\text{social norm pressure}}, \tag{3.7}$$

where $\bar{F} = \dfrac{\sum_j d_{ji} F_j(t)}{\sum_j d_{ji}}$ is the weighted average of the frequency of cooperators in the network. Further assume that the actual cost of each strategy is stochastic with a known cost and a random cost, given by $U_{\mathcal{C}} = C_{\mathcal{C}} + \epsilon_{\mathcal{C}}$

and $U_{\mathcal{D}} = C_{\mathcal{D}} + \epsilon_{\mathcal{D}}$. Since we are considering $\epsilon_{\mathcal{C}}$ and $\epsilon_{\mathcal{D}}$ to be additional random costs, their maximum values are of most interest. Thus, we assume that $\epsilon_{\mathcal{C}}$ and $\epsilon_{\mathcal{D}}$ follow the extreme value (Gumbel) distribution. Conveniently, the difference between two extreme value distributed random variables follows a logistic distribution (Hofbauer and Sigmund, 2003). That is, $\epsilon_d = \epsilon_{\mathcal{C}} - \epsilon_{\mathcal{D}} \sim$ Logistic$(0, \frac{1}{\beta})$ with CDF $\dfrac{1}{1+e^{-\beta x}}$. Thus, when a player evaluates their strategy they will defect with probability $P_{\mathcal{D}} = P(U_{\mathcal{D}} < U_{\mathcal{C}}) = P(\epsilon_{\mathcal{D}} - \epsilon_{\mathcal{C}} < C_{\mathcal{C}} - C_{\mathcal{D}})$ (or cooperate with probability $P_{\mathcal{C}} = P(U_{\mathcal{D}} > U_{\mathcal{C}}) = P(\epsilon_{\mathcal{D}} - \epsilon_{\mathcal{C}} > C_{\mathcal{C}} - C_{\mathcal{D}})$) given by the logistic distribution.

Finally, the rate of switching is given as the probability of choosing a strategy, multiplied by the rate at which one evaluates their strategy:

$$r_{i,\mathcal{DC}}(F_i, B_i) = \frac{s}{1 + e^{\beta[C_{i,\mathcal{C}}(B_i) - C_{i,\mathcal{D}}(F_i, B_i)]}}, \tag{3.8}$$

$$r_{i,\mathcal{CD}}(F_i, B_i) = \frac{s}{1 + e^{\beta[C_{i,\mathcal{D}}(F_i, B_i) - C_{i,\mathcal{C}}(B_i)]}}, \tag{3.9}$$

where s is the level of conservatism of the population interpreted as the rate at which a player evaluates their strategy. If s is small the population switches strategies infrequently. β is a parameter controlling the level of stochasticity. Large β means the population deterministically chooses a strategy based on cost, whereas a small β will make the switching more random as seen in Figure 3.2. Furthermore, the last equation in (3.1) can be written as

$$r_{i,\mathcal{DC}}(F_i, B_i)(1 - F_i) - r_{i,\mathcal{CD}}(F_i, B_i)F_i = r_{i,\mathcal{DC}}(F_i, B_i) - sF_i. \tag{3.10}$$

The switching rates described in (3.8) and (3.9) arrive from a sound derivation and are quite intuitive and often referred to as the logit best-response model for choice probabilities. However, as previously discussed the approximation of complex functions by mathematically tractable functions is an incredibly

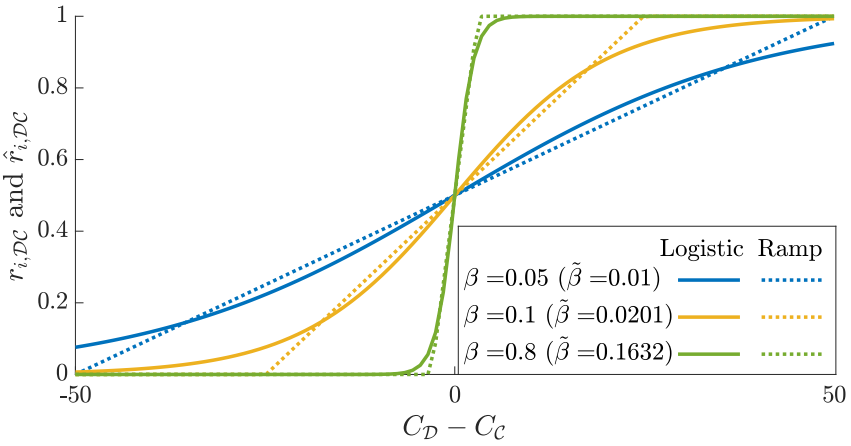

Figure 3.2: Shows the comparison of the logistic function (given in (3.8)) and the approximating ramp function in (3.12) for various values of β and the corresponding $\tilde{\beta}$ values. We take $s = 1$ here.

useful tool. For this reason we note that the logistic function ($\frac{1}{1+e^{\beta x}}$) is readily approximated by the ramp function

$$\frac{1}{1+e^{-\beta x}} \approx \begin{cases} 0 & x \leq -c^*, \\ \frac{1}{2} + \tilde{\beta} x & -c^* \leq x \leq c^*, \\ 1 & c^* \leq x, \end{cases} \tag{3.11}$$

where $c^* = \frac{1}{2\tilde{\beta}}$ and $\tilde{\beta}$ is a parameter found by minimising $\mathcal{L}^1$ norm of the difference between the two functions for a given value of β. Thus, $r_{i,\mathcal{DC}}(F_i, B_i)$ is approximated by

$$\hat{r}_{i,\mathcal{DC}}(F_i, B_i) = s \cdot \begin{cases} 0 & 1/2 + \tilde{\beta}(C_{i,\mathcal{D}} - C_{i,\mathcal{C}}) \leq 0, \\ 1/2 + \tilde{\beta}(C_{i,\mathcal{D}} - C_{i,\mathcal{C}}) & 0 < 1/2 + \tilde{\beta}(C_{i,\mathcal{D}} - C_{i,\mathcal{C}}) < 1, \\ 1 & 1 \leq 1/2 + \tilde{\beta}(C_{i,\mathcal{D}} - C_{i,\mathcal{C}}). \end{cases} \tag{3.12}$$

Further, the piecewise function can be equivalently written as

$$\hat{r}_{i,\mathcal{D},\mathcal{C}}(F_i, B_i) = s \cdot \max\{0, \min\{1, \frac{1}{2} + \tilde{\beta}(C_{i,\mathcal{D}} - C_{i,\mathcal{C}})\}\}. \tag{3.13}$$

The difference between $r_{i,\mathcal{DC}}(F_i, B_i)$ and $\hat{r}_{i,\mathcal{DC}}(F_i, B_i)$ is shown in Figure 3.2.

The parameters and their values corresponding to the ecological components of model (3.1) are summarized in Table 3.1. In-depth discussion and de-

scriptions of the ecological parameters can be found in (Heggerud, Wang, and Lewis, 2020; Wang, Kuang, and Loladze, 2008) and the references therein. The parameters corresponding to the socio-economic dynamics are summarized in Table 3.2 and are taken from the ranges in (Iwasa, Uchida, and Yokomizo, 2007) and are justified by arguing a comparable scale of all terms in (3.6) and (3.7).

Table 3.1: Definitions and values for ecological parameters of system (3.1). References to parameter values can be found in (Diehl, Berger, and Wöhrl, 2005; Whitton, 2012; Berger et al., 2006).

Par.	Meaning	Value	Biological Values
r	Maximum CB specific production rate	1	1 $/day$
Q_m	CB cell quota at which growth ceases (minimum)	0.004	0.004 gP/gC
Q_M	CB cell quota at which nutrient uptake ceases (maximum)	0.04	0.04 gP/gC
z_m	Depth of epilimnion	7	$> 0 - 10m$
ν_r	CB respiration loss rate	0.35	0.05-0.6 $/day$
D	Water exchange rate	0.02	m/day
H	Half saturation coefficient of light-dependent CB production	120	120 $\mu mol/(m^2 \cdot s)$
ρ_m	Maximum CB phosphorus uptake rate	1	0.2-1 $gP/gC/day$
M	Half saturation coefficient for CB nutrient uptake	1.5	1.5 mgP/m^3
K_{bg}	Background light attenuation	0.3	0.3-0.9 $/m$
k	Algal specific light attenuation	0.0004	0.0003-0.0004 m^2/mgC
I_{in}	Light intensity at water surface	300	300 $\mu mol/(m^2 \cdot s)$

Table 3.2: Definitions and values for the socio-economic parameters of system (3.1)

Par.	Meaning	Value	Units
$p_{i,\mathcal{C}}$	Concentration of influx of dissolved inorganic phosphorus for strategy $\mathcal{C}$.	50	mgP/m^3
$p_{i,\mathcal{D}}$	Concentration of influx of dissolved inorganic phosphorus for strategy $\mathcal{C}$.	770	mgP/m^3
s	Rate players make a decision to change strategies.	0.001	day^{-1}
β	Level of determinism in changing strategies.	0.1	$(\text{cost unit})^{-1}$
$\tilde{\beta}$	Slope of approximated line in (3.11)	0.0201	$(\text{cost unit})^{-1}$
$c_{i,\mathcal{C}}$	Baseline cost to cooperate.	50	(cost unit)
$c_{i,\mathcal{D}}$	Baseline cost to defect.	1	(cost unit)
ϕ	Cost conversion coeff. for CB	10	$(\text{cost unit})/mgC/m^3$
α	Cost conversion for social pressure due to CB	3	(cost unit)
ξ	Strength of frequency dependence for social pressure	10	$-$
ψ	Level of social concern for CB	0.02	$(mgC/m^3)^{-1}$
d_{ji}	connectedness of lake j to i.	-	-
$d_{\mathcal{D}}$	Cost conversion coeff. of social norms for defecting.	1	(cost unit)
$d_{\mathcal{C}}$	Cost conversion coeff. of social norms for cooperating.	1	(cost unit)

3.3 Dynamics of a single lake model

In this section we consider the single lake version of model (3.1) where the external network pressure is treated as a constant. We separately consider the dynamics under phosphorus limitation and iron limitation, proceeding with

a phase line and phase plane analysis, respectively. In each case bistability scenarios arise and bifurcation results are obtained.

In this chapter we assume that when considering phosphorus almost all ecological processes occur on a fast time scale, thus the QSSA reduces the model to a single equation that represents the human dynamics on the slow timescale. When iron is considered, only the cell quota and CB dynamics occur on the fast time scale thus, the QSSA reduces the model to two differential equations on the slow timescale that represent the human and available iron dynamics. Hence, two types of analysis are performed. First, we consider a phase line analysis for the phosphorus system in Section 3.3.1. Second, we perform a phase plane analysis for the iron system in Section 3.3.2

To start, assume that all other lakes are in a fixed state allowing us to drop the subscript i. Thus the cost difference $C_{\mathcal{C}} - C_{\mathcal{D}} = c_{\mathcal{C}} - c_{\mathcal{D}} - \alpha(1+\xi F)\psi B + d_{\mathcal{C}}(1-\bar{F}) - d_{\mathcal{D}}\bar{F}$ can be written as $c_C - c_{\mathcal{D}} - \alpha(1+\xi F)\psi B + \hat{\delta}$, where $\hat{\delta}$ is treated as a parameter. In this section we study the following model:

$$\begin{cases} \dfrac{dB}{dt} = rB(1-\dfrac{Q_m}{Q})h(B) - \nu_r B - \dfrac{D}{z_e}B, \\ \dfrac{dQ}{dt} = \rho(Q,P) - rQ(1-\dfrac{Q_m}{Q})h(B), \\ \dfrac{dP}{dt} = \dfrac{D}{z_e}(I(F(t)) - P) - B\rho(P,Q), \\ \dfrac{dF}{dt} = r_{\mathcal{DC}}(F,B)(1-F) - r_{\mathcal{CD}}(F,B)F = \dfrac{s}{1+e^{\beta(C_{\mathcal{C}}-C_{\mathcal{D}})}} - sF. \end{cases} \tag{3.14}$$

3.3.1 Dynamics of the phosphorus explicit model

In this section we simplify system (3.14) and use parameter values given for the phosphorus system in Tables 3.1 and 3.2. The simplifications lead to a single differential equation that is analyzed on the phase line to gain in-

depth understanding of the single lake dynamics and the bistable nature of the system.

Nondimensionalization of the single lake model

We begin by nondimensionalizing system (3.14) by letting $\tau = rt$, $u = kz_m B$, $v = \frac{Q}{Q_M}$, $w = \frac{P}{M}$, and F remains unchanged as F is dimensionless by definition. Making these substitutions into system (3.14) yields:

$$\begin{cases} \dfrac{du}{d\tau} = u(1 - \dfrac{Q_m}{Q_M}\dfrac{1}{v})h(au) - \dfrac{(\nu_r + \frac{D}{z_e})}{r}u \\ \dfrac{dv}{d\tau} = \dfrac{\rho_m}{rQ_M}\dfrac{Q_M - Q_M v}{Q_M - Q_m}\dfrac{w}{1+w} - (v - \dfrac{Q_m}{Q_M})h(au), \\ M\dfrac{dw}{d\tau} = \dfrac{D}{rz_e}(p_C F + p_D(1-F) - Mw) - \dfrac{\rho_M}{rkz_e}u\dfrac{Q_M - Q_M v}{Q_M - Q_m}\dfrac{w}{1+w}, \\ \dfrac{dF}{d\tau} = \dfrac{s}{r}\left(\dfrac{1}{1 + e^{\beta(c_C - c_D - \alpha(1+\xi F)\psi au + \hat{\delta})}} - F\right). \end{cases} \tag{3.15}$$

Upon substitution of the nondimensional parameters given in Table 3.3 we have:

$$\begin{cases} \dfrac{du}{d\tau} = u(1 - \dfrac{1}{\gamma}\dfrac{1}{v})\hat{h}(u) - (\epsilon\beta_1 + \beta_2)u \\ \dfrac{dv}{d\tau} = \omega(1-v)\dfrac{w}{1+w} - (v - \dfrac{1}{\gamma})\hat{h}(u), \\ \dfrac{dw}{d\tau} = \epsilon(\kappa_1 F - \beta_1 w) + \kappa_2(1-F) - \lambda u(1-v)\dfrac{w}{1+w}, \\ \dfrac{dF}{d\tau} = \epsilon\left(\dfrac{1}{1 + e^{\eta - \sigma(1+\xi F)u)}} - F\right), \end{cases} \tag{3.16}$$

where

$$\hat{h}(u) = \frac{1}{u + k_1}\log\left(\frac{1+I}{1 + I\exp(-u - k_1)}\right), \tag{3.17}$$

is the non-dimensional light dependent growth term from (3.2) and its nondimensional approximation stemming from (3.5) is given as

$$\hat{h}(u) \approx \hat{h}_{app}(u) = \frac{1}{au + b}, \tag{3.18}$$

where $b = 1/\hat{h}(0)$ and $a = \frac{1}{\hat{h}(1)} - b$.

Table 3.3: Dimensionless parameters for system (3.16) and equation (3.27).

Parameter	Definition	Value
β_1	$\frac{D}{sz_m}$	0.2857
β_2	ν_r/r	0.35
ω	$\frac{\rho_m}{r(Q_M - Q_m)}$	5.556
γ	$\frac{Q_M}{Q_m}$	10
κ_1	$\frac{p_C}{M}\beta_1$	9.5238
κ_2	$\frac{p_D}{M}\frac{D}{rz_m}$	1.4667
λ	$\frac{Q_M}{Q_M - Q_m}\frac{\rho_m}{Mrkz_m}$	52.9
k_1	$z_m K_{bg}$	2.1
I	I_{in}/H	2.5
η	$\beta(c_C - c_D + \hat{\delta})$	-5 to 7
$\hat{\eta}$	$\tilde{\beta}(c_C - c_D + \hat{\delta})$	-1 to 1.5
σ	$\alpha\beta\psi/kz_m$	2.1429
$\hat{\sigma}$	$\alpha\tilde{\beta}\psi/kz_m$	0.4307
ϵ	s/r	<0.01

Application of the quasi steady state approximation

We now further reduce the model by utilizing the QSSA. The nondimensional system (3.16) contains the parameter $\epsilon = s/r$, where s is given as the rate at which players reevaluate strategies and r is the maximal growth rate of CB. The rate at which players are able to reevaluate their strategy is very small in comparison to many ecological processes. Here we assume that the ecological dynamics of the CB occur on the order of days or weeks, whereas the social dynamics, or the maximum rate a player can switch strategies, is on the order of several months, or years. Thus, ϵ is a small parameter.

By re-scaling time with the small parameter ϵ in system (3.16) we apply the QSSA. We introduce a new time scale $\tilde{\tau} = \epsilon\tau$ creating a slow time scale. The time scale $\tilde{\tau}$ is the slow timescale in which the human (F) dynamics occur, while τ is the fast timescale where most of the ecological dynamics occur. We note that certain aspects of the ecological dynamics such as water exchange rates can also occur on the slow timescale. Upon re-scaling time to $\tilde{\tau}$ we arrive at the following system:

$$\begin{cases} \epsilon\dfrac{du}{d\tilde{\tau}} = u(1-\dfrac{1}{\gamma v})\hat{h}(u) - (\epsilon\beta_1 + \beta_2)u, \\ \epsilon\dfrac{dv}{d\tilde{\tau}} = \omega(1-v)\dfrac{w}{1+w} - (v-\dfrac{1}{\gamma})\hat{h}(u), \\ \epsilon\dfrac{dw}{d\tilde{\tau}} = \epsilon(\kappa_1 F - \beta_1 w) + \kappa_2(1-F) - \lambda u(1-v)\dfrac{w}{1+w}, \\ \epsilon\dfrac{dF}{d\tilde{\tau}} = \epsilon\dfrac{1}{1+e^{\eta-\sigma(1+\xi F)u)}} - \epsilon F. \end{cases} \tag{3.19}$$

Now, by the QSSA, which assumes that the fast dynamics are in an equilibrium state, and letting ϵ go to zero we arrive at the differential algebraic system:

$$\begin{cases} \dfrac{dF}{d\tilde{\tau}} = \dfrac{1}{1+e^{\eta-\sigma(1+\xi F)u}} - F, & \text{(3.20a)} \\ 0 = \kappa_2(1-F) - \lambda u(1-v)\dfrac{w}{1+w}, & \text{(3.20b)} \\ 0 = u(1-\dfrac{1}{\gamma v})\hat{h}(u) - \beta_2 u, & \text{(3.20c)} \\ 0 = \omega(1-v)\dfrac{w}{1+w} - (v-\dfrac{1}{\gamma})\hat{h}(u). & \text{(3.20d)} \end{cases}$$

Denote $u^*(F)$ as the solution to the algebraic system (3.20b)-(3.20d). The following theorem ensures that there is a unique solution to the algebraic system for the given parameter values.

Theorem 3.1. *There exists a unique positive solution to the algebraic system defined by equations* (3.20b) *to* (3.20d) *if* $(1-\frac{1}{\gamma})\hat{h}(\frac{\omega\kappa_2(1-F)}{\beta_2\lambda}) - \beta_2 > 0$.

Proof. First, by multiplying equation (3.20b) by ω/λ and adding equation (3.20c) multiplied by v and equation (3.20d) multiplied by u we arrive at the equation:

$$0 = \frac{\omega}{\lambda}\kappa_2(1-F) - \beta_2 uv, \tag{3.21}$$

$$\iff u = \frac{\omega\kappa_2(1-F)}{\beta_2\lambda v} = G(v). \tag{3.22}$$

Substituting $u = G(v)$ into equation (3.20c) divided by u gives

$$0 = (1 - \frac{1}{\gamma v})\hat{h}(G(v)) - \beta_2 = S(v). \tag{3.23}$$

$G(v)$ is a decreasing function of v and furthermore, recall that $\hat{h}(u) = \frac{1}{u+k_1}\log\left(\frac{1+I}{1+I\exp(-u-k_1)}\right)$ is a decreasing function of u, by construction. Thus, $S(v)$ is a strictly increasing function of v which guarantees uniqueness. Now, by construction of the biological system, $v \in [\frac{1}{\gamma}, 1]$ and $S(1/\gamma) < 0$. Thus, if $S(1) = (1 - \frac{1}{\gamma})h(\frac{\omega\kappa_2(1-F)}{\beta_2\lambda}) - \beta_2 > 0$ then by the intermediate value theorem a solution to (3.23) exists. Lastly, equations (3.20b) and (3.20d) yield linear equations in w ensuring uniqueness.

□

Remark 3.2. *Theorem 3.1 also applies when using $\hat{h}_{app}(u)$ in place of $\hat{h}(u)$. The condition for existence and uniqueness of a positive solution remains the same and an explicit form of $u^*(F)$ can be obtained.*

Remark 3.3. *When the condition in Theorem 3.1 is not satisfied a unique trivial solution can only exist when $F = 1$. Otherwise, no positive solution exists.*

An approximation for the cyanobacteria abundance

In this Subsection we explicitly compute $u^*(F)$ by utilizing the previously established approximation for $\hat{h}(u)$, given in (3.18), and solving (3.20b)-(3.20d).

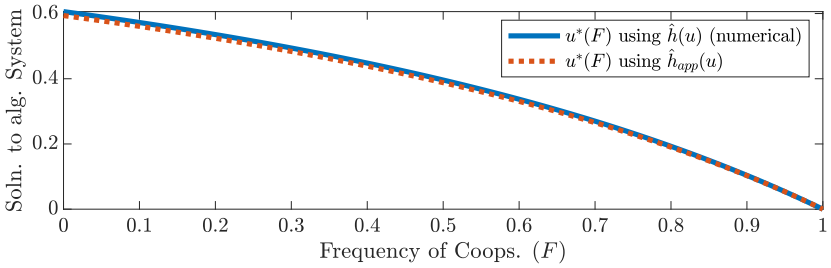

Figure 3.3: Comparison of the approximation given by (3.25) and the numerical solution for $u^*(F)$

Without approximations or simplifications the unique positive solution to (3.20b)-(3.20d) is verified to exist by Theorem 3.1 but can only be implicitly given.

Proceeding, from equation (3.22):

$$v = \frac{\omega\kappa_2(1-F)}{\lambda\beta_2 u} = p_1\frac{(1-F)}{u}. \tag{3.24}$$

We explicitly solve for $u^*(F)$ by utilizing the approximation for $\hat{h}(u)$ given by $\hat{h}_{app}(u)$ in (3.18), using v as in (3.24), and solving (3.20c) for u gives

$$u^*(F) = \frac{\gamma p_1(1-\beta_2 b)(1-F)}{\beta_2 a\gamma p_1(1-F)+1} = \frac{a_1(1-F)}{a_2(1-F)+1}, \tag{3.25}$$

where $a_1 = \gamma p_1(1-\beta_2 b) > 0$ and $a_2 = \beta_2 a\gamma p_1 > 0$.

Remark 3.4. *As shown in Figure 3.3 the explicit version of* $u^*(F)$*, as in* (3.25)*, is a reasonable approximation to the numerical solution of* (3.20b)-(3.20d)*. Note that both solutions give* $u^*(1) = 0$*. However, in reality even with 100% cooperation we would predict a small but non-zero CB abundance due to the non-zero pollution rate of the cooperators. In our QSSA this term* ($\kappa_1 F$) *disappears, and is hence essentially deemed negligible resulting in* $u^*(1) = 0$*.*

A simplifying approximation for the governing differential equation

We now apply the approximation discussed in (3.13) to (3.20a) to solve for equilibrium values. From Section 3.3.1 we obtained an explicit approximation

of the solution to the algebraic system (3.20b)-(3.20d) given by (3.25). Thus, the entire system (3.20) is reduced to the following equation:

$$\frac{dF}{d\tilde{\tau}} = \frac{1}{1 + e^{\eta - \sigma(1+\xi F)u^*(F)}} - F, \tag{3.26}$$

where $u^*(F)$ is given by (3.25). We further simplify (3.26) by using the nondimensionalized version of the approximation given in (3.13). Thus, (3.26) is approximated by

$$\frac{dF}{d\tilde{\tau}} = \max\left\{0, \min\left\{1, \frac{1}{2} - \hat{\eta} + J(F)\right\}\right\} - F, \tag{3.27}$$

where

$$J(F) = \hat{\sigma}(1 + \xi F)u^*(F) = \hat{\sigma}(1 + \xi F)\frac{a_1(1-F)}{a_2(1-F)+1}, \tag{3.28}$$

and the remaining nondimensional parameters are given in Table 3.3.

Equilibrium and phase line analysis of the simplified single lake phosphorus model

Here we discuss the possible equilibrium, their stability and bifurcation structure of equation (3.27) with respect to the parameter $\hat{\eta}$. Equation (3.27) has four possible steady state solutions given by $F_l^* = 0, F_1^* = 1, F_h^*$, and F_u^* where F_h^* and F_u^* are internal equilibrium given by the solution to $J(F) = F + \hat{\eta} - 1/2$. The analysis is supplemented graphically in Figure 3.5 where intersections of the nonlinear curve $J(F)$ with the linear curve $F + \hat{\eta} - 1/2$ for various values of $\hat{\eta}$ represent the equilibria. Furthermore the structure of the equilibrium is shown in a bifurcation diagram (see Figure 3.4) where three critical values of $\hat{\eta}$ are highlighted. By (3.27) an internal equilibrium must satisfy the equation

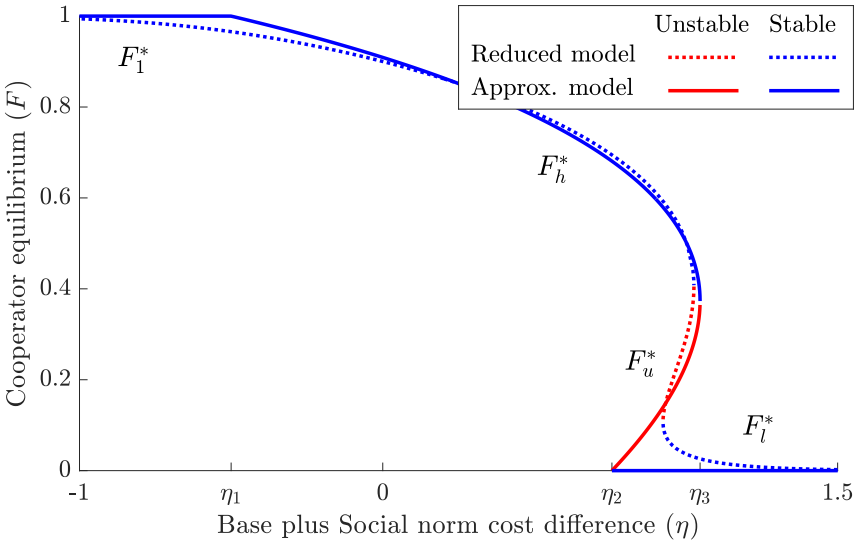

Figure 3.4: Solid line: Bifurcation plot of equilibria solutions to the approximated model (3.27) with respect to $\hat{\eta}$. Dotted line: Bifurcation plot of the reduced model (3.26) with η values scaled to $\hat{\eta}$ values. Note the two plots are qualitatively similar other than F_l^* is small but non zero and F_1^* does not exist in the full model and is explained in Remark 3.8.

$J(F) = F + \hat{\eta} - 1/2$ for some $F \in [0, 1]$.

$$J(F) = F + \hat{\eta} - 1/2, \tag{3.29}$$

$$\iff 0 = -F + 1/2 - \hat{\eta} + \hat{\sigma}(1 + \xi F)\frac{a_1(1-F)}{a_2(1-F)+1}, \tag{3.30}$$

$$= (1/2 - \hat{\eta} - F)(a_2(1-F)+1) + \sigma(1+\xi F)(a_1(1-F)), \tag{3.31}$$

$$= F^2(a_2 - \sigma a_1 \xi) + F(\sigma a_1(\xi - 1) - 1 - a_2 - a_2(1/2 - \hat{\eta})) + \sigma a_1 + (1/2 - \hat{\eta})(a_2 + 1), \tag{3.32}$$

for some $F \in [0, 1]$. The solutions to this equation are shown graphically in Figure 3.5b as the intersections of the curve $J(F)$ with $F + \hat{\eta} - 1/2$. Let Δ

denote the discriminant of (3.32). Then

$$\Delta = \left[\sigma a_1(\xi - 1) - 1 - a_2 - a_2(\frac{1}{2} - \hat{\eta}))\right]^2 - 4(a_2 - \sigma a_1 \xi)\left(\sigma a_1 + (\frac{1}{2} - \hat{\eta}) + a_2(\frac{1}{2} - \hat{\eta})\right), \tag{3.33}$$

$$= a_2^2(\frac{1}{2} - \hat{\eta})^2 + \hat{B}(\frac{1}{2} - \hat{\eta}) + \hat{C}, \tag{3.34}$$

where $\hat{B} = [2\,a_2\,(a_2 - a_1\,\sigma\,(\xi - 1) + 1) - (a_2 + 1)\,(4\,a_2 - 4\,a_1\,\sigma\,\xi)]$ and $\hat{C} = (a_2 - a_1\,\sigma\,(\xi - 1) + 1)^2 - a_1\,\sigma\,(4\,a_2 - 4\,a_1\,\sigma\,\xi)$. Two solutions to (3.29) exist when $\Delta > 0$ however, since Δ is given as a quadratic function in $1/2 - \hat{\eta}$, Δ is not positive everywhere for all values of $\hat{\eta}$. Note that for the given parameter values $B^2 - 4a_2^2\hat{C} > 0$, thus $\Delta = 0$ has two solutions given by

$$\hat{\eta}_{3,4} = -\left(\frac{-\hat{B} \pm \sqrt{\hat{B}^2 - 4a_2^2\hat{C}}}{2a_2^2}\right) + \frac{1}{2}, \pm 4\sqrt{-a_1\,\sigma\,(a_2 - a_1\,\sigma\,\xi)\,(a_2 + \xi + a_2\,\xi)}$$

$$= \frac{-\,2\,a_2 - {a_2}^2 + 2\,a_1\,a_2\,\sigma + 4\,a_1\,\sigma\,\xi + 2\,a_1\,a_2\,\sigma\,\xi}{2\,{a_2}^2}, \tag{3.35}$$

where $a_1\,\sigma\,\xi - a_2 > 0$ for our parameter region. Numerically we have $\hat{\eta}_3 = 1.0464$ and $\hat{\eta}_4 = 32.3$. Thus, if $\hat{\eta} < \hat{\eta}_3$ two solutions exist to (3.32). Also, if $\hat{\eta} > \eta_4$ two solutions to (3.32) exist, but the solutions are values of F that are much greater than one and are not considered. These solutions occur for values of F that exceed the vertical asymptote of $J(F)$. Thus, we conclude that $\eta < \eta_3$ is a necessary condition for solutions to (3.29) to be in $[0, 1]$ and that the solutions are given by

$$F_h^* = \frac{3\,a_2 - 2\,a_2\,\hat{\eta} + 2\,a_1\,\sigma - 2\,\sqrt{\Delta} - 2\,a_1\,\sigma\,\xi + 2}{4\,(a_2 - a_1\,\sigma\,\xi)}, \tag{3.36}$$

$$F_u^* = \frac{3\,a_2 - 2\,a_2\,\hat{\eta} + 2\,a_1\,\sigma + 2\,\sqrt{\Delta} - 2\,a_1\,\sigma\,\xi + 2}{4\,(a_2 - a_1\,\sigma\,\xi)}, \tag{3.37}$$

with $F_h^* > F_u^*$. Furthermore,

$$\frac{dF_u^*}{d\hat{\eta}} = -\frac{-a_2 + \frac{\frac{d\Delta}{d\hat{\eta}}}{2\sqrt{\Delta}}}{2\ (a_1\,\sigma\,\xi - a_2)}. \tag{3.38}$$

When $\hat{\eta} < \hat{\eta}_3$, $\frac{d\Delta}{d\hat{\eta}} < 0$ since Δ is a concave up quadratic and $\hat{\eta}_3$ is the left root. Thus it is easily verified that $\dfrac{dF_u^*}{d\hat{\eta}} > 0$ when $\hat{\eta} < \hat{\eta}_3$.

Observe that

$$\frac{dF_h^*}{d\hat{\eta}} = \frac{a_2 + \frac{\frac{d\Delta}{d\hat{\eta}}}{2\sqrt{\Delta}}}{2\ (a_1\,\sigma\,\xi - a_2.)}. \tag{3.39}$$

We show that $a_2 + \frac{\frac{d\Delta}{d\hat{\eta}}}{2\sqrt{\Delta}} < 0$. Since Δ is positive and $\frac{d\Delta}{d\hat{\eta}}$ is negative for $\hat{\eta} < \hat{\eta}_3$ we examine

$$2a_2\sqrt{\Delta} < -\frac{d\Delta}{d\hat{\eta}}, \tag{3.40}$$

$$\iff 4a_2^2\Delta < (-\frac{d\Delta}{d\hat{\eta}})^2, \tag{3.41}$$

$$\iff 4a_2^2(a_2^2\hat{\eta}^2 + \hat{B}\hat{\eta} + \hat{C}) < (2a_2^2\hat{\eta} + \hat{B})^2, \tag{3.42}$$

$$\iff 4a_2^4\hat{\eta}^2 + 4a_2^2\hat{B}\hat{\eta} + 4a_2^2\hat{C} < 4a_2^2\hat{\eta}^2 + 2a_2^2\hat{B}\hat{\eta} + \hat{B}^2, \tag{3.43}$$

$$\iff 0 < \hat{B}^2 - 4a_2^2\hat{C}, \tag{3.44}$$

which is verified true as in (3.35). Thus, $\dfrac{dF_h^*}{d\hat{\eta}} < 0$ for $\hat{\eta} < \hat{\eta}_3$.

Since the internal equilibrium of our system are given by F_h^* and F_u^*, and we have further shown that F_u^* is an increasing function of $\hat{\eta}$, while F_h^* is decreasing. We now search for the critical points for $\hat{\eta}$ in which $F_h^* < 1$ and $F_u^* > 0$. First, when $\hat{\eta} = \hat{\eta}_1 = -1/2$, we note that $F_h^* = 1$ as seen visually from Figure 3.5b and verified mathematically from both (3.36) and (3.29). Second, when $\hat{\eta} = \hat{\eta}_2 = 1/2 + \sigma a_1/(a_2 + 1)$, we note that $F_u^* = F_l^* = 0$ as seen visually from Figure 3.5b and verified mathematically from both (3.37) and (3.29). Lastly, we note that $F_h^* = F_u^*$ when $\hat{\eta} = \hat{\eta}_3$ and for $\hat{\eta} > \hat{\eta}_3$,

F_h^* and F_u^* have imaginary parts and are not considered equilibrium. The above discussion leads us to the following theorem regarding stability and bifurcations of (3.27).

Theorem 3.5. *The equilibrium and stability of* (3.27) *are given by the following:*

- *(i) If* $\hat{\eta} < \hat{\eta}_1 = -1/2$ *then* F_1^* *is the only equilibrium to exist and is globally stable.*
- *(ii) If* $\hat{\eta}_1 < \hat{\eta} < \hat{\eta}_2$ *then* F_h^* *is the only equilibrium to exist and is globally stable.*
- *(iii) If* $\hat{\eta}_2 < \hat{\eta} < \hat{\eta}_3$ *then* F_l^*, F_u^* *and* F_h^* *exist. Bistability occurs where* F_l^* *and* F_h^* *are locally stable, and* F_u^* *is unstable.*
- *(iv) If* $\hat{\eta} > \hat{\eta}_3$ *then* F_l^* *is the only equilibrium to exist and is globally stable.*

Furthermore, we define a saddle node bifurcation as a point when two steady states collide and annihilate each other as a bifurcation parameter changes. Following this definition we conclude the following corollaries.

Corollary 3.6. *A saddle node bifurcation occurs at the point* $(F, \hat{\eta}) = (F_h^*, \hat{\eta}_3)$.

Corollary 3.7. *A saddle node bifurcation occurs at the point* $(F, \hat{\eta}) = (F_l^*, \hat{\eta}_2)$.

Proof of Theorem 3.5. First, we note that $\hat{\eta}_1 < \hat{\eta}_2 < \hat{\eta}_3$ and $J(F) > 0$ for all $F \in (0, 1)$. Assume that $\hat{\eta} < \hat{\eta}_1 < -1/2$ then $F + \hat{\eta} - 1/2 < 0$ for all $F \in [0, 1]$ and $J(F) > F + \hat{\eta} - 1/2$ for all $F \in (0, 1)$. Hence, $\dfrac{dF}{d\tilde{\tau}} > 0$ for all $F \in (0, 1)$ and $\dfrac{dF}{d\tilde{\tau}} = 0$ for $F = 1$, thus proving (i).

When $\hat{\eta} = \hat{\eta}_1$, $F_h^* = F_1^* = 1$. Since $\frac{dF_h^*}{d\hat{\eta}} < 0$, and necessary condition for $F_h^* \in [0,1]$ is $\hat{\eta} > \hat{\eta}_1$. Now, assume that $\hat{\eta}_1 < \hat{\eta} < \hat{\eta}_2$, then $F_u^* < 0$ because $F_u^* = F_l^* = 0$ when $\hat{\eta} = \hat{\eta}_2$ and $\frac{dF_h^*}{d\hat{\eta}} > 0$. Moreover, $J(F) = F + \hat{\eta} - 1/2$ has only one solution for $F \in [0,1]$ then by the concavity of $J(F)$:

$$J''(F) = -\frac{2\,a_1\,\sigma\,\left(a_2 + \xi + a_2\,\xi\right)}{\left(a_2(1-F)+1\right)^3} < 0, \tag{3.45}$$

for all F, $J(F) > F + \hat{\eta} - 1/2$ for all $F \in [0, F_h^*)$ and $J(F) < F + \hat{\eta} - 1/2$ for all $F \in (F_h^*, 1]$. Hence, $J(F) + 1/2 - \hat{\eta} > 0$ for all $F \in [0, F_u^*)$ and $J(F) + 1/2 - \hat{\eta} < 1$ for all $F \in (F_u^*, 1]$. This implies that $\frac{dF_h^*}{d\hat{\eta}} > 0$ for all $F \in [0, F_h^*)$ and $\frac{dF_h^*}{d\hat{\eta}} < 0$ for all $F \in (F_h^*, 1]$ thus proving (ii).

When $\hat{\eta} = \hat{\eta}_3$, $F_h^* = F_u^*$ as seen in (3.36) and (3.37). Now assume that $\hat{\eta}_2 < \hat{\eta} < \hat{\eta}_3$, then $1 > F_h^* > F_u^* > 0$ by their respective monotonicity. Since $J(F) = F + \hat{\eta} - 1/2$ for $F = F_h^*$ and $F = F_u^*$, we deduce that $0 < J(F) + 1/2 - \hat{\eta} < 1$ near F_h^* and F_u^*. Furthermore, by the concavity of $J(F)$, $J(F) > F + \hat{\eta} - 1/2$ for all $F \in (F_u^*, F_h^*)$ and $J(F) < F + \hat{\eta} - 1/2$ for all $F \notin [F_u^*, F_h^*]$ thus proving that F_h^* is locally stable, and F_u^* is unstable. Lastly, if $F < F_u^*$ then $J(F) < F + \hat{\eta} - 1/2$. Which furthermore implies that $J(F) - \hat{\eta} + 1/2 \leq 0$ for F near $F = 0$, thus proving that $F = 0$ locally stable and concluding (iii)

Finally, assume $\hat{\eta} > \hat{\eta}_3$, then both F_h^* and F_u^* are imaginary roots and not considered to be equilibrium. Furthermore, $J(F) < F + \hat{\eta} - 1/2$ for all $F \in [0,1]$ and hence, $J(F) - \hat{\eta} + 1/2 < 1$ for all $F \in [0,1]$ implying that $\frac{dF}{d\tilde{\tau}} < 0$ for all for all $F \in (0,1]$ and $\frac{dF}{d\tilde{\tau}} = 0$ for $F = 0$ proving that $F = F_l^*$ is globally stable concluding (iv). □

Proof of Corollary 3.6. The two equilibria F_h^* and F_u^*, which are stable and unstable respectively collide, are equivalent at $\hat{\eta} = \hat{\eta}_3$ and do not exist for

$\hat{\eta} > \hat{\eta}_3$. Furthermore, when $\hat{\eta} = \hat{\eta}_3$, $0 < J(F) - \hat{\eta} + 1/2 < 1$ near $F_u^* = F_h^*$, since $J(F) - \hat{\eta} + 1/2 = F$ and $\frac{dF}{d\tilde{\tau}} = 0$ at $F_u^* = F_h^*$. Lastly, we check that $\frac{d(J(F)+1/2-\hat{\eta}-F)}{dF} = 0$ which is equivalent to $J'(F) = 1$ at F_h^* and $\eta = \eta_3$.

Recall F_h^* as given in (3.37) and $\hat{\eta}_3$ as in (3.35). Then at $\hat{\eta} = \hat{\eta}_3$:

$$F_h^* = F_l^* = -\frac{\sqrt{-a_1\,\sigma\,(a_2 - a_1\,\sigma\,\xi)\,(a_2 + \xi + a_2\,\xi)} - a_2 - {a_2}^2 + a_1\,\sigma\,\xi + a_1\,a_2\,\sigma\,\xi}{{a_2}^2 - a_1\,a_2\,\sigma\,\xi}. \tag{3.46}$$

Thus, via substitution and tedious computations that are verified using MATLAB's symbolic software

$$J'(F_h^*) = \frac{a_1\,\sigma\,(\xi - 2\,F_h^*\,\xi + a_2\,\xi - 2\,F_h^*\,a_2\,\xi + {F_h^*}^2\,a_2\,\xi - 1)}{(a_2 - F_h^*\,a_2 + 1)^2}, \tag{3.47}$$

$$= \frac{a_1\,\sigma \left(\begin{array}{l} \xi + a_2\,\xi - 1 \\ \quad + \frac{2\,\xi\left(\sqrt{-a_1\,\sigma\,(a_2 - a_1\,\sigma\,\xi)\,(a_2+\xi+a_2\,\xi)} - a_2 - {a_2}^2 + a_1\,\sigma\,\xi + a_1\,a_2\,\sigma\,\xi\right)}{{a_2}^2 - a_1\,a_2\,\sigma\,\xi} \\ \quad + \frac{2\,a_2\,\xi\left(\sqrt{-a_1\,\sigma\,(a_2 - a_1\,\sigma\,\xi)\,(a_2+\xi+a_2\,\xi)} - a_2 - {a_2}^2 + a_1\,\sigma\,\xi + a_1\,a_2\,\sigma\,\xi\right)}{{a_2}^2 - a_1\,a_2\,\sigma\,\xi} \\ \quad + \frac{a_2\,\xi\left(\sqrt{-a_1\,\sigma\,(a_2 - a_1\,\sigma\,\xi)\,(a_2+\xi+a_2\,\xi)} - a_2 - {a_2}^2 + a_1\,\sigma\,\xi + a_1\,a_2\,\sigma\,\xi\right)^2}{({a_2}^2 - a_1\,a_2\,\sigma\,\xi)^2} \end{array} \right)}{\left(a_2 + \frac{a_2\left(\sqrt{-a_1\,\sigma\,(a_2 - a_1\,\sigma\,\xi)\,(a_2+\xi+a_2\,\xi)} - a_2 - {a_2}^2 + a_1\,\sigma\,\xi + a_1\,a_2\,\sigma\,\xi\right)}{{a_2}^2 - a_1\,a_2\,\sigma\,\xi} + 1 \right)^2} \tag{3.48}$$

$$= 1. \tag{3.49}$$

□

Proof of Corollary 3.7. In (3.29) we see that F_u^* and F_l^* are equivalent (collide) at $\eta = \eta_2$ and are equal to zero. Furthermore, for $\eta < \eta_2$ neither steady state exists as $F_u^* < 0$ as F_u^* is a increasing function of η and $0 = J(F_l^*) + 1/2 - \eta_2$ implies that $J(F_l^*) + 1/2 - \eta > 0$ for $\eta < \eta_2$. Thus the point $(F, \hat{\eta}) = (F_l^*, \hat{\eta}_2)$ is a saddle node bifurcation. □

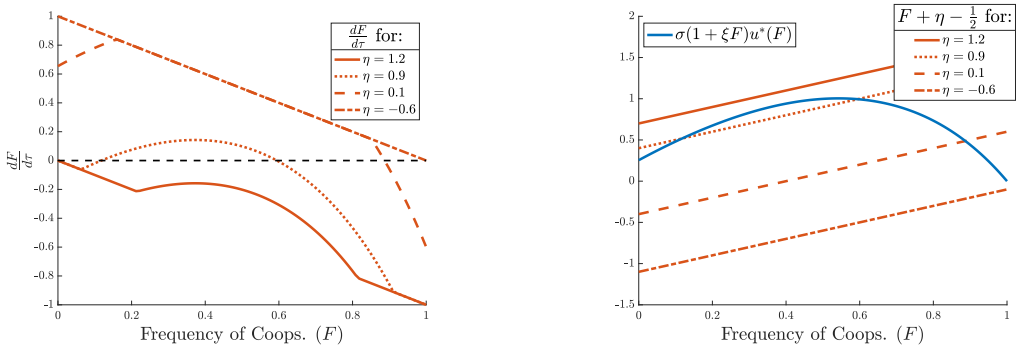

(a) (b)

Figure 3.5: (a) Phase line of equation (3.27) for the four cases given in Theorem 3.5. (b) Curve $J(F)$ and line $F+\hat{\eta}-1/2$ for four values of $\hat{\eta}$ corresponding to the cases in Theorem 3.5. The points of intersection give the equilibria of equation (3.27)

The bifurcations discussed in 3.6 and 3.7 are illustrated intuitively in Figures 3.4 and by noting the intersections of $J(F)$ with $F+\hat{\eta}-12$ in Figure 3.5.

Remark 3.8. *In the non-approximated model* (3.26) *the equilibrium* $F_1^* = 1$ *does not exist. The equilibrium* F_h^* *approaches one, but does not equal and there is no transition from* F_1^* *to* F_h^* *seen in Figure 3.4. Furthermore, the equilibrium* F_l^* *will be small, but non zero. These differences are explained by the linear approximation made at the tails of the logistic curve being set to one or zero accordingly as shown in Figure 3.2. Furthermore, we conjecture that the flows near corresponding equilibrium are topologically equivalent between the two models* (3.26) *and* (3.27) *and that the analysis presented for* (3.26) *holds for* (3.27)*.*

Theorem 3.5 gives an understanding of the possible regime outcomes of the single lake dynamics based on the parameter $\hat{\eta}$, which describes the difference in both baseline and external social norm costs between the two strategies. The results of Theorem 3.5 are summarized graphically in Figure 3.5.

3.3.2 Dynamics of the iron explicit model

Here we consider different parameter values where the nutrient of focus is iron instead of phosphorus. These new parameter values allow us to look at the dynamics of the coupled CB and socio-economic model in the phase plane. The parameter values chosen for Section 3.3.1 (given in Tables 3.1 and 3.2) represent a typical system in which phosphorus pollution occurs. However, we now consider the situation where iron is the focal nutrient. When considering iron instead of phosphorus we must alter certain assumptions and parameters in our model. First, the values of Q_M and Q_m are decreased by nearly an order of magnitude as implied by the extended Redfield ratio (Cunningham and John, 2017; North et al., 2007). Similarly, the uptake rate (ρ_m) is smaller (Downs, Schallenberg, and Burns, 2008; Larson, Liu, and Passy, 2015; Cunningham and John, 2017). However the half saturation constant may not need to decrease, meaning the phytoplankton are inefficient at 'finding' iron at low concentrations. As before, we nondimensionalize the system, but where P now represents the iron concentration and the values of only the following parameters are changed: $Q_M = .4e^{-4}$,$Q_m = .4e^{-5}$, $\rho_M = 1e^{-3}$, $\xi = 5$, $p_{\mathcal{D}} = 100$,$p_{\mathcal{C}} = 50$. All other parameter values remain as in Tables 3.1 and 3.2 but are interpreted for iron.

Nondimensionalization of the single lake model

We now continue with the non-dimensionalization of system (3.14) by the making the substitutions, $\tau = rt$, $u = kz_m B$, $v = \frac{Q}{Q_M}$, $w = \frac{P}{p_{\mathcal{C}}}$, yielding:

$$\begin{cases} \dfrac{du}{d\tau} = u(1 - \dfrac{Q_m}{Q_M}\dfrac{1}{v})h(au) - \dfrac{(\nu_r + \frac{D}{z_e})}{r}u, \\ \dfrac{dv}{d\tau} = \dfrac{\rho_m}{rQ_M}\dfrac{Q_M - Q_M v}{Q_M - Q_m}\dfrac{w}{M/p_{\mathcal{C}} + w} - (v - \dfrac{Q_m}{Q_M})h(au), \\ p_{\mathcal{C}}\dfrac{dw}{d\tau} = \dfrac{D}{rz_e}(p_{\mathcal{C}}F + p_{\mathcal{D}}(1-F) - p_{\mathcal{C}}w) - \dfrac{\rho_M}{rkz_e}u\dfrac{Q_M - Q_M v}{Q_M - Q_m}\dfrac{w}{M/p_{\mathcal{C}} + w}, \\ \dfrac{dF}{d\tau} = \dfrac{s}{r}\left(\dfrac{1}{1 + e^{\beta(c_C - c_{\mathcal{D}} - \alpha(1+\xi F)\psi au + \hat{\delta})}} - F\right). \end{cases} \tag{3.50}$$

Upon substitution of the dimensionless parameters that given in Table 3.4 we arrive at:

$$\begin{cases} \dfrac{du}{d\tau} = u(1 - \dfrac{1}{\gamma}\dfrac{1}{v})\hat{h}(u) - (\epsilon\beta_1 + \beta_2)u, \\ \dfrac{dv}{d\tau} = \omega(1-v)\dfrac{w}{\mu + w} - (v - \dfrac{1}{\gamma})\hat{h}(u), \\ \dfrac{dw}{d\tau} = \epsilon\left(\beta_1(F + \kappa(1-F) - w) - \lambda u(1-v)\dfrac{w}{\mu + w}\right), \\ \dfrac{dF}{d\tau} = \epsilon\left(\dfrac{1}{1 + e^{\hat{\eta} - \sigma(1+\xi F)u)}} - F\right), \end{cases} \tag{3.51}$$

where $\hat{h}(u)$ is the nondimensional light dependent growth originating from (3.2) given by (3.17) and approximated by (3.18).

Application of the quasi steady state approximation

We now apply the QSSA to (3.51). As in Section 3.3.1 we introduce the new timescale $\tilde{\tau} = \epsilon\tau$. $\tilde{\tau}$ now represents the slow timescale in which the socio-economic and iron dynamics mainly occur, whereas the CB growth dynamics occur on the fast time scale τ. Lastly, we apply the QSSA and let $\epsilon \to 0$ arriving at the system:

Table 3.4: Dimensionless parameters for the iron system (3.51)

Parameter	Definition	Value
β_1	$\frac{D}{sz_m}$	0.2857
β_2	ν_r/r	0.35
ω	$\frac{\rho_m}{r(Q_M - Q_m)}$	2.7778
γ	$\frac{Q_M}{Q_m}$	10
κ	$\frac{p_{\mathcal{D}}}{p_{\mathcal{C}}}$	2
μ	$\frac{M}{p_{\mathcal{C}}}$	0.03
λ	$\frac{Q_M}{Q_M - Q_m}\frac{\rho_m}{p_{\mathcal{C}} s k z_m}$	0.7937
k_1	$z_m K_{bg}$	2.1
I	I_{in}/H	2.5
η	$\beta(c_{\mathcal{C}} - c_{\mathcal{D}} + \hat{\delta})$	-
σ	$\alpha\beta\psi/kz_m$	2.1429
ϵ	s/r	<0.001

$$
\begin{cases}
0 = u(1 - \frac{1}{\gamma}\frac{1}{v})\hat{h}(u) - \beta_2 u, & \text{(3.52a)} \\
0 = \omega(1-v)\frac{w}{\mu + w} - (v - \frac{1}{\gamma})\hat{h}(u), & \text{(3.52b)} \\
\frac{dw}{d\tilde{\tau}} = \beta_1(F + \kappa(1-F) - w) - \lambda u(1-v)\frac{w}{\mu + w} = g(F, w), & \text{(3.52c)} \\
\frac{dF}{d\tau} = \frac{1}{1 + e^{\eta - \sigma(1+\xi F)u)}} - F = f(F, w), & \text{(3.52d)}
\end{cases}
$$

reducing our problem to a differential- algebraic system. Denote $u^*(w)$ and $v^*(w)$ as a solution to the algebraic system defined by (3.52a) and (3.52b). The following theorem gives a condition to guarantee existence of uniqueness of a solution to the algebraic system.

Theorem 3.9. *There exists a unique positive solution,* $(\hat{u}(w), \hat{v}(w))$*, to the*

algebraic system defined by (3.52a) *and* (3.52b) *if* $\left(1-\dfrac{1}{\gamma\hat{v}(w)}\right)\hat{h}(0)-\beta_2>0$. *The trivial solution* $(0,\bar{v}(w))$ *always exists.*

Proof. Observe that $(0,\bar{v}(w))$ where

$$\bar{v}(w)=\frac{\omega\dfrac{w}{\mu+w}+\frac{1}{\gamma}\hat{h}(0)}{\omega\dfrac{w}{\mu+w}+\hat{h}(0)}, \tag{3.53}$$

solves (3.52a) and (3.52b). Now, we compute the positive solution by first adding equation (3.52a) multiplied by v/u to equation (3.52b) arriving at

$$0=\omega(1-v)\frac{w}{\mu+w}-\beta_2 v. \tag{3.54}$$

Thus,

$$\hat{v}(w)=\frac{\omega\dfrac{w}{\mu+w}}{\omega\dfrac{w}{\mu+w}+\beta_2}=\frac{\omega w}{\omega w+\beta_2(\mu+w)}. \tag{3.55}$$

Now we see that $\hat{v}(w)$ is only dependent on parameters as w is treated as a parameter in the algebraic system. Thus, (3.52a) can be reduced to a problem with a single unknown:

$$0=(1-\frac{1}{\gamma\hat{v}(w)})\hat{h}(u)-\beta_2. \tag{3.56}$$

Recall, by the construction of $h(B)$ in (3.2) it and its nondimensional analog, $\hat{h}(u)=\frac{1}{u+k_1}\log\left(\frac{1+I}{1+I\exp(-u-k_1)}\right)$, are monotone decreasing functions and $\lim_{u\to\infty}\hat{h}(u)=0$. Thus, if

$$(1-\frac{1}{\gamma\hat{v}(w)})\frac{1}{k}\log(\frac{1+I}{1+Ie^{-k}})-\beta_2>0, \tag{3.57}$$

then a unique positive solution exists via the intermediate value theorem. □

Note that the condition in the theorem is also satisfied for values of w, such that $w>w_c$, where w_c is the critical point such that $\bar{v}^(w_c)=\hat{v}(w_c)$. w_c can

be written explicitly as

$$w_c = -\frac{\frac{1}{\gamma}\hat{h}(0)\mu\beta_2}{\omega\beta_2 + \frac{1}{\gamma}\hat{h}(0)\omega + \frac{1}{\gamma}\beta_2\hat{h}(0) - \omega\hat{h}(0)}. \tag{3.58}$$

The equation $\bar{v}(w) = \hat{v}(w)$ is reduced to a linear equation in w thus verifying w_c is unique. For $w < w_c$ the only solution to the system (3.52a) and (3.52b) is given by $(0, \bar{v}(w))$. For $w > w_c$ the positive solution $(\hat{u}(w), \hat{v}(w))$ also exists and $(0, \bar{v}(w_c) = (\hat{u}(w_c), \hat{v}(w_c))$. It can be shown that the trivial equilibrium of the fast subsystem is unstable if $w > w_c$ thus, we take the solutions to system (3.52a) and (3.52b) as

$$u^*(w) = \max\{0, \hat{u}(w)\} \qquad \text{and} \qquad v^*(w) = \max\{\bar{v}(w), \hat{v}(w)\}, \tag{3.59}$$

where $\hat{u}(w)$ is the solution to (3.56).

Phase Plane analysis of the simplified single lake iron model

We now proceed with studying (3.52) in the phase plane. Changing the value for η in system (3.52) will result in various phase portraits that are topologically different. One such instance shows a bistable scenario that is lost through either one of two saddle-node bifurcations.

In the following we assume that $u^*(w), v^*(w)$ are defined as in (3.59). The bifurcation plot, with respect to η of system (3.52) is shown in Figure 3.6. Recall that the parameter $\eta = c_{\mathcal{C}} - c_{\mathcal{D}} + \hat{\delta}$ partly describes the differences in base costs and network social norm costs faced by the cooperator and defector, respectively.

The first case we explore is for η values that are relatively 'large'. Figure 3.7 shows the phase portrait for values of η that represent the base costs of cooperating to be relatively much higher than that of the defector. In this case the

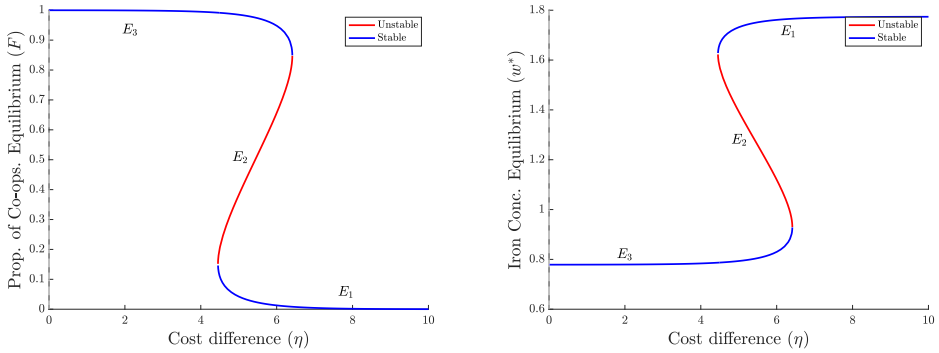

Figure 3.6: Bifurcation diagrams for system (3.52c) and (3.52d). Left: equilibrium values for the proportions of cooperators (F). Right: Equilibrium values for the concentration of iron.

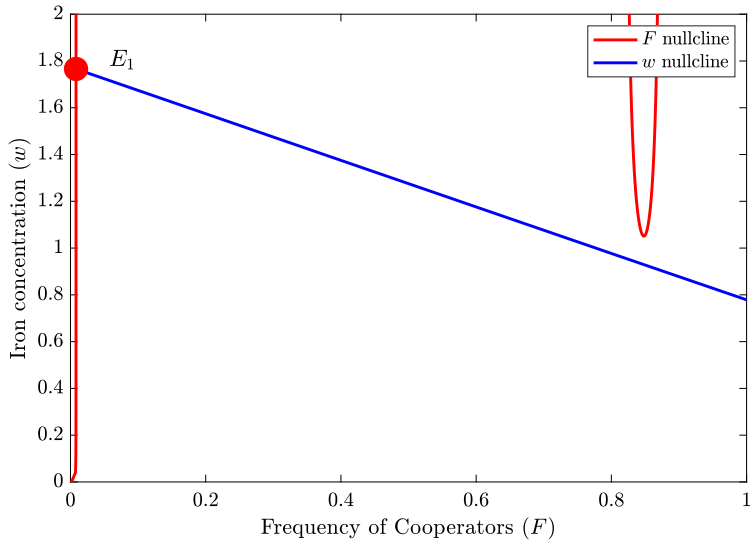

Figure 3.7: Phase plane for 'large' values of η. E_1 is the only equilibrium and attracts all solutions.

equilibrium E_1, defined by a low level of cooperation and a relatively high concentration of iron, is numerically globally attracting and the only equilibrium to exist. We show via graphical arguments the local stability below:

It is enough to observe the sign changes of $f(F, w)$ and $g(F, w)$ as we cross the nullclines near the equilibrium point E_1 given in the phase plane (see Figure 3.7). The Jacobian of system ((3.52c) and (3.52d)) has the following form:

$$A|_{E_1} = \begin{pmatrix} f_F & f_w \\ g_F & g_w \end{pmatrix}_{E_1} = \begin{pmatrix} - & + \\ - & - \end{pmatrix}. \tag{3.60}$$

By the signs given in $A|_{E_1}$ we conclude that, $Tr(A|_{E_1}) < 0$ and $det(A_{E_1}) > 0$. Thus, the matrix $A|_{E_1}$ has eigenvalues with negative real parts and we conclude that equilibrium E_1 is locally stable.

Now we look at the case where η is relatively 'small'. Here the values of η represent the base costs of cooperating to be relatively close to that of the defectors. Figure 3.8 shows the phase portrait for this scenario. Here, the equilibrium E_3, defined by a high level of cooperation and a relatively low concentration of iron, is numerically globally attracting and the only equilibrium to exist. This means the phase portrait in Figure 3.8 represents an environmentally favourable outcome. We show the local stability below.

Near the equilibrium point, E_3 in Figure 3.8 , we observe the sign changes of $f(F, w)$ and $g(w, F)$ as the nullclines are crossed. The Jacobian of system (3.52c) and (3.52d) has the following form:

$$A|_{E_3} = \begin{pmatrix} f_F & f_w \\ g_F & g_w \end{pmatrix}_{E_3} = \begin{pmatrix} - & + \\ - & - \end{pmatrix}. \tag{3.61}$$

We conclude that $Tr(A|_{E_3}) < 0$ and $det(A_{E_3}) > 0$. Thus, the matrix $A|_{E_3}$ has eigenvalues with negative real parts and we conclude that equilibrium E_3 is locally stable.

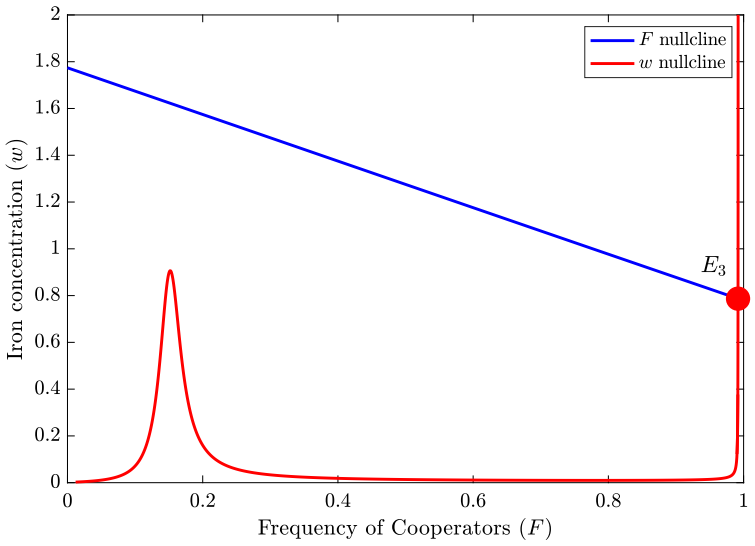

Figure 3.8: Phase plane for 'small' values of η. E_3 is the only equilibrium and attracts all solutions.

Now we show the dynamics for intermediate values of η such that a bistable scenario occurs. These values of η represent an intermediate region where the cost of cooperating and defecting are close to being balanced. Figure 3.9 shows the phase portrait of the bistable scenario, where the topology near equilibrium E_1 and E_3 are qualitatively consistent to that shown in Figures 3.7 and 3.8, respectively. That is, E_1 and E_3 are both locally stable for our chosen parameter region. A new equilibrium, E_2, appears as seen in Figure 3.9 which we now show is unstable. First by graphical methods, the Jacobian evaluated near E_2 is,

$$A|_{E_2} = \begin{pmatrix} f_F & f_w \\ g_F & g_w \end{pmatrix}_{E_2} = \begin{pmatrix} + & + \\ - & - \end{pmatrix}. \tag{3.62}$$

From this alone, we can not make any conclusions. Graphically, the gradients evaluated on the nullclines are such that $\frac{dw}{dF}|_{g=0} < 0$, $\frac{dw}{dF}|_{f=0} < 0$, and $\frac{dw}{dF}|_{g=0} >$

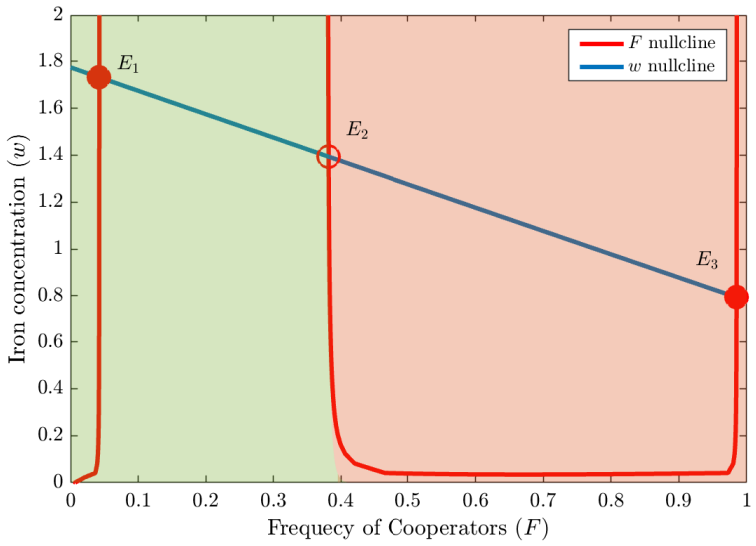

Figure 3.9: Phase plane for 'intermediate' values of η. In this case E_1 and E_3 have similar topology as in Figures 3.7 and 3.8 and thus have the same stability. The shaded regions represent the attraction basin of the respective equilibrium. E_2 is unstable.

$\frac{dw}{dF}|_{f=0}$, near E_2. Furthermore,

$$\left.\frac{dw}{dF}\right|_{g=0} = -\frac{g_F}{g_w} > \left.\frac{dw}{dF}\right|_{f=0} = -\frac{f_F}{f_w}, \tag{3.63}$$

$$\begin{aligned}
&\implies -\frac{g_F}{g_w} > -\frac{f_F}{f_w},\\
&\implies \frac{g_F}{g_w} < \frac{f_F}{f_w},\\
&\implies f_w \frac{g_F}{g_w} < f_F,\\
&\implies f_w g_F > f_F g_w,\\
&\implies 0 > f_F g_w - f_w g_F,\\
&\implies det(A) < 0.
\end{aligned}$$

Thus, E_2 is an unstable saddle. Note that the above comes from taking the derivative of the level set $f(F, w) = 0$ and graphical observation.

Remark 3.10. *In Figures 3.7 and 3.9 we note that there is a region of F values where the F nullcline does not exist. This atypical phenomenon is explained by the dependency of the nullcline on the solution to the algebraic system* (3.52a) *and* (3.52b)*, $u^*(w)$. That is, the F nullcline is given by the solutions to*

$$0 = \frac{1}{1 + e^{\eta - \sigma(1+\xi F)u^*(w))}} - F, \tag{3.64}$$

$$\iff u^*(w) = \frac{\log(\frac{1}{F} - 1) - \eta}{-\sigma(1 + \xi F)}. \tag{3.65}$$

The right hand side of (3.65) *has one local max, one local min, and one inflection point in* $[0, 1]$*. Also, note that as $F \to 0$ the RHS of* (3.65) *goes to $-\infty$ and as $F \to 1$ the RHS of* (3.65) *goes to $+\infty$. However, $u^*(w)$ is a saturating function of w, and is bounded between zero and some positive constant. The positive bound results from CB self-shading and light limitation. Thus, for certain values of F, the right hand side of* (3.65) *exceeds the upper bound of $u^*(w)$ resulting in no solution to the equation. Furthermore, vertical asymptotes occur as F approaches the regions of nonexistence accordingly.*

We have shown that the socio-economic and ecological regime is highly connected to costs associated with each strategy. The dynamic properties have been explored in the phase plane which included a high cooperation regime, a low cooperation regime, and a bistable scenario.

3.4 Dynamics of a network system

We now return to the network model proposed in (3.1) with parameter values given for the phosphorus dynamics in Tables 3.1 and 3.2. Here we consider the nondimensional version of (3.1) and, upon further simplifying assumptions, reduce the entire network model to a system of two ODEs which are studied in the phase plane. A series of two parameter bifurcation plots are provided

to show regime outcomes for various parameter regions associated with the socio-economic dynamics.

3.4.1 Reduction of the network model

We now make a series of simplifying assumptions to reduce the network model (3.1) to a system of two ODEs.

We wish to further understand how socio-economic pressures can lead to regime shifts. In section 3.3 we consider these pressures on a local scale, we now consider these pressures when they originate from distant social connections. For this reason, let us consider a network with N lakes. Assume that each lake is modelled with identical parameter values and that if the network is not connected, each lake exhibits the bistable dynamics discussed in the phase line analysis (Section 3.3.1). Note that the nondimensionalization of the network model (3.1) is equivalent to what is shown in (3.16) with the explicit subscripts for lake i and the term $\hat{\delta}$ is to be a function of the weighted average of the frequency of cooperators in the network.

Assume a given lake is initially either in the high cooperation state (F_h^*) or the low cooperation state (F_l^*) at equilibrium as discussed in Figures 3.5a and 3.4. Since the system is bistable, we can assume that our network has $N-k$ lakes in the low cooperation state (F_l^*) and K lakes in the high cooperation (F_h^*) state.

By assuming that every lake in the network has the same environmental parameters we can conclude that the dynamics of lakes with the same initial conditions will be identical. We introduce two new state variables F_h and F_l. F_h represents the dynamics of frequency of cooperators that start in a high cooperation state. F_l is the dynamics of those that start in a low cooperation

state. Indeed a requirement based on these assumptions is that $F_h(0) > F_l(0)$.

Then, $\hat{\delta}(\bar{F}(t))$ is rewritten as

$$\hat{\delta}(\bar{F}(t)) = \hat{\delta}(F_l, F_h) = \delta_{\mathcal{C}}(1 - \bar{F}) - \delta_{\mathcal{D}}\bar{F}. \tag{3.66}$$

Since all lakes of the same regime are in the same state, then $\bar{F} = \frac{(k)F_h + (N-k)F_l}{N}$. Furthermore, assuming that the ecological dynamics of each lake are in steady state and occur on a faster timescale (by the QSSA discussed in Section 3.3.1) the entire network is reduced to a two dimensional system of equations:

$$\frac{dF_h}{d\tau_1} = \frac{1}{1 + e^{\eta - u^*(F_h)(1+\xi F_h) + \delta(F_l, F_h)}} - F_h = f_1(F_h, F_l), \tag{3.67a}$$

$$\frac{dF_l}{d\tau_1} = \frac{1}{1 + e^{\eta - u^*(F_l)(1+\xi F_l) + \delta(F_l, F_h)}} - F_l = f_2(F_h, F_l), \tag{3.67b}$$

where $u^*(F)$ is the unique equilibrium of the ecological system discussed in Theorem 3.1. The system (3.67) then represents the coupled socio-economic and ecological dynamics of a network of lakes where F_h and F_l represent the social dynamics of lakes that start in a high and low cooperation regime, respectively.

3.4.2 Phase plane analysis of the reduced network model

We now use the phase plane to explore the possible long term dynamics of the network dependent on socio-economic parameters. Three stable steady states can occur that correspond to high, low and mixed levels of cooperation throughout the network. By manipulating parameters a network shift from mixed to either high or low cooperation can occur.

Note that under the condition $\hat{\delta}(F_l, F_h) = 0$ the system is decoupled and each lake would exhibit bistable behaviour. Further note that given our assumptions we must limit the phase plane to the region $F_l \leq F_h$. We assume that the system will start the prescribed initial condition of $N - K$ lake in

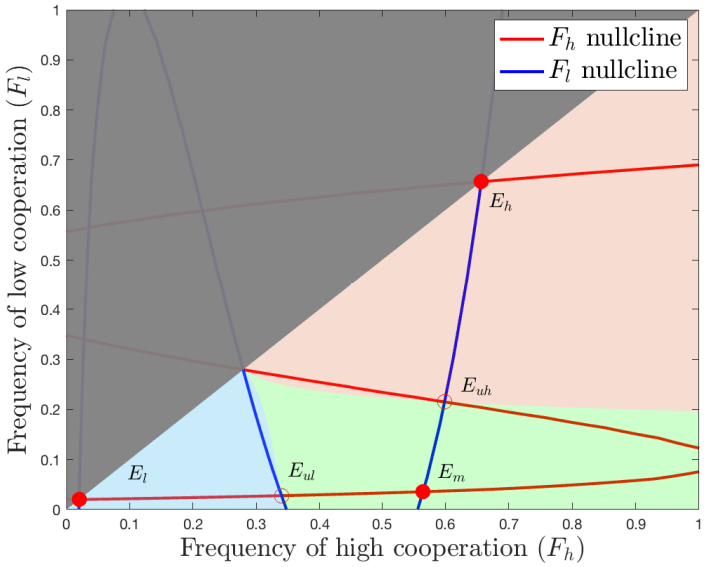

Figure 3.10: The phase plane of F_h and F_l for similar social norm pressure. The region above the line $F_l = F_h$ is excluded based on the condition $F_l < F_h$. The shaded regions represent the attraction basins of the stable equilibrium, the initial condition is located within the green region. In this case no regime shifts occur based on the prescribed initial condition.

a low cooperation state (corresponding F_l^*) and k lakes in the high cooperation state (corresponding to F_h^*). This means that the initial condition of our system is $F_h(0) = F_h^*$ and $F_l(0) = F_l^*$.

The stable equilibria are E_l, E_h, and E_m and the unstable equilibria are E_{ul} and E_{uh} as shown in Figure 3.10. The stability of E_l, E_h, and E_m can be easily shown through graphical arguments similar to that in Section 3.3.2. That is, the Jacobian of system (3.67) near E_l has the form

$$A|_{E_l} = \left(\begin{array}{cc} \frac{df_1}{dF_h} & \frac{df_1}{dF_l} \\ \frac{df_2}{dF_h} & \frac{df_2}{dF_l} \end{array} \right) \Bigg|_{E_l} = \begin{pmatrix} - & + \\ + & - \end{pmatrix}. \tag{3.68}$$

Thus, $Tr(A|_{E_l}) < 0$. Moreover,

$$\left.\frac{dF_l}{dF_h}\right|_{f_1=0} = -\frac{df_1}{dF_h} \Big/ \frac{df_1}{dF_l} > \left.\frac{dF_l}{dF_h}\right|_{f_2=0} = -\frac{df_2}{dF_h} \Big/ \frac{df_2}{dF_l}, \tag{3.69}$$

$$\begin{aligned}
&\implies -\frac{df_1}{dF_h}/\frac{df_1}{dF_l} > -\frac{df_2}{dF_h}/\frac{df_2}{dF_l}, \\
&\implies -\frac{df_1}{dF_h}\frac{df_2}{dF_l} < -\frac{df_1}{dF_l}\frac{df_2}{dF_h}, \\
&\implies det(A|_{E_l}) > 0.
\end{aligned}$$

Thus, E_l is stable. The stability of E_m and E_h can be verified in an identical fashion as E_l. The instability of E_{uh} and E_{ul} is concluded similarly with

$$A|_{E_{ul}} = \begin{pmatrix} + & + \\ + & - \end{pmatrix} \implies det(A|_{E_{ul}}) < 0, \tag{3.70}$$

and

$$A|_{E_{uh}} = \begin{pmatrix} - & + \\ + & + \end{pmatrix} \implies det(A|_{E_{uh}}) < 0. \tag{3.71}$$

E_l is representative of a low cooperation regime in the entire network, E_h is representative of a high cooperation regime in the entire network, and E_m is representative of the regime where some lakes cooperate and high levels and some at low levels and are not qualitatively different from the initial condition of the network (i.e. $N-k$ lakes remain in a low cooperation state and k lakes remain in a high cooperation state). We explore the loss of stability or disappearance of E_m. That is, when E_m loses stability or vanishes the dynamics must either shift to E_l, or E_h and the shift will be decided by the basins of attraction near bifurcation points. From graphical methods, we can show that when E_m exists it is stable. However, E_m can disappear through one of two saddle node bifurcations: (i) The equilibrium E_{uh} collides with E_m and (ii) The equilibrium E_{ul} collides with E_m.

Case (i): bifurcation when E_{uh} collides with E_m

In this case, we see that the lower two branches of the F_l nullcline would be to the left of the rightmost branch of the F_h nullcline as depicted in Figure 3.11.

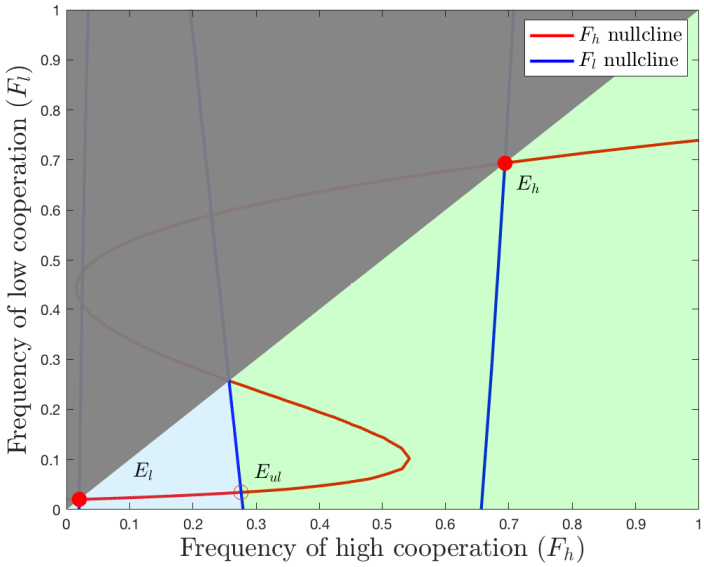

Figure 3.11: Phase plane after E_m collides with E_{uh}. This phase plane corresponds with higher pressure to cooperate. The region above the line $F_l = F_h$ is excluded based on the condition $F_l < F_h$. The shaded regions represent the attraction basins of the stable equilibrium, the initial condition is located within the green region. In this case a regime shift to high cooperation occurs based on the prescribed initial condition.

The separatrix is approximately the middle branch of the F_h nullcline and runs vertically through E_{ul}. With initial conditions such that k lakes are in a high cooperation state and $N-k$ lakes in a low cooperation state the network dynamics will eventually tend to E_h based on the attraction basins. The phase plane of this situation is shown in Figure 3.11.

Case (ii): Bifurcation when E_{ul} collides with E_m

Here the two rightmost branches of the F_l nullcline will be above the lowest branch of the F_h nullcline. The separatrix is now the (roughly) middle branch of the F_h nullcline and runs horizontally through E_{uh}. With initial conditions such that k lakes are in a high cooperation state and $N-k$ lakes in a low cooperation state the network dynamics will eventually tend to E_l based on

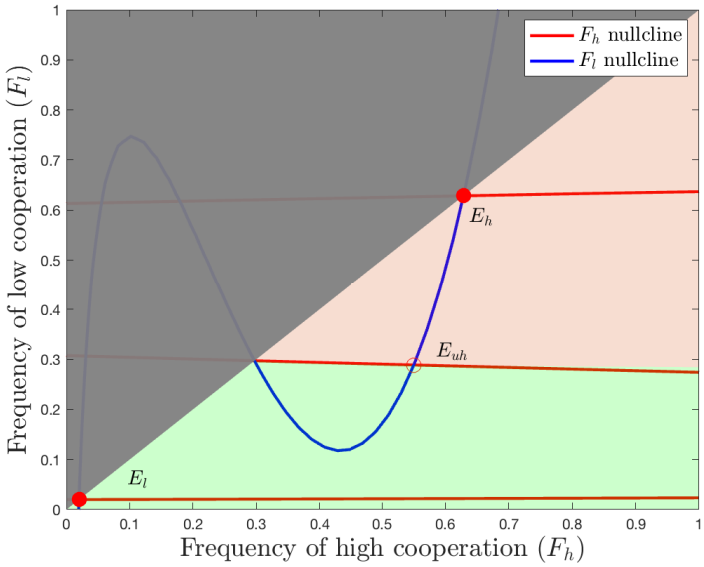

Figure 3.12: Phase plane after E_m collides with E_{ul}. This phase plane corresponds with lower pressure to cooperate. The region above the line $F_l = F_h$ is excluded based on the condition $F_l < F_h$. The shaded regions represent the attraction basins of the stable equilibrium, the initial condition is located within the green region. In this case a regime shift to low cooperation occurs based on the prescribed initial condition.

the attraction basins. The phase plane of this situation is shown in Figure 3.12

We have shown via phase plane analysis that three main dynamical outcomes occur. First, when additional network pressure is small then the system will stay in a state of mixed regime, i.e. k lakes in high cooperation state and $N - k$ lakes in a low cooperation state as in Figure 3.10. Second, when additional network pressure adds sufficiently more costs for the defectors a bifurcation occurs such that all lakes will tend to a high cooperation state as in Figure 3.11. Lastly, when additional network pressures add sufficiently more costs to the cooperators a bifurcation occurs such that all lakes will tend a low cooperation state as in Figure 3.12.

3.4.3 Bifurcation conditions

We now discuss necessary conditions for the bifurcations to occur. These necessary conditions are based on model parameters and thus offer insight to the parameter values that result in certain regime shifts giving insight to effective mitigation for environmentally favourable outcomes.

Graphically we notice that the signs of $A|_{E_m}$ do not change as we vary parameter values. However, near either bifurcation point we require the signs $A|_{E_{ul}}$ or $A|_{E_{uh}}$ to change. This observation leads us to the following two theorems.

Remark 3.11. *Two neccessary conditions for the bifurcations to occur are highlighted:*

(i) If the system is close to the bifurcation point where E_{ul} collides with E_m then $\frac{df_1}{dF_h}|_{E_{ul}} < 0$.

(ii) If the system is close to the bifurcation point where E_{uh} collides with E_m then $\frac{df_2}{dF_l}|_{E_{uh}} < 0$.

Remark 3.11 is justified by graphical inspection. First, when sufficiently far away from the bifurcation point discussed in (i) the Jacobian, $A|_{E_{ul}} = \begin{pmatrix} + & + \\ + & - \end{pmatrix}$. A necessary condition at the bifurcation point is $det(A|_{E_{ul}}) = 0$. Now, at the bifurcation point we require $A|_{E_{ul}} = A|_{E_m}$, and graphically we can see that near the bifurcation point only the first entry in $A|_{E_{ul}}$ will change sign. Thus, near the bifurcation point $\frac{df_1}{dF_h}|_{E_{ul}}$ must be negative. The argument for (ii) follows identical logic to the above discussion.

Thus, by Remark 3.11 we have necessary conditions for the bifurcations to occur. These conditions involve model parameters, thus offering insight

towards system characteristic that promote, or prevent, bifurcation from occurring.

3.4.4 Bifurcation diagrams for the reduced network

We now explore the possible regime shifts dependent on the socio-economic parameters $\delta_{\mathcal{C}}, \delta_{\mathcal{D}}$, k and N and focus on the bifurcations related to E_m. The model parameters considered offer insight towards implementing additional costs as to prevent non-environmentally favourable outcomes or to promote environmentally favourable regime shifts.

Figures 3.13, 3.14, and 3.15, show two parameter bifurcation diagrams for the combination of parameters $\delta_{\mathcal{C}}$, $\delta_{\mathcal{D}}$ and k/N. We assume that the initial condition of (3.67) corresponds to populations in the bistable state of the single lake model i.e., $F_h(0) = F_h^*$ and $F_l(0) = F_l^*$. The region denoted with 'high coop.' represents the region in parameter space where lake populations will tend to a high cooperation regime (Figure 3.11). Conversely, the region denoted with 'low coop.' corresponds to the network shifting to a low cooperation regime (Figure 3.12). The region denoted 'mixed coop' represents when there is no regime shift (Figure 3.10). There are two remaining regions in the parameter space where either E_l or E_h disappear. These regions correspond to the bifurcation that would occur when either i) E_{ul} and E_l collide, and ii) E_{uh} and E_h collide and are denoted with 'high coop. only', and 'low coop. only', respectively. In both cases the resultant regime will not change, the key difference is that bistability is lost.

Remark 3.12. *There is a cusp bifurcation shown in Figures 3.14 and 3.15. The cusp bifurcation is the point in which E_m,E_{ul}, and E_{uh} all collide and one unstable equilibrium remains. Above the cusp bifurcation no bifurcation occurs,*

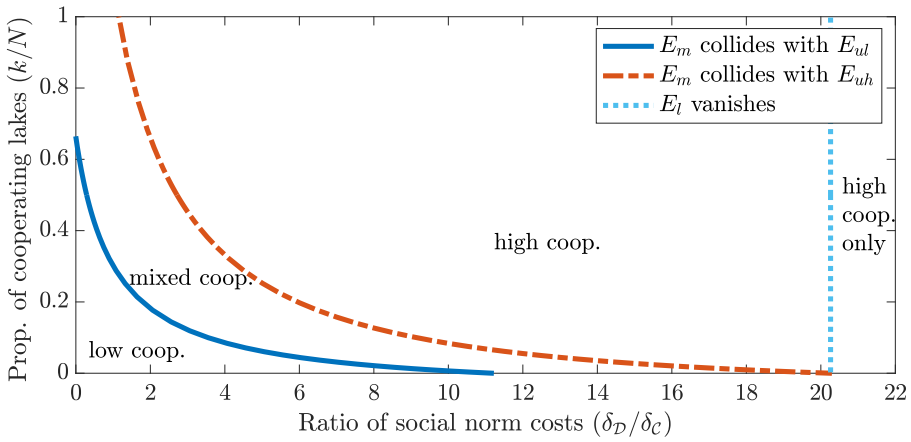

Figure 3.13: Shows the two parameter bifurcation for $\delta_{\mathcal{C}} = 0.6$. The solid line is the curve in parameter space where E_m collides with E_{ul}. Below the solid is described in Case (ii). The dashed line is the curve in parameter space where E_m collides with E_{uh}. Above the dashed line is described in Case (i). The region between the curves is where the equilibrium E_m persists. To the right of the dotted line E_l vanishes and the equilibrium E_h is the only equilibrium.

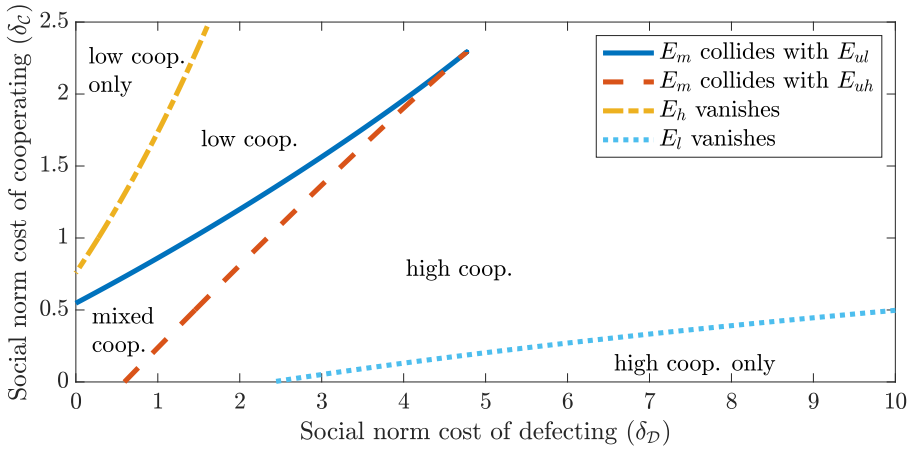

Figure 3.14: Shows the two parameter bifurcation for $k/N = 0.5$. The orange dashed line is the curve in parameter space where E_m collides with E_{uh}. The region below this line is described in Case (i). The solid blue line is the curve in parameter space where E_m collides with E_{ul}. The region above this line is described in Case (ii). The solid and dashed lines meet at a cusp bifurcation (see Remark 3.12). The other two lines show when E_l or E_h vanish. Crossing these lines transition from bistable state to a monostable state.

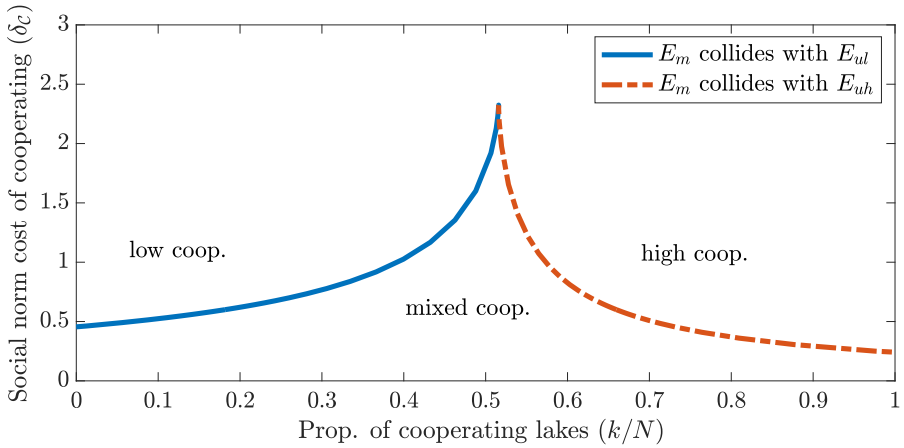

Figure 3.15: Shows the two parameter bifurcation for $\delta_{\mathcal{D}} = 2\delta_{\mathcal{C}}$. The solid line is the curve in parameter space where E_m collides with E_{ul}. Above the solid is described in Case (ii). The dashed line is the curve in parameter space where E_m collides with E_{uh}. Above the dashed line is described in Case (i).The solid and dashed lines meet at a cusp bifurcation (see Remark 3.12).

but the location of the unstable equilibrium varies and the size of the attracting basins changes accordingly. Thus, above the cusp bifurcation we label the region 'high coop.' if remaining unstable equilibrium is along the bottom-most branch of the F_l nullcline, and label the region 'low coop.' if it is along the rightmost branch of the F_h nullcline. Figure 3.16 shows two phase portraits near the cusp bifurcation.

The series of two parameter bifurcation plots presented in Figures 3.13, 3.14, and 3.15 give insight to parameter values that will yield a favourable regime shift. Interestingly, the parameters $\delta_{\mathcal{C}}$, $\delta_{\mathcal{D}}$, k and N can be altered strategically with three possible outcomes. First, for values that greatly increase the pressure to cooperate, such as large k/N, small $\delta_{\mathcal{C}}$, or large $\delta_{\mathcal{D}}$ the network will shift to a high cooperation regime. Second, for small k/N, large $\delta_{\mathcal{C}}$, or small $\delta_{\mathcal{D}}$ ($\delta_{\mathcal{D}}/\delta_{\mathcal{C}}$ is small) the network will shift to a low cooperation regime. However, for the third case, there are intermediate values of each of the parameters such

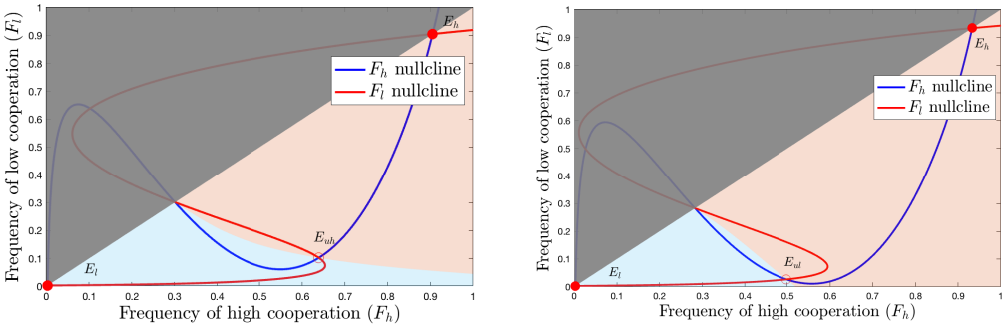

Figure 3.16: Shows the phase portrait just beyond the cusp bifurcation in Figures 3.14 and 3.15. The left phase portrait shows the unstable equilibrium on the rightmost branch of the F_h nullcline, thus this parameter region is labelled as 'low coop'. The right phase portrait shows the unstable equilibrium on the bottom-most branch of the F_l nullcline, thus is labelled as the 'high coop.' region.

that no regime shift will occur.

3.5 Discussion

The study of CB dynamics is important to effectively mitigate potential risks associated with toxin production and ecosystem health as well as to reduce the associated agricultural, recreational, and water treatment costs. However, CB dynamics are intertwined with human dynamics through anthropogenic nutrient pollution (Paerl, 2014). In order to make meaningful management strategies to reduce the effects of CHABs we must also consider the associated socio-economic dynamics.

In this chapter we study the coupled socio-economic dynamics and abundance of CB in a single lake, and a network of lakes. The model presented is an extension of previously studied socio-economic and phytoplankton models. Similar systems have been studied but only consider the nutrient dynamics and neglect the deeper issue of CB abundance (Iwasa, Uchida, and Yokomizo,

2007; Iwasa, Suzuki-Ohno, and Yokomizo, 2010). This distinction is important as many landowners are more concerned with the risks associated with CHABs as a result of eutrophication than the eutrophic conditions themselves. For this reason we explicitly consider the influence human dynamics have on CB abundance. This is done by extending the models established by Iwasa, Uchida, and Yokomizo (2007) and Iwasa, Suzuki-Ohno, and Yokomizo (2010) to consider CB abundance as the main environmental concern. The CB model is derived from a series of stoichiometric models (Wang et al., 2007; Berger et al., 2006; Heggerud, Wang, and Lewis, 2020). The coupling of the ecological and socio-economic models yields the existence of multiple stable states and hysteresis creating deeper implications for effective management of such systems.

We consider the dynamics of our model for both phosphorus and iron. In the case of phosphorus the ecological dynamics occur on a faster timescale than the human dynamics. This observation allows us to apply the QSSA, simplifying the analysis. We further apply a series of approximations and arrive at a single tractable differential equation that describes the entire single lake system. Equilibria and their stability are studied through a bifurcation analysis with respect to the parameter η in Theorem 3.5. The results are supported by graphical inspection, inspired by the analysis of the classical Spruce Budworm model (Ludwig, Jones, and Holling, 1978). For the iron case, the nutrient dynamics occur on the same timescale as the human dynamics with the CB and cell quota remaining on the faster timescale. We again apply the QSSA and graphically study the system in the phase plane. The graphical results show two saddle node bifurcation points with respect to the parameter η. Each bifurcation point results in a loss of bistability and either

the high or low cooperation equilibrium become globally attracting. This type of dynamic is akin to the typical hysteresis phenomenon (Carpenter, 2005; Beisner, Haydon, and Cuddington, 2003).

Lastly, we extend the phase line analysis to study the long term behaviour of a network of lakes. We assume that each lake is ecologically similar and that the only connections among lakes are through social interactions. The analysis is done in the phase plane where multiple stable states exist. Each state corresponds to a regime of high, low or mixed levels of cooperation throughout the network. Two main bifurcation branches are observed which correspond to the loss of the mixed cooperation equilibrium. Through a series of bifurcation diagrams we gain understanding as to what the long term regime outcome is based on parameter values pertaining to social pressures.

The results presented in this chapter all have various implications towards policy and management strategies. In the phase line analysis of the phosphorus model our main result, Theorem 3.5, gives analytical conditions for bifurcation points. The bifurcation points correspond to the loss of bistability as the parameter η is changed. Recall that η represents the difference in baseline costs to cooperate and defect plus the difference in costs of external social pressures. That is, a large η represents a larger cost to cooperate, whereas a small η represents a larger cost to defect. Our results are not surprising in the sense that large η leads to lower cooperation and vice versa, but what is noteworthy to managers is the presence of hysteresis. A lake could be in a high cooperation state and suddenly shift to a low cooperation state if η exceeds its bifurcation point (η_3). However, attempts to lower η back down to η_3 will not be sufficient in re-achieving the high cooperation state due to the presence of the hysteresis phenomenon.

The results of the iron system reiterate the conclusions of the phosphorus system with respect to bistability, but explicitly show the high and low pollution states. Additionally, the dynamics of iron and phosphorus are assumed to act on different timescales with respect to CB and anthropogenic inputs (Whitton, 2012; Cunningham and John, 2017). We assume that phosphorus dynamics occur on a similar scale to the ecological dynamics, whereas iron dynamics occur on the slower time scale similar to the human dynamics. This distinction is important when suggesting management strategies for a specific nutrient as the transient dynamics of the systems can differ significantly and moreover, the response of the human system may not yield a satisfactory response in the ecology for significantly longer periods of time (Hastings, 2016).

In general, adding costs that are associated with social norm pressures on the defectors can help sway the long term outcomes to be environmentally favourable. For instance, a large associated social norm pressure to cooperate, combined with a low associated pressure to defect will result in an overall environmentally favourable outcome. Also, when social network connections are added the initial state of the network can be a predictor of the regime outcome. We show that when a large majority of lakes start in a high cooperation state, it is unlikely that parameters can be changed enough so that the long term outcome will be a state of low cooperation, although mixed levels of cooperation throughout the network is possible.

We have shown that bistability is observed in a single lake system. These results reiterates what has been hypothesized to occur in many nutrient explicit lake systems (Carpenter, 2005; Iwasa, Suzuki-Ohno, and Yokomizo, 2010) although in our case bistability does not occur in the CB model without the

socio-economic coupling (Wang et al., 2007; Heggerud, Wang, and Lewis, 2020). However, when a network system is considered our results show that tristability occurs as in Figure 3.10. To our knowledge no such ecological system has been shown to exhibit such behaviour. The implication of tristability is interesting in the sense that three regime outcomes are possible and that attempts to shift regimes may require significantly more effort. That is, if the system is in a low cooperation regime, it must first transition to a mixed regime state before achieving the environmentally favourable outcome. Furthermore, a system in the mixed regime can be perturbed in either direction to cause a regime shift, as opposed to the bistable case where perturbations can only shift the regime in one direction. In this sense tristable systems are more fragile to environmental fluctuations which can both be beneficial if transitioning from a less favourable regime, or detrimental if in a favourable state. Future work of this study should include deeper consideration of tristable systems and their implications towards management.

In much of our analysis we make the QSSA or similar simplification. Although these simplifications make the model tractable for analysis they do take away some key aspects of the dynamics, mainly the possibility for interesting transient dynamics. Our results pertain to only long-term dynamics which may be insufficient in the eyes of policy makers as the ecology can change drastically on a smaller timescale (Heggerud, Wang, and Lewis, 2020; Hastings, 2010; Hastings et al., 2018). Furthermore, certain mechanisms are deemed negligible via the QSSA which, although reasonable, do take away from the dynamics of the full system.

The socio-economic component of our model uses the logit best-response dynamics to model human decision making and is extended from Iwasa, Uchida,

and Yokomizo (2007) and Iwasa, Suzuki-Ohno, and Yokomizo (2010). We present justifications for using this form, although the replicator dynamics are, perhaps, more commonly used. Indeed the replicator dynamics are more mathematically friendly, but they are based on the assumption of completely rational individuals (Sun and Hilker, 2021), or individuals that base their decision solely on decreasing cost by assuming a strategy that was beneficial to another individual. The best-response dynamics assumes that an individual bases their decision partly on the current environmental state and the associated social norms (Farahbakhsh, Bauch, and Anand, 2021; Sun and Hilker, 2021). Replication dynamics assumes that eventually the population will entirely assume a strategy whereas the best-response dynamics will have persistence of both strategies. Furthermore, we assume that individuals in our system understand the link between nutrient pollution and bloom formation, and further do not learn a strategy from interacting with other individuals. For our system we deem the assumptions around the best-response dynamics more reasonable. However, for deeper mathematical understanding the simpler form of the replicator dynamics may prove useful.

Our analysis of the network model is greatly simplified with the strict assumption that all lakes had identical ecological dynamics and socio-economic parameters. This assumption may be inaccurate in reality, but allows for a simplistic understanding of the potential regimes, and shifts among them. We assume the social norm pressures from the network are dependent on the proportion of cooperators at each lake, when in reality this pressure is also dependent on the population size at each lake. Additionally, explicit weighted network connections can result in coupling between pairs of lakes in which we expect to see scenarios where regime shifts can propagate through the net-

work (Keitt, Lewis, and Holt, 2001). In future extensions of our model these assumptions should be revisited and addition of weighted network connections that are non-uniform should be considered. By relaxing our assumptions on the network model we expect many new and exciting results pertaining to social dynamics and propagation of regime shifts.

The current study shows the importance of the interconnection of ecological and socio-economic dynamics in aquatic systems by portraying the various dynamical outcomes that can occur in the coupled system. Social pressures and ostracism influence the role an individual assumes with respect to environmental issues by adding associated costs. Furthermore, social pressures can lead to favourable regime shifts within a network of lakes giving valuable insight to policies and mitigation strategies. This study builds a valuable framework for future studies of coupled CB and socio-economic systems.

Chapter 4

Niche differentiation in the light spectrum promotes coexistence of phytoplankton species: a spatial modelling approach

4.1 Introduction

Phytoplankton are microscopic photosynthetic aquatic organisms that are the main primary producers of many aquatic ecosystems, and play a pivotal role at the base of the food chain. However, the overabundance of phytoplankton species, or algal blooms as it is often referred to, regularly leads to adverse effects both environmentally and economically (Huisman et al., 2018; Reynolds, 2006; Watson et al., 2015). For these reasons the study of phytoplankton dynamics is important to enhance the positive effects of phytoplankton while limiting any adverse outcomes. Phytoplankton dynamics depend on inorganic materials, dissolved nutrients and light, creating energy for the entire aquatic ecosystem via photosynthesis (Reynolds, 2006). As the world becomes more industrialized anthropogenic sources of nutrients drastically increase, more often than not, resulting in eutrophication. Eutrophication is defined as the excess amount of nutrients in a system required for life. Thus, in eutrophic

conditions light will prevail as the limiting resource for phytoplankton productivity (Paerl and Otten, 2013; Watson et al., 2015).

Resource limitation, whether it be light or nutrient limitation, is bound to lead to competition amongst species. By the competitive exclusion principle, any two species competing for the same resource can not stably coexist. However, several cases exist in nature that seemingly contradict the competitive exclusion principle such as Darwin's finches, North American Warblers, Anoles, and of course phytoplankton. However, these contradictions are easily explained through niche differentiation. The paradox of the plankton (a.k.a Hutchinson paradox) stems from ostensible contradiction between the diversity of phytoplankton typically observed in a water body and the competitive exclusion principle, since phytoplankton superficially compete for the same resources (Hutchinson, 1961). Several modelling attempts have been made to shed light on this paradox by considering spatial heterogeneity throughout the water column (Jiang et al., 2019; Jiang, Lam, and Lou, 2021; Hsu and Lou, 2010). However competitive advantage, leading to exclusion, is gained by a species who has better overall access to light, whether it be through buoyancy regulation or increased turbulent diffusion.

Classically, light has been treated as a single resource and competitive exclusion is regularly predicted by mathematical models (Heggerud, Wang, and Lewis, 2020; Huisman and Weissing, 1994; Wang et al., 2007; Jiang et al., 2019; Jiang, Lam, and Lou, 2021; Hsu and Lou, 2010). However, further investigation shows that phytoplankton species can absorb and utilize wavelengths with varying efficiencies, implying non-uniform absorption spectra (Burson et al., 2018; Luimstra et al., 2020; Holtrop et al., 2021; Stomp et al., 2007a). A species' absorption spectrum measures the amount of light absorbed, of a

specific wavelength, by the species. Figure 4.1 gives examples of absorption spectra for four different species of phytoplankton. These differences between the absorption spectra imply niche differentiation among species and can, in part, help to explain Hutchinson's paradox.

Light limitation in aquatic systems occurs through several different mechanisms. For instance, incident light can be variable due to atmospheric attenuation, Rayleigh scattering and the solar incidence angle. All of these factors contribute to the amount of light that enters the water column. Moreover, light is attenuated by molecules and organisms as it penetrates through the vertical water column. Typically this attenuation is modelled using Lambert-Beer's law which assumes an exponential form of light absorbance by water molecules and seston (suspended organisms, minerals, compounds, gilvin, tripton and etc.). However, the amount of light attenuated is not strictly uniform with respect to wavelengths. For example, pure water absorbs green and red wavelengths more than blue, giving water its typical bluish tone whereas waters rich in gilvin, that absorb blue light, typically appear yellow. Additionally, as mentioned, phytoplankton species' absorption spectra are non-uniform across the light spectrum thus contributing to the variable light attenuation. Because absorption depends on wavelength, the available light profile can change drastically throughout the depth of the water column, giving rise to water colour and another mechanism for species persistence. For these reasons modelling of phytoplankton dynamics should explicitly consider light and its availability throughout the water column.

Several attempts have been made to study phytoplankton competition and dynamics. Single species models have been well established and give good understanding of the governing dynamics of phytoplankton in general (Heggerud,

Wang, and Lewis, 2020; Hsu and Lou, 2010; Du and Mei, 2011; Shigesada and Okubo, 1981). These studies include various modelling approaches including stoichiometric modelling (Heggerud, Wang, and Lewis, 2020), non-local reaction-diffusion equations (Hsu and Lou, 2010; Du and Mei, 2011) and complex limnological interactions (Zhang et al., 2021). Non-local reaction diffusion equations are beneficial to the study of phytoplankton population because they are capable of capturing light availability after attenuation throughout the water column, modelling diffusion and buoyancy/sinking of phytoplankton, and there exists a myriad of mathematical tools and theories to aid in their analysis. One such mathematical theory that we utilize in this chapter is the monotone dynamical systems theory popularized by Smith (Smith, 1995). The theory of monotone dynamical systems is a powerful tool to study the global dynamics of a complex competition system as utilized in (Jiang et al., 2019; Jiang, Lam, and Lou, 2021; Hsu and Lou, 2010).

In this chapter we extend spatially explicit mathematical models for phytoplankton dynamics to consider competition amongst phytoplankton species with niche differentiation in the absorption spectrum (Jiang et al., 2019; Jiang, Lam, and Lou, 2021; Stomp et al., 2007b). Furthermore, the underwater light spectrum, and its attenuation, modelled by the Lambert-Beer law, explicitly depends on the wavelengths of light. In Section 4.2 we propose a reaction-diffusion-advection phytoplankton competition model that non-locally depends on phytoplankton abundance and light attenuation. In Section 4.3 we provide several preliminary results regarding persistence of semi-trivial equilibrium via the associated linearized eigenvalue problem. In Section 4.4 we introduce an index to serve as a proxy for the level of niche differentiation amongst two species and provide coexistence results based on this index. In the absence of

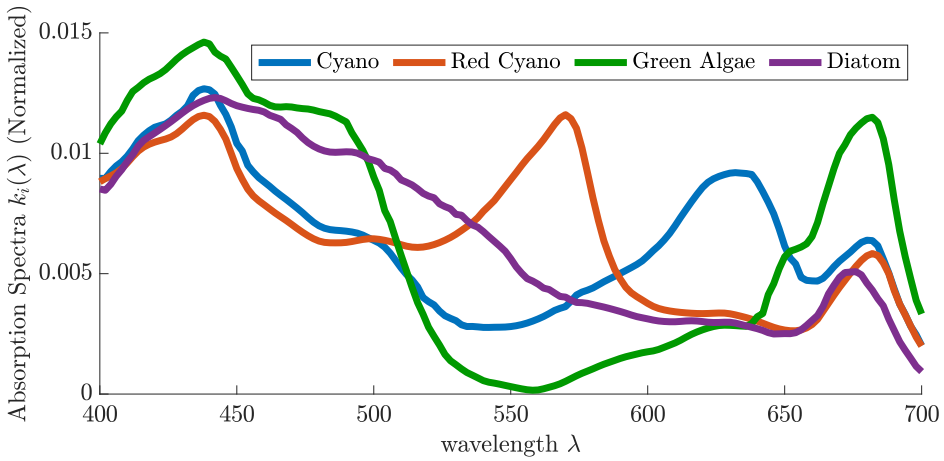

Figure 4.1: Normalized absorption spectra for four phytoplankton species: green cyanobacteria (*Synechocystis* strain), red cyanobacteria (*Synechococcus* strain), green algae (*Chlorella* strain) and a diatom (*Nitzschia* strain) (Luimstra et al., 2020; Burson et al., 2018; Stomp et al., 2007b). The differences of absorption spectra among species imply niche differentiation throughout the spectrum. $k_i(\lambda)$ has units m^2/cell.

niche differentiation we establish the competitive exclusion results based on advantages gained through buoyancy or diffusion. In Section 4.5 we numerically explore how niche differentiation via i) specialist versus specialist competition, and ii) specialist versus generalist competition can overcome competitive advantages that would otherwise result in competitive exclusion. We then consider the case when more than two species compete and show that upon sufficient niche differentiation multiple species can coexist in Section 4.6. Finally, we offer a realistic competition scenario where the absorption spectra of two competing species are given in Figure 4.1 and background attenuation is modelled based on typical oligotrophic, mesotrophic and eutrophic water conditions. This chapter offers a clear explanation of Hutchinson's paradox. That is, through sufficient niche differentiation in the light spectrum phytoplankton species can coexist.

4.2 The model

In this section we extend a two species non-local reaction-diffusion-advection model proposed in several papers (Jiang et al., 2019; Jiang, Lam, and Lou, 2021; Hsu and Lou, 2010; Du and Hsu, 2010) to consider niche differentiation via absorption spectra separation. The PDE system assumes sufficient nutrient conditions so that light is the only factor limiting phytoplankton growth. However, the species are capable of utilizing incident wavelengths at varying efficiency as highlighted in Figure 4.1 (Stomp et al., 2007b; Burson et al., 2018; Luimstra et al., 2020; Holtrop et al., 2021). Because of the attenuation of light through the vertical water column, the diffusivity of the phytoplankton and the potential for buoyancy regulation (advection) the system is spatially explicit. That is, let x denote the vertical depth within the water column then $u(x,t)$ and $v(x,t)$ are the population density of competing phytoplankton species at depth x and time t. We generalize the model in (Jiang et al., 2019; Jiang, Lam, and Lou, 2021; Stomp et al., 2007b) to the spatial context:

$$\begin{cases} \partial_t u_1 = D_1 \partial_x^2 u_1 - \alpha_1 \partial_x u_1 \\ \qquad\qquad\qquad +[g_1(\gamma_1(x,t)) - d_1(x)]u_1 & \text{for } 0 < x < L,\ t > 0, \\ \partial_t u_2 = D_2 \partial_x^2 u_2 - \alpha_2 \partial_x u_2 \\ \qquad\qquad\qquad +[g_2(\gamma_2(x,t)) - d_2(x)]u_2 & \text{for } 0 < x < L,\ t > 0, \\ D_i \partial_x u_i(x,t) - \alpha_i u_i(x,t) = 0 & \text{for } x = 0, L,\ t > 0,\ i = 1,2 \\ u_1(x,0) = u_{1,0}(x),\ u_2(x,0) = u_{2,0}(x) & \text{for } 0 < x < L. \end{cases} \tag{4.1}$$

In this model the turbulent diffusion coefficients $D_1, D_2 > 0$ and sinking/buoyancy coefficients $\alpha_1, \alpha_2 \in \mathbb{R}$ are assumed to be constants. The functions $d_1(x), d_2(x) \in C([0,L])$ are the death rate of the species at depth x and $\gamma_1(x,t)$ is the number of absorbed photons available for photosynthesis by species u_1

and is given by

$$\gamma_1(x,t) = \int_{400}^{700} a_1(\lambda)k_1(\lambda)I(\lambda,x)\,d\lambda, \tag{4.2}$$

where $k_1(\lambda)$ and $k_2(\lambda)$ are the absorption spectra of species u_1 and u_2, respectively. The absorption spectrum is the proportion of incident photons of a given wavelength absorbed by the cell. The respective quantity $\gamma_2(x,t)$ for species u_2 is similarly defined. For each given wavelength λ, the quantities $a_1(\lambda)$ (resp. $a_2(\lambda)$) converts the absorption spectrum of species u_1, (and u_2) into the action spectrum, or the proportion of absorbed photons used for photosynthesis, of phytoplankton species u_1 (resp. u_2). In many cases photons are absorbed and utilized with similar efficiency, thus we take $a_1(\lambda) = a_2(\lambda) = 1$. Sunlight enters the water column with an incident light spectrum $I_{\text{in}}(\lambda)$ and $I(\lambda,x,t)$ is the light intensity of wavelength λ at depth x which, according to the Lambert-Beer's law, given by

$$I(\lambda,x,t) = I_{\text{in}}(\lambda)\exp\left[-K_{BG}(\lambda)x - k_1(\lambda)\int_0^x u_1(y,t) - k_2(\lambda)\int_0^x u_2(y,t)\right], \tag{4.3}$$

where $K_{BG}(\lambda)$ is the background attenuation of the incident light spectrum. We also assume that the specific growth rates $g_1(s)$ and $g_2(s)$ of both phytoplankton species are increasing and saturating functions of the number of absorbed photons available for photosynthesis, i.e.

$$g_1(0) = 0, \quad g_1'(s) > 0 \quad \text{for } s \geq 0, \quad g_1(+\infty) < +\infty, \tag{4.4}$$

and the same holds for $g_2(s)$ as well. A common choice of growth function is the Monod equation given by

$$g_i(s) = \frac{\bar{g}_i s}{\overline{\gamma}_i + s}, \qquad i = 1,2, \tag{4.5}$$

where $\bar{g}_i$ is the maximal growth rate of species u_i and $\overline{\gamma}_i$ is the half-saturation coefficient. Lastly, we assume there is no net movement across the upper and

lower boundaries of the water column, resulting in the zero-flux boundary conditions for $x = 0, L$.

4.3 Preliminary results

In this section we establish several preliminary theorems for coexistence and competitive exclusion that are used throughout the paper. From the eigenvalue we establish conditions for a single species to persist in absence of a competitor. From this we are able to use the associated linearized eigenvalue problem to establish a sufficient condition for coexistence and competitive exclusion.

Throughout the chapter we refer the readers to the following definition and condition. Define the functions $f_i : [0, L] \times [0, \infty) \times [0, \infty) \to \mathbb{R}$ by:

$$f_i(x, p_1, p_2) = g_i\left(\int_{400}^{700} a_i(\lambda)k_i(\lambda)I_{\text{in}}(\lambda)\exp\left[-K_{BG}(\lambda)x - \sum_{j=1}^{2} k_j(\lambda)p_j\right]\right) - d_i(x). \tag{4.6}$$

Then it is not hard to verify that, for $i = 1, 2$, the function f_i satisfies

(H) $\dfrac{\partial f_i}{\partial p_j} < 0$ and $\dfrac{\partial f_i}{\partial x} < 0$ for $(x, p_1, p_2) \in [0, L] \times \mathbb{R}^2_+,\ j = 1, 2.$

Although we only consider the autonomous system here, we remark that most of the theoretical results can be generalized to the case of a temporally periodic environment.

4.3.1 Persistence of a single species

In this subsection we fully characterize the long-term dynamics of system (4.1) in the absence of competition, i.e when $u_{1,0} \equiv 0$ or $u_{2,0} \equiv 0$. We begin by defining the following eigenvalue problem.

Definition 4.1. *For given constants $D > 0$ and $\alpha \in \mathbb{R}$, and given function $h(x) \in C([0, L])$, define $\mu(D, \alpha, h) \in \mathbb{R}$ to be the principal eigenvalue of the following boundary value problem:*

$$\begin{cases} 0 = D\partial_{xx}\phi - \alpha\partial_x\phi + h(x)\phi + \mu\phi & \text{for } (x,t) \in [0,L] \times \mathbb{R}^+, \\ D\partial_x\phi - \alpha\phi = 0 & \text{for } (x,t) \in \{0,L\} \times \mathbb{R}^+. \end{cases} \tag{4.7}$$

We now introduce two useful lemmas concerning some characteristics of the principal eigenvalue $\mu(D, \alpha, h)$ of (4.7).

Lemma 4.2. *Suppose either (i) $\int_0^L e^{\alpha x/D} h(x) dx > 0$, or (ii) $\int_0^L e^{\alpha x/D} h(x) dx = 0$, and $h'(x)$ is not identically zero in $[0, L]$, then $\mu(D, \alpha, h) < 0$.*

Proof. Let $\tilde{\phi}(x) = e^{-\alpha x/D}\phi(x)$, where ϕ is a principal eigenfunction of $\mu(D, \alpha, h)$, and satisfies $\phi > 0$ in $[0, L]$. Then (4.7) can be rewritten as

$$\begin{cases} 0 = D\partial_x \left(e^{\alpha x/D} \partial_x \tilde{\phi} \right) + e^{\alpha x/D}(h(x) + \mu)\tilde{\phi} & \text{for } (x) \in [0,L], \\ \partial_x \tilde{\phi} = 0 & \text{for } (x) \in \{0,L\}. \end{cases} \tag{4.8}$$

Notice that $\tilde{\phi} > 0$ in $[0, L]$, by the strong maximum principle. One can divide the above equation by $\tilde{\phi}$ and integrate over $[0, L]$ to get

$$\begin{aligned} 0 &= D \int_0^L \frac{1}{\tilde{\phi}} \partial_x \left(e^{\alpha x/D} \partial_x \tilde{\phi} \right) dx + \int_0^L e^{\alpha x/D}(h(x) + \mu)\, dx, \\ &= -D \int_0^L \partial_x \left(\frac{1}{\tilde{\phi}} \right) \left(e^{\alpha x/D} \partial_x \tilde{\phi} \right) dx + \int_0^L e^{\alpha x/D}(h(x) + \mu)\, dx, \\ &= D \int_0^L e^{\alpha x/D} \frac{|\partial_x \tilde{\phi}|^2}{\tilde{\phi}^2}\, dx + \int_0^L e^{\alpha x/D}(h(x) + \mu)\, dx. \end{aligned}$$

Note that we used the Neumann boundary condition of $\tilde{\phi}$ to perform the integrate by parts in the second equality. Hence,

$$-\mu \int_0^L e^{\alpha x/D}\, dx = D \int_0^L e^{\alpha x/D} \frac{|\partial_x \tilde{\phi}|^2}{\tilde{\phi}^2}\, dx + \int_0^L e^{\alpha x/D} h(x)\, dx. \tag{4.9}$$

Suppose to the contrary that $\mu \geq 0$, then it follows from (4.9) that $\int_0^L e^{\alpha x/D} h(x)\, dx \leq 0$. Hence, case (i) is impossible, and we must have case (ii),

which implies

$$\int_0^L e^{\alpha x/D} \frac{|\partial_x \tilde{\phi}|^2}{\tilde{\phi}^2}\, dx = \int_0^L e^{\alpha x/D} h(x)\, dx = 0.$$

Hence, $\partial_x \tilde{\phi} \equiv 0$ which by (4.8) implies either $\tilde{\phi} \equiv 0$ or $h(x) \equiv 0$, which leads to a contradiction. □

Lemma 4.3. *If $h(x) \in C^1([0, L])$ satisfies $h'(x) < 0$ in $[0, L]$, then*

(a) $\dfrac{\partial \mu}{\partial \alpha}(D, \alpha, h) > 0$ *for any* $D > 0$ *and* $\alpha \in \mathbb{R}$.

(b) $\dfrac{\partial \mu}{\partial D}(D, \alpha, h) > 0$ *for any* $D > 0$ *and* $\alpha \leq 0$.

(c) *If* $\mu(D_0, \alpha_0, h) = 0$ *for some* D_0 *and* $\alpha_0 \geq h(0)L$, *then* $\frac{\partial \mu}{\partial D}(D_0, \alpha_0, h) < 0$.

Proof. Assertion (a) follows from Jiang et al. (2019, Lemma 4.8), while assertions (b) and (c) follow from Jiang et al. (2019, Lemma 4.9). □

In the following we call $E_1 = (\tilde{u}_1, 0)$ and $E_2 = (0, \tilde{u}_2)$ the exclusion equilibria. The eigenvalue problem given in Definition 4.1 is well associated to the system (4.1) linearized around E_1 or E_2. The main result of this section is given below and provides a condition for the existence and attractiveness of the semi-trivial solutions E_1 and E_2. They are consequences of the monotone dynamical system theory and derived from the results in (Jiang et al., 2019).

Proposition 4.4. *Suppose*

(P) $\mu(D_i, \alpha_i, f_i(x, 0, 0)) < 0$ *for* $i = 1, 2$.

Then the system (4.1) *has two non-negative equilibria* $E_1 = (\tilde{u}_1, 0)$ *and* $E_2 = (0, \tilde{u}_2)$. *Moreover,* E_1 *(resp.* E_2*) attracts all solutions of* (4.1) *with initial condition* $(u_{1,0}, u_{2,0})$ *such that*

$$u_{1,0} \geq, \not\equiv 0 \quad \textit{and} \quad u_{2,0} \equiv 0 \quad (\text{resp.} \quad u_{1,0} \equiv 0 \quad \textit{and} \quad u_{2,0} \geq, \not\equiv 0).$$

Proof. See Jiang et al. (2019, Proposition 3.11). □

By applying Lemma 4.2 the following corollary gives an explicit condition for **(P)**.

Corollary 4.5. *Let f_i be defined in* (4.6)*. If*

$$\int_0^L e^{\alpha_i x/D_i} f_i(x,0,0)\,dx > 0 \quad \text{for } i = 1,2, \tag{4.10}$$

then **(P)** *holds and the conclusions of Proposition 4.4 concerning the existence and attractivity of semi-trivial solutions E_1 and E_2 hold.*

In terms of the physical parameters, (4.10) reads

$$\int_0^L e^{\alpha_i x/D_i} g_i \left(\int_{400}^{700} a_i(\lambda) k_i(\lambda) I_{\text{in}}(\lambda) e^{-K_{BG}(\lambda)x} \right) dx > \int_0^L e^{\alpha_i x/D_i} d_i(x)\,dx, \tag{4.11}$$

giving an explicit condition for the attractivity and existence of the exclusion equilibrium E_1 and E_2.

4.3.2 Coexistence in two species competition

We now consider the outcomes of a two species competition and establish sufficient conditions for coexistence. We begin by connecting the system (4.1) to the general theory of monotone dynamical systems, allowing for the study of global dynamics (Smith, 1995). For this purpose, consider the cone $\mathcal{K} = \mathcal{K}_1 \times (-\mathcal{K}_1)$, where

$$\mathcal{K}_1 = \left\{ \phi \in C([0,L]) \,:\, \int_0^x \phi(y)\,dy \geq 0 \quad \text{for all } x \in [0,L] \right\}. \tag{4.12}$$

The cone $\mathcal{K}$ has non-empty interior, i.e. $\operatorname{Int}\mathcal{K} = (\operatorname{Int}\mathcal{K}_1) \times (-\operatorname{Int}\mathcal{K}_1)$, where

$$\operatorname{Int}\mathcal{K}_1 = \left\{ \phi \in \mathrm{C}([0,\mathrm{L}]) \,:\, \phi(0) > 0 \int_0^{\mathrm{x}} \phi(\mathrm{y})\,\mathrm{dy} > 0 \quad \text{for all } \mathrm{x} \in [0,\mathrm{L}] \right\}. \tag{4.13}$$

For $i = 1, 2$, let $(u_i(x,t), v_i(x,t))$ be two sets of solutions of (4.1) with initial conditions $(u_{i,0}(x), v_{i,0}(x))$. Since f_1 and f_2 satisfy **(H)**, it follows by Jiang et al. (2019, Corollary 3.4) that

$$(u_{2,0}-u_{1,0}, v_{2,0}-v_{1,0}) \in \mathcal{K}\backslash\{(0,0)\} \Rightarrow (u_{2,0}-u_{1,0}, v_{2,0}-v_{1,0})(\cdot,t) \in \operatorname{Int} K \quad \forall t > 0.$$

In other words, the system (4.1) generates a semiflow that is strongly monotone with respect to the cone $\mathcal{K}$. It follows from the property of monotone dynamical systems that the long-time dynamics of the system (4.1) can largely be determined by the local stability of the equilibrium.

We now characterize the local stability of E_1.

Proposition 4.6 ((Jiang et al., 2019, Proposition 4.5))**.** *Suppose the parameters are chosen such that* **(P)** *holds, i.e. the two species system has two exclusion equilibria* $E_1 = (\tilde{u}_1, 0)$ *and* $E_2 = (0, \tilde{u}_2)$*.*

(a) *The equilibria* E_1 *is linearly stable (resp. linearly unstable) if* $\mu_u > 0$ *(resp.* $\mu_u < 0$*), where*

$$\mu_u := \mu(D_2, \alpha_2, f_2(x, \int_0^x \tilde{u}_1(y)\, dy, 0)). \tag{4.14}$$

(b) *The equilibria* E_2 *is linearly stable (resp. linearly unstable) if* $\mu_v > 0$ *(resp.* $\mu_v < 0$*), where*

$$\mu_v := \mu(D_1, \alpha_1, f_1(x, \int_0^x \tilde{u}_2(y)\, dy, 0)). \tag{4.15}$$

Proof. We only prove assertion (a), since assertion (b) follows by a similar argument. To determine the local stability of the exclusion equilibrium E_1, we consider the associated linearized eigenvalue problem at $E_1 = (\tilde{u}_1, 0)$, which is

given by

$$\begin{cases} D_1\phi_{xx} - \alpha_1\phi_x + f_1(x, \int_0^x \tilde{u}_1(y)\,dy, 0)\phi \\ \quad -\tilde{u}_1 g_1'(\gamma_1)[A_{11}(x)\int_0^x \phi(y)\,dy + A_{12}(x)\int_0^x \psi(y)\,dy] + \mu\phi = 0 & \text{in } [0,L], \\ D_2\psi_{xx} - \alpha_2\psi_x + f_2(x, \int_0^x \tilde{u}_1(y)\,dy, 0)\psi + \mu\psi = 0 & \text{in } [0,L], \\ D_1\phi_x - \alpha_1\phi = D_2\psi_x - \alpha_2\psi = 0 & \text{for } x = 0, L, \end{cases} \tag{4.16}$$

where

$$A_{ij}(x) = \int_{400}^{700} k_i(\lambda) I(\lambda, x) k_j(\lambda)\,d\lambda \tag{4.17}$$

and

$$\gamma_i(x) = \int_{400}^{700} k_i(\lambda) I_{in}(\lambda) \exp\left[-K_{BG}(\lambda)x - k_1(\lambda)\int_0^x \tilde{u}_1(y)\,dy\right] d\lambda. \tag{4.18}$$

Recall that we have taken $a_i \equiv 1$. Thanks to the monotonicity of the associated semiflow, the linearized problem (4.16) has a principal eigenvalue in the sense that $\mu_1 \leq \operatorname{Re}\mu$ for all eigenvalues μ of (4.16), and that the corresponding eigenfunction can be chosen in $\mathcal{K} \setminus \{(0,0)\}$. In particular, E_1 is linearly stable (resp. linearly unstable) if $\mu_1 > 0$ (resp. $\mu_1 < 0$).

Next, we apply Jiang et al. (2019, Proposition 4.5), which says that

$$\operatorname{sgn}\mu_1 = \operatorname{sgn}\mu_u,$$

where μ_u, given in (4.14), is the principal eigenvalue of the second equation in (4.16). Hence, E_1 is linearly stable (resp. linearly unstable) if $\mu_1 > 0$ (resp. $\mu_1 < 0$). □

If both E_1 and E_2 exist we can conclude the existence of a positive equilibrium solution by the following proposition.

Proposition 4.7. *Assume* **(P)** *so that the semi-trivial equilibrium, E_1 and E_2 exist. Suppose further that*

$$\mu_u \cdot \mu_v > 0,$$

then (4.1) *has at least one positive equilibrium* $(\hat{u}_1, \hat{u}_2)$.

Proof. If $\mu_u \cdot \mu_v > 0$, then the exclusion equilibria E_1 and E_2 are either both linearly stable or both linearly unstable. The existence of positive equilibrium thus follows from Hess (1991, Remark 33.2 and Theorem 35.1). □

In case both E_1 and E_2 are linearly unstable, both species persist in a robust manner.

Proposition 4.8. *Assume* **(P)** *so that the semi-trivial equilibria E_1, E_2 exist. Suppose*

$$\mu_u < 0 \quad \text{and} \quad \mu_v < 0, \tag{4.19}$$

(i.e. both E_1 and E_2 are unstable) then the following holds.

(i) *There exists $\delta_0 > 0$ that is independent of the initial data such that*

$$\liminf_{t\to\infty} \min_{i=1,2} \int_{0<x<L} u_i(x,t) \geq \delta_0;$$

(ii) *System* (4.1) *has at least one coexistence, equilibrium* $(\hat{u}_1, \hat{u}_2)$ *that is locally asymptotically stable.*

Proof. By (4.19), both exclusion equilibria E_1, E_2 are linearly unstable. The result follows from Hess (1991, Theorems 33.3). □

The signs of the principal eigenvalue μ_u and μ_v are often difficult to determine. We now establish an explicit condition for coexistence. To this end, observe from Corollary 4.5 and (4.11) that a sufficient condition for

$$\mu_v = \mu(D_1, \alpha_1, f_1(x, 0, \int_0^x \tilde{u}_2(y,t)\, dy)) < 0. \tag{4.20}$$

is given by

$$\int_0^L e^{\alpha_1 x/D_1} g_1 \left(\int_{400}^{700} a_1(\lambda) k_1(\lambda) I_{\text{in}}(\lambda) e^{-K_{BG}(\lambda)x - k_2(\lambda)\int_0^x \tilde{u}_2(y,t)\,dy} \right) dx > \int_0^L e^{\alpha_1 x/D_1} d_1(x,t)\,dx. \quad (4.21)$$

For $i = 1, 2$, we will obtain an explicit upper bound for $\int_0^x \tilde{u}_i(y)\,dy$. To this end, define

$$M_i := \inf \Bigg\{ M > 0 : \int_0^x f_i(y, 0, M \int_0^y e^{-\alpha_i z/D_i}\,dz) e^{-\alpha_i y/D_i}\,dy \le 0 \text{ in } [0,L] \times [0,T] \Bigg\}. \quad (4.22)$$

Lemma 4.9. *For $i = 1, 2$,*

$$\int_0^x \tilde{u}_i(y,t)\,dy \le \frac{M_i D_i}{\alpha_i}(1 - e^{-\alpha_i x/D_i}) \quad \textit{for all } (x,t) \in [0,L] \times [0,T].$$

Proof. Indeed, with such a choice of M_i, the function $M_i e^{-\alpha_i x/D_i}$ will then qualify as an super-solution for the single species equation for species i, in the sense of Jiang et al. (2019, Subsection 3.2). Hence, by comparison, we have

$$M_i e^{-\alpha_i x/D_1} - \tilde{u}_i \in \mathcal{K}_1,$$

that is,

$$\int_0^x \tilde{u}_i(y,t)\,dy \le \int_0^x M_i e^{-\alpha_i y/D_i}\,dy = \frac{M_i D_i}{\alpha_i}(1 - e^{-\alpha_i x/D_i}) \quad \text{for } (x) \in [0,L].$$

This completes the proof. □

By the above discussion, a sufficient condition for (4.21) is

$$\int_0^L e^{\alpha_1 x/D_1} g_1 \left(\int_{400}^{700} a_1(\lambda) k_1(\lambda) I_{\text{in}}(\lambda,t) e^{-K_{BG}(\lambda)x - k_2(\lambda)\frac{M_2 D_2}{\alpha_2}(1 - e^{-\alpha_2 x/D_2})} \right) dx > \int_0^L e^{\alpha_1 x/D_1} d_1(x)\,dx. \quad (4.23)$$

Furthermore, an upper bound, M_1, for $\int_0^x \tilde{u}_1(y,t)\,dy$ is easily established following the arguments in Lemma 4.9. Thus, a sufficient condition for (4.19) is given by (4.23) and

$$\int_0^L e^{\alpha_2 x/D_2} g_2\left(\int_{400}^{700} a_2(\lambda)k_2(\lambda)I_{\text{in}}(\lambda)e^{-K_{BG}(\lambda)x - k_1(\lambda)\frac{M_1 D_1}{\alpha_1}(1-e^{-\alpha_1 x/D_1})}\right) dx > \int_0^L e^{\alpha_2 x/D_2} d_2(x)\,dx. \quad (4.24)$$

Thus, we have concluded an explicit form for a sufficient condition for coexistence.

4.4 Extreme cases of niche differentiation: competitive outcomes

In this section we explicitly consider niche differentiation via the absorption spectra, $k_1(\lambda)$ and $k_2(\lambda)$. We consider the extreme cases of differentiation, where the niches either completely overlap, or do not overlap at all. Sufficient conditions for exclusion or coexistence are given. We establish the following definition to serve as a proxy for niche differentiation.

Definition 4.10.

$$\mathcal{I}_S(k_1,k_2) = \frac{\|k_1 - k_2\|_{L^1}}{\|k_1\|_{L^1} + \|k_2\|_{L^1}}. \quad (4.25)$$

We refer to $\mathcal{I}_S(k_1,k_2)$ as the index of spectrum differentiation among two species. If the two species have the same absorption spectra then $\mathcal{I}_S(k_1,k_2) = 0$ whereas if their absorption spectra are completely non-overlapping then $\mathcal{I}_S(k_1,k_2) = 1$.

4.4.1 Coexistence for disjoint niches

We first consider the case where competition for light is at the extreme minimum, i.e.

$$\mathcal{I}_S(k_1(\lambda), k_2(\lambda)) = 1,$$

and give a sufficient condition for coexistence. First, we assume the absorption spectra are completely non-overlapping, which promotes coexistence.

Corollary 4.11. *Suppose* **(P)** *holds, so that the exclusion equilibria E_1 and E_2 exist. If, in addition, $\mathcal{I}_S(k_1(\lambda), k_2(\lambda)) = 1$, then the coexistence results of Proposition 4.8 hold.*

Proof. First note that $\mathcal{I}_S(k_1(\lambda), k_2(\lambda)) = 1$ is equivalent to $k_1(\lambda)k_2(\lambda) = 0$ for each λ. It suffices to observe that

$$f_2(x, \int_0^x \tilde{u}_1(y)\, dy, 0) = f_2(x, 0, 0), \quad \text{and} \quad f_1(x, 0, \int_0^x \tilde{u}_2(y)\, dy) = f_1(x, 0, 0)$$

so that **(P)** implies $\mu_u < 0$ and $\mu_v < 0$. The rest follows from Proposition 4.8. □

4.4.2 Competitive exclusion for identical niches

Next, we consider the case where the absorption spectra overlap completely ($\mathcal{I}_S(k_1, k_2) = 0$) to consider maximum competition for light. Recall our assumption that $a_1(\lambda) = a_2(\lambda) = 1$. Thus, Under these assumptions we establish the competitive exclusion scenarios in the following theorems.

Theorem 4.12. *(Jiang et al., 2019, Theorem 2.2) Assume $\mathcal{I}_S(k_1, k_2) = 0$. Let $D_1 = D_2$, $\alpha_1 < \alpha_2$, $f_1 = f_2$, $d_1 = d_2$. If* **(P)** *holds (i.e. both E_1, E_2 exist), then the first species u_1 drives the second species u_2 to extinction, regardless of initial condition.*

Proof. By the theory of monotone dynamical systems (see, e.g. Hsu, Smith, and Waltman (1996, Theorem B) and Lam and Munther (2016, Theorem 1.3)), it suffices to establish the linear instability of the exclusion equilibria E_2, and the non-existence of positive equilibria.

Step 1. We claim that $\mu_v < 0$, i.e. $E_2 = (0, \tilde{u}_2)$ is linearly unstable.

Recall that $\tilde{u}_2$ is the unique positive solution to

$$\begin{cases} D_2\tilde{u}_{xx} - \alpha_2\tilde{u}_x + f_2(x, 0, \int_0^x \tilde{u}(y)\,dy)\tilde{u} = 0 & \text{in } [0, L], \\ D_2\tilde{u}_x - \alpha_2\tilde{u} = 0 & \text{for } x = 0, L, \end{cases}$$

where f_2 is given in (4.6) and satisfies **(H)**. Since $\tilde{u}_2$ can be regarded as a positive eigenfunction, we deduce that $\mu(D_2, \alpha_2, f_2(x, 0, \int_0^x \tilde{u}_2(y)\,dy)) = 0$.

Since $D_1 = D_2$, $\alpha_1 < \alpha_2$ and $f_1 = f_2$, we may apply Lemma 4.3(a) to get

$$\mu_v = \mu(D_1, \alpha_1, f_1(x, 0, \int_0^x \tilde{u}_2(y)\,dy)) < \mu(D_2, \alpha_2, f_2(x, 0, \int_0^x \tilde{u}_2(y)\,dy)) = 0.$$

Thus E_2 is linearly unstable.

Step 2. The system (4.1) has no positive equilibrium.

Suppose to the contrary that (u_1^*, v_*^2) is a positive equilibrium, then deduce that

$$\mu(D_i, \alpha_i, f_i(x, \int_0^x u_1^*(y)\,dy, \int_0^x u_2^*(y)\,dy)) = 0 \quad \text{for } i = 1, 2,$$

where the respective eigenfunctions are given by $u_i^* > 0$. However, this is in contradiction with Lemma 4.3(a). □

Theorem 4.13. *(Jiang et al., 2019, Theorem 2.3) Assume $\mathcal{I}_S(k_1, k_2) = 0$. Let $D_1 < D_2$, $\alpha_1 = \alpha_2 \geq [f_1(L, 0, 0) - d_1]L$, $f_1 = f_2$, $d_1 = d_2$. If (**P**) holds (i.e. both E_1, E_2 exist), then the faster species u_2 drives the slower species u_1 to extinction, regardless of initial condition.*

Proof. By the theory of monotone dynamical systems (see, e.g. Hsu, Smith, and Waltman (1996, Theorem B) and Lam and Munther (2016, Theorem 1.3)),

it suffices to establish the linear instability of the exclusion equilibria E_2, and the non-existence of positive equilibria.

Step 1. We claim that $\mu_v < 0$, i.e. $E_2 = (0, \tilde{u}_2)$ is linearly unstable.

Recall that $\tilde{u}_2$ is the unique positive solution to

$$\begin{cases} D_2\tilde{u}_{xx} - \alpha_2\tilde{u}_x + f_2(x, 0, \int_0^x \tilde{u}(y)\,dy)\tilde{u} = 0 & \text{in } [0, L], \\ D_2\tilde{u}_x - \alpha_2\tilde{u} = 0 & \text{for } x = 0, L, \end{cases}$$

where f_2 is given in (4.6) and satisfies **(H)**. Since $\tilde{u}_2$ can be regarded as a positive eigenfunction, we deduce that $\mu(D_2, \alpha_2, f_2(x, 0, \int_0^x \tilde{u}_2(y)\,dy)) = 0$.

Since $D_1 < D_2$, $\alpha_1 = \alpha_2 \geq [f_1(0, 0, 0)]L$ and $f_1 = f_2$, we may apply Lemma 4.3(c) to get

$$\mu_v = \mu(D_1, \alpha_1, f_1(x, 0, \int_0^x \tilde{u}_2(y)\,dy)) < \mu(D_2, \alpha_2, f_2(x, 0, \int_0^x \tilde{u}_2(y)\,dy)) = 0.$$

(Otherwise there exists $D_3 \in (D_1, D_2)$ such that $\mu(D_3, \alpha_1, f_1(x, 0, \int_0^x \tilde{u}_2(y)\,dy)) = 0$ and $\frac{\partial\mu}{\partial D}(D_3, \alpha_1, f_1(x, 0, \int_0^x \tilde{u}_2(y)\,dy)) \leq 0$.) Thus E_2 is linearly unstable.

Step 2. The system (4.1) has no positive equilibrium.

Suppose to the contrary that (u_1^*, v_*^2) is a positive equilibrium, then deduce that

$$\mu(D_i, \alpha_i, f_i(x, \int_0^x u_1^*(y)\,dy, \int_0^x u_2^*(y)\,dy)) = 0 \quad \text{for } i = 1, 2,$$

where the respective eigenfunctions are given by $u_i^* > 0$. However, this is in contradiction with Lemma 4.3(c). □

Theorem 4.14. *(Jiang et al., 2019, Theorem 2.4) Assume $\mathcal{I}_S(k_1, k_2) = 0$. Let $D_1 < D_2$, $\alpha_1 = \alpha_2 \geq 0$, $f_1 = f_2$, $d_1 = d_2$. If (**P**) holds (i.e. both E_1, E_2 exist), then the slower species u_1 drives the faster species u_2 to extinction, regardless of initial condition.*

Proof. The proof is the same as Theorem 4.12, where we use Lemma 4.3(b) instead of Lemma 4.3(a). □

Note that $\mathcal{I}_S(k_1, k_2) = 0$ is equivalent to $k_1(\lambda) = k_2(\lambda)$ for all λ. The above theorems can be summarized into a single sentence: Suppose both species consume light in the same efficiency, the species that remains at, or moves towards the water's surface at a higher rate will exclude the other species. That is, if both species are sinking either the one sinking slower, or with higher diffusion will exclude. If both species are buoyant then the less buoyant species or the more diffusive species will be excluded.

4.5 Numerical investigation of niche differentiation

To complement the theorems established in Sections 4.3 and 4.4 we present several numerical simulations that show the relatively large regions in parameter space that allow for coexistence. We numerically explore two main competition scenarios: 1) Niche differentiation through specialization of different wavelengths and 2) niche differentiation through specialist and generalist (with respect to light) competition. In each scenario we consider the intermediate levels of niche differentiation evaluated by $\mathcal{I}_S(k_1, k_2)$.

4.5.1 Competition outcomes for specialization on separate parts of the light spectrum

Here we assume that the two species with relatively narrow niches are competing for light. We numerically show that through niche differentiation a species can resist competitive exclusion. These results imply that without the assumption of $\mathcal{I}_S(k_1, k_2) = 0$ the theorems in Section 4.4.1 do not hold and that when species' absorption spectra do not significantly overlap, coexistence is readily observed.

To investigate the extent of which niche differentiation promotes coexistence we consider two scenarios. First, we let $k_1(\lambda)$ and $k_2(\lambda)$ be unimodal functions that are horizontal translations of each other. That is, let $k_i(\lambda)$ be given by a truncated Gaussian distribution (-75,75) with mean zero and variance σ denoted by $g^*(\lambda)$. Then $k_i(\lambda) = g^*(\lambda - \lambda_{i,0})$ where $\lambda_{i,0} \in [475, 625]$ is the peak absorbance in the visible light spectrum. This ensures $k_1(\lambda)$ and $k_2(\lambda)$ have the same L^1 norm and are identical in their degree of specialization, giving no advantage through the absorption spectra alone. We then allow the peaks of $k_2(\lambda)$ to vary along the light spectrum ($\lambda_{2,0} \in [475, 625]$) while keeping $k_1(\lambda)$ fixed $\lambda_{1,0} = 475$. By varying the peak of $k_2(\lambda)$ we in-turn vary $\mathcal{I}_S(k_1, k_2)$. Examples of this are shown graphically with the blue curves in Figure 4.2c. We also assume that the incident light $I_{in}(\lambda)$ is a unimodal function with peak incidence at $\lambda = \lambda_I$. To understand the implications incident light has on coexistence we alter λ_I in the range $[450, 650]$). Two example curves for $I_{in}(\lambda)$ are shown in orange in figure 4.2c.

Second, we alter $\mathcal{I}_S(k_1, k_2)$ as above but with a uniform incident light function and allow a competitive advantage through advection by altering the advection rate of species u_2, α_2. Recall that u_1 has competitive advantage when $\alpha_1 < \alpha_2$, and u_2 has competitive advantage when $\alpha_1 > \alpha_2$ (see Theorem 4.12).

By varying $\mathcal{I}_S(k_1, k_2)$ we can then explore the competitive outcomes for various scenarios where exclusion is known to occur when niche differentiation is not considered. Furthermore, we show that the incident light function ($I_{in}(\lambda)$), together with the absorption spectra $k_1(\lambda), k_2(\lambda)$, play important roles in the competition outcome by allowing competitive advantages to be overcome, or diminished. Our results of this section are shown in Figure 4.2 and are sum-

marized by the following key points:

P1: Competitive advantage is given to the species whose absorption spectrum overlaps the most with the available incident light. However, significant niche differentiation can promote coexistence for scenarios where incident light does not strongly favour a single species.

P2: Competitive exclusion through an advection advantage can be overcome by niche differentiation.

Figure 4.2a shows the coexistence regions when varying the location of the peak of incident light and the distance between the two absorption spectra $k_1(\lambda)$ and $k_2(\lambda)$ (given by $\mathcal{I}_S(k_1, k_2)$). The point P2 is justified by the following observations in Figure 4.2a. We see that exclusion is exhibited for extreme values of $\lambda_{1,0} - \lambda_I$ and non-zero $\mathcal{I}_S(k_1, k_2)$. When the values of $\lambda_{1,0} - \lambda_I$ are extreme, one of the species' absorption spectrum overlaps with the incident light significantly more giving it a competitive advantage. However, when the values of $\lambda_{1,0} - \lambda_I$ are intermediate and $\mathcal{I}_S(k_1, k_2)$ then each species has sufficient overlap with the incident light spectrum and any competitive advantage is diminished, promoting coexistence.

Figure 4.2b shows the coexistence region when varying the advection rate of species u_2 (α_2) and the distance between the two absorption spectra $k_1(\lambda)$ and $k_2(\lambda)$ (given by $\mathcal{I}_S(k_1, k_2)$). It was established in Section 4.4.2 that a more buoyant species will exclude the less buoyant species when $\mathcal{I}_S(k_1, k_2) = 0$ and is visualized in Figure 4.2b. However, we observe that for sufficiently large values of $\mathcal{I}_S(k_1, k_2)$ the competitive exclusion caused by advection advantage is overcome and coexistence occurs.

When considering two species with unimodal absorption spectra, it is pos-

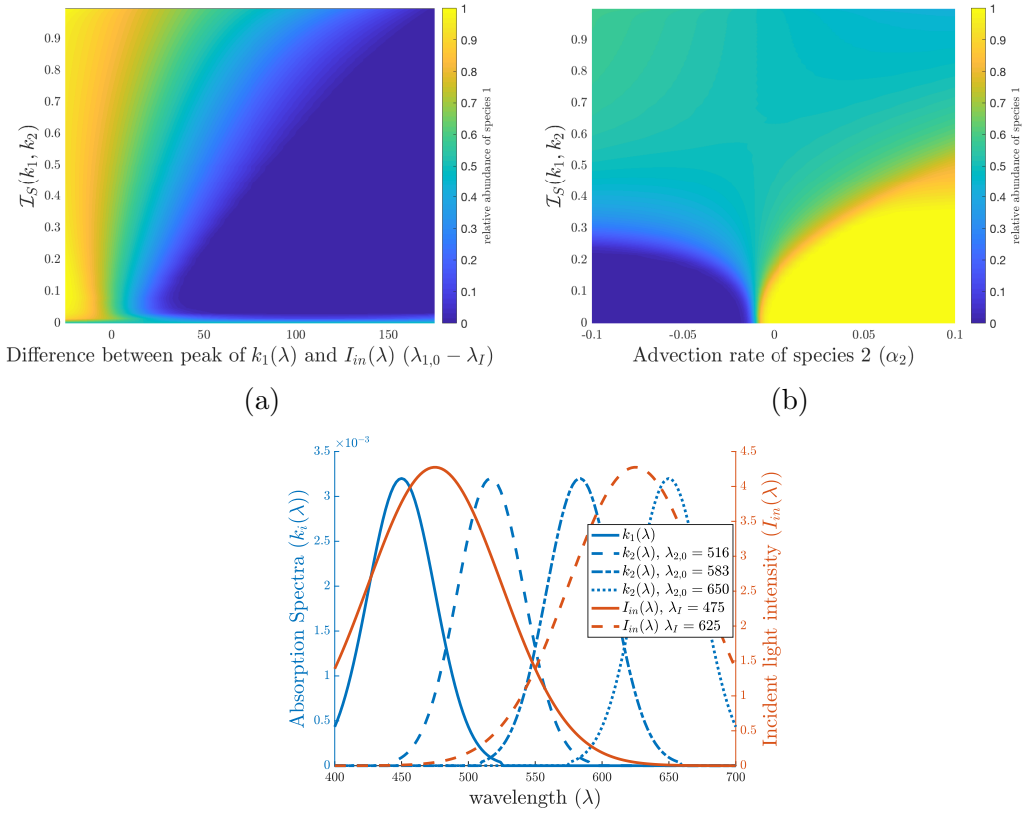

Figure 4.2: (a) and (b) show coexistence regions for two competing species with narrow niches. The heat map is given by $\frac{|u_1|}{|u_1|+|u_2|}$. In (c) we show the shape of $k_i(\lambda)$ for four reference values of $\lambda_{i,0}$ in blue, and $I_{in}(\lambda)$ for two reference values of λ_I in orange. In (a) we show the competition outcome as the distance between $\lambda_{1,0}$ and λ_I is changed, versus the degree of niche differentiation between the two species. In (b) we show the competition outcome as the advection rate, α_2, is changed versus the degree of niche differentiation between the two species under uniform incident light. In (b) we fix $\alpha_1 = -0.01$ m/h. $I_{in}(\lambda)$ has units of photons/m^2·s and $k_i(\lambda)$ is in units of m^2/cell.

sible to overcome competitive exclusion by allowing for niche differentiation in the light spectrum.

4.5.2 Outcomes for generalist versus specialist competition

In this section we numerically explore niche differentiation in the light spectrum through competition between a specialist and a generalist. We say that a generalist species is a species whose absorption spectrum is uniform (or nearly uniform) across all visible wavelengths. Whereas we say a specialist species is one whose absorption spectrum is unimodal or narrow. That is, a specialist absorbs a specific wavelength, or small subset of wavelengths with a higher rate than other wavelengths.

We explore the mechanism of specialist vs. generalist competition in overcoming competitive exclusion by explicitly comparing absorption spectra. We take $k_2(\lambda)$ to be constant (generalist) and choose $k_1(\lambda)$ such that $|k_1(\lambda)| = |k_2(\lambda)|$ in the L^1 norm. We further assume that $k_1(\lambda)$ is given by a truncated normal distribution, between 400 and 700 nm, with a fixed mean. By using the truncated normal distribution for $k_1(\lambda)$ we are able to change the degree of specialization of species 1 by changing the variance of the distribution as shown in Figure 4.3c. We consider two scenarios to analyze the promotion of coexistence via the niche differentiation mechanism of specialist versus generalist competition. First, we assume an unimodal incident light $I_{in}(\lambda)$ as in Figure 4.2a and vary the location of its peak with respect to the peak of the specialists absorption spectrum ($k_1(\lambda)$). Additionally, we vary the degree of specialization of species u_1 by changing the variance of the truncated normal distribution that defines its absorption spectrum. That is, by changing the variance we change the narrowness of its niche and thus change the values of

$\mathcal{I}_S(k_1, k_2)$.

Second, we change $\mathcal{I}_S(k_1, k_2)$ as described above but with a uniform incident light function. We allow a competitive advantage through advection by altering the advection rate of species u_2, α_2. Recall that u_1 has competitive advantage when $\alpha_1 < \alpha_2$, and u_2 has competitive advantage when $\alpha_1 > \alpha_2$(see Theorem 4.12).

By varying $\mathcal{I}_S(k_1, k_2)$ we are able to show the competitive outcomes when niche differentiation via a specialist versus generalist competition is permitted. Our results of this section are shown in Figure 4.3 and can be summarized by the following key points:

P3 Intermediate values of specialization will promote coexistence. Otherwise, the specialist is excluded if its niche is too narrow, or excludes if its niche overlaps with the incident light significantly.

P4 Competitive exclusion through an advection advantage can be overcome by niche differentiation.

In Figure 4.3a we show the relative abundance of species 1 for various degrees of specialization and overlap with the incident light function. Species 1 is a strong competitor for a narrow set of wavelengths, whereas species 2 is a weak competitor for a broad set of wavelengths. When species 1 is highly specialized ($\mathcal{I}_S(k_1, k_2)$ close to one) it strongly out-competes species 2 for a small amount of photons, however species 2 has little competition for the remaining photons and is that able to exclude species 1. Furthermore, if the incident light does not overlap well with species 1 niche then species 1 is faced with limited resource and is thus excluded. On the other hand, for intermediate specialization and relatively small distance between the peaks of $k_1(\lambda)$

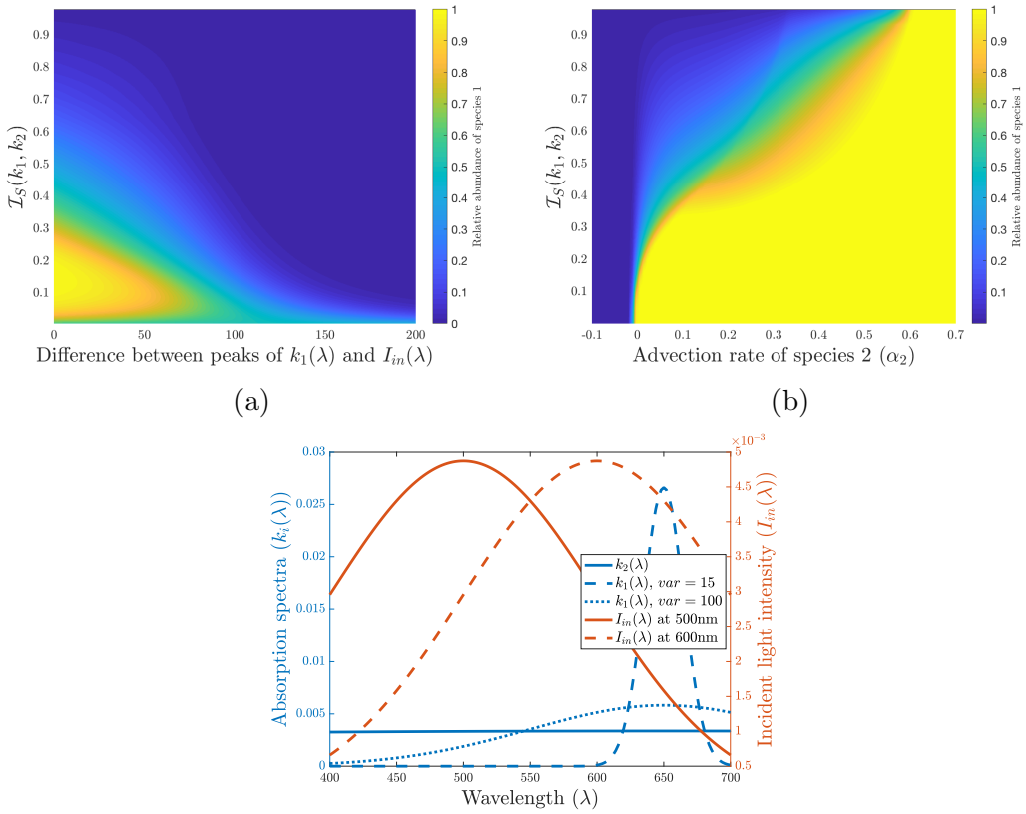

Figure 4.3: (a) and (b) show coexistence regions for a specialist (species 1), competing with a generalist (species 2). The heat map is given by $\frac{|u_1|}{|u_1|+|u_2|}$. In both (a) and (b) we fix $k_2(\lambda)$ and change the specialization of species 1 by flattening or widening the absorption spectrum as shown by the blue lines in (c). In (a) we compare the competition outcome with relation to the distance between the specialists peak absorption and the incident lights peak intensity and the distance between the two absorption spectra. In (b) we vary the generalists advection rate and fix $\alpha_1 = -0.01$ m/h while also adjusting $\mathcal{I}_S(k_1, k_2)$. We take $I_{in}(\lambda)$ to be uniform. In (c) we show samples of the absorption spectra in blue and incident light (for (b)) in orange. $I_{in}(\lambda)$ has units of photons/m^2·s and $k_i()$ is in units of m^2/cell.

and $I_{in}\lambda$ species 1 will out-compete species two for nearly all of the resources and thus excluding species 2. Coexistence is then observed when the specialist tends to a generalist niche ($\mathcal{I}_S(k_1, k_2)$ is close to zero) because weak competition occurs along the entire light spectrum and no significant advantage is given. Additionally, for intermediate values of $\mathcal{I}_S(k_1, k_2)$ and sufficient overlap between incident light and species 1 niche, coexistence is permitted by the balance between the specialist strongly competing for a sufficient but narrow amount of resource and the generalist weakly competing for wide amount of resource that is not utilized by the specialist.

In Figure 4.3b we show the relative abundance of species 1 for various degrees of specialization and advection rates of species 2 under uniform incident light. Recall in Theorem 4.12 we show that competitive exclusion occurs if one species has an advection advantage and there is no niche differentiation. Here we see that niche differentiation in the light spectrum ($\mathcal{I}_S(k_1, k_2) > 0$) allows for coexistence even though one species has a competitive advantage through advection. We note that if the generalist has an advection advantage then it will always exclude the specialist. On the other hand, if the specialist has the advection advantage it will exclude the generalist unless it becomes too specialized, in which case sufficient light is available for the generalist and either coexistence occurs, or in the case of extreme specialization, the specialist is excluded. Furthermore, there is a region where the competitive advantage of advection is so strong for the specialist that it will always exclude the generalist.

4.6 Coexistence of N species

In this section, we will show the possibility of coexistence of N species, for any number $N \geq 1$. We numerically verify this result by considering competition among 5 species with varying advection rates.

We introduce the N-species model analogous to (4.1):

$$\begin{cases} \partial_t u_i = D_i \partial_x^2 u_i - \alpha_i \partial_x u_i \\ \qquad\qquad +[g_i(\gamma_i(x,t)) - d_i(x)]u_i & \text{for } 0 < x < L,\ 1 \leq i \leq N, \\ D_i \partial_x u_i(x,t) - \alpha_i u_i(x,t) = 0 & \text{for } x = 0,\ L,\ t > 0,\ 1 \leq i \leq N, \\ u_i(x,0) = u_{i,0}(x) & \text{for } 0 < x < L,\ 1 \leq i \leq N, \end{cases} \tag{4.26}$$

where $D_i > 0$, $\alpha_i \in \mathbb{R}$ and d_i are the diffusion rate, buoyancy coefficient and death rate of the i-th species, respectively. The function $\gamma_i(x,t)$ is the number of absorbed photons available for photosynthesis by the i-th species and is given by

$$\gamma_i(x,t) = \int_{400}^{700} a_i(\lambda) k_i(\lambda) I(\lambda, x)\, d\lambda, \tag{4.27}$$

and

$$I(\lambda, x) = I_{\text{in}}(\lambda) \exp\left[-K_{BG}(\lambda) x - \sum_{i=1}^{N} k_i(\lambda) \int_0^x u_i(y,t)\, dy \right]. \tag{4.28}$$

Theorem 4.15. *Let the incident light spectrum $I_{in}(\lambda)$ be positive on an open set in $[400, 700]$. Then for each $N \geq 1$, there exists a choice of $\{a_i(\lambda)\}_{i=1}^N$ and $\{k_i(\lambda)\}_{i=1}^N$ such that all N species can persist in (4.26), i.e. for any positive initial condition, the solution $(u_i)_{i=1}^N$ of (4.26) satisfies*

$$\liminf_{t\to\infty} \left[\inf_{0\leq x\leq L} u_i(x,t) \right] > 0 \quad \text{for each } 1 \leq i \leq N.$$

Proof. By the hypotheses of the theorem, there exists λ_1, λ_2 such that $400 \leq \lambda_1 < \lambda_2 \leq 700$ and that $I_* := \inf_{[\lambda_1,\lambda_2]} I_{in}(\lambda) > 0$. Let $\{J_i\}_{i=1}^N$ be a partition

of $[\lambda_1, \lambda_2]$, and choose the functions $k_i(\lambda)$ such that $\operatorname{Supp} k_i \subset \operatorname{Int} J_i$. In particular, the support of k_i do not overlap. Hence,

$$I(\lambda, x) = I_{\text{in}}(\lambda) \exp\left[-K_{BG}(\lambda)x - k_i(\lambda)\int_0^x u_i(y,t)\,dy\right] \quad \text{in } \operatorname{Supp} k_i,$$

and the i-th species u_i satisfies effectively a single species equation

$$\begin{cases} \partial_t u_i = D_i\partial_x^2 u_i - \alpha_i \partial_x u_i + [g_i(\gamma_i(x,t)) - d_i(x)]u_i & \text{for } 0 < x < L,\ t > 0, \\ D_i\partial_x u_i - \alpha_i \partial_x u_i = 0 & \text{for } x = 0, L,\ t > 0, \end{cases}$$

with γ_i being independent of u_j for $j \neq i$. Precisely,

$$\gamma_i(x,t) = \int_{400}^{700} a_i(\lambda)k_i(\lambda)I_{\text{in}}(\lambda)\exp\left[-K_{BG}(\lambda)x - k_i(\lambda)\int_0^x u_i(y,t)\,dy\right]\,d\lambda. \tag{4.29}$$

Next, we choose a_i to be a positive constant (independent of λ) such that

$$\mu(D_i, \alpha_i, g_i(a_i \int k_i(\lambda)I_{in}(\lambda)\exp(-K_{BG}(\lambda)x)) - d_i) < 0.$$

This is possible since

$$\lim_{a\to\infty} \mu(D_i, \alpha_i, g_i(a \int k_i(\lambda)I_{in}(\lambda)\exp(-K_{BG}(\lambda)x)) - d_i) = -\infty.$$

It then follows from Jiang et al. (2019, Proposition 3.11) that, provided $u_i(\cdot, 0) \not\equiv 0$, we have

$$u_i(\cdot, t) \to \tilde{u}_i \quad \text{in } C([0, L]),\ \text{as } t \to \infty,$$

where $\tilde{u}_i$ is the unique positive solution of

$$\begin{cases} D_i\partial_x^2 u_i - \alpha_i \partial_x u_i + [g_i(\tilde{\gamma}_i(x)) - d_i]u_i & \text{for } 0 < x < L, \\ D_i\partial_x u_i(x) - \alpha_i u_i(x) = 0 & \text{for } x = 0,\ L, \end{cases}$$

with $\tilde{\gamma}_i(x)$ given by

$$\hat{\gamma}_i(x) = \int_{400}^{700} a_i(\lambda)k_i(\lambda)I_{\text{in}}(\lambda)\exp\left[-K_{BG}(\lambda)x - k_i(\lambda)\int_0^x \tilde{u}_i(y,t)\,dy\right]\,d\lambda.$$

This completes the proof. □

We now explore the possibility of coexistence of five phytoplankton species under niche differentiation. We assume that all five species $D_i = D_j$, $d_i = d_j$, and $g_i = g_j$ for all i, j and that $\alpha_1 = 0.01$ with $\alpha_i = i \cdot \alpha_1$ for all i. We assume that all absorption spectra are unimodal given by the truncated normal distribution. Each $k_i(\lambda)$ is a horizontal translation of one another. We alter the peak absorption (or the mean) to allow for niche differentiation similarly to Figures 4.2c and 4.3c. We also assume that the incident light ($I_{in}(\lambda)$) is unimodal with peak absorption at 575 nm allowing for a competitive advantage. We compare the relative abundances of the five species at time t defined by

$$\bar{u}_i(t) = \frac{|u_i(x,t)|_{L^1}}{\sum_{j=1}^{N} |u_j(x,t)|_{L^1}}, \tag{4.30}$$

where the L^1 norm here is with respect to space. We further denote the relative abundance at steady steady as $\bar{u}_i^*$. In addition we define the N species niche differentiation index as

$$\mathcal{I}_i = \frac{1}{N-1} \sum_{j=1, j\neq i}^{N} \mathcal{I}_S(k_i, k_j). \tag{4.31}$$

Consequently the average niche differentiation index is given as

$$\bar{\mathcal{I}} = \frac{1}{N} \sum_{i}^{N} \mathcal{I}_i. \tag{4.32}$$

Figure 4.4 gives the numerical results of the five species competition. Competitive exclusion occurs when niche differentiation is not sufficient and the species with the lowest advection rate (species 1) excludes all other species. However, as the niche differentiation is increased, more species are able to coexist and all five species can persist when niche differentiation is significant enough.

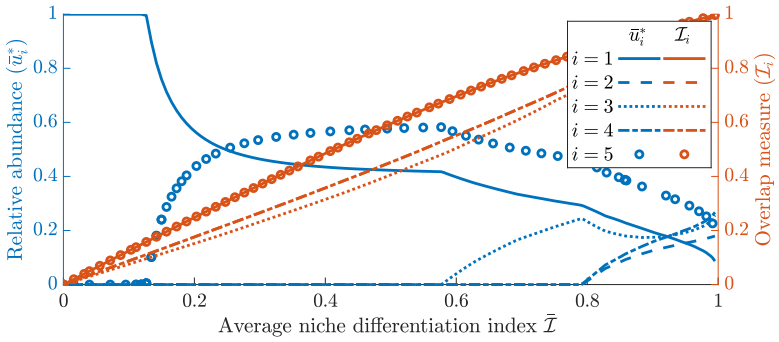

(a)

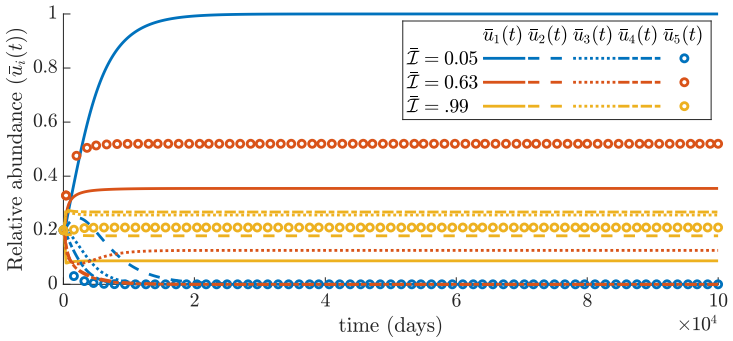

(b)

Figure 4.4: (a) gives the steady state relative abundance ($\bar{u}_i^*$) of 5 competing species and their respective overlap measure defined in (4.31). The x-axis is labelled as the average overlap measure $\bar{\mathcal{I}}$ given in (4.32). (b) gives the time dynamics of the relative abundance of the 5 competing species ($\bar{u}_i(t)$) for three different values of $\bar{\mathcal{I}}$. All other model parameters are the same among species expect the competitive advantage obtained through buoyancy: $\alpha_1 = 0.01$ m/h, $\alpha_2 = 0.02$ m/h, $\alpha_3 = 0.03$ m/h, $\alpha_4 = 0.04$ m/h, $\alpha_5 = 0.05$ m/h.

4.7 Red versus Green cyanobacteria competition

In this section we numerically explore a more realistic competition scenario between two phytoplankton species. To incorporate realistic biological assumptions into our model we consider two main things. First, the background attenuation of water is not uniform across the visible light spectrum and depends on the amount of dissolved and particulate organic matter (gilvin and tripton) in the water. Second, the absorption spectra considered in Section 4.5 are idealistic for investigation and are not typical for a phytoplankton species. Thus, in this section we consider absorption spectra given empirically as in Figure 4.1 and explore competition outcomes.

4.7.1 Background attenuation in water

Here we introduce a reasonable function to more accurately model background attenuation of water, gilvin and tripton and phytoplankton.

We divide the background attenuation into two parts to account for the attenuation of pure water and gilvin and tripton

$$K_{BG}(\lambda) = K_W(\lambda) + K_{GT}(\lambda), \tag{4.33}$$

where $K_W(\lambda)$ is readily found in the literature and shown in Figure 4.5 (Stomp et al., 2007b; Pope and Fry, 1997). $K_{GT}(\lambda)$ is also found in literature and is given by the following form (Kirk, 2010):

$$K_{GT}(\lambda) = K_{BG}(\lambda_r)\exp(-S(\lambda - \lambda_r)), \tag{4.34}$$

where λ_r is a reference wavelength with a known turbidity and S is the slope of the exponential decline. Following literature we take reasonable values for

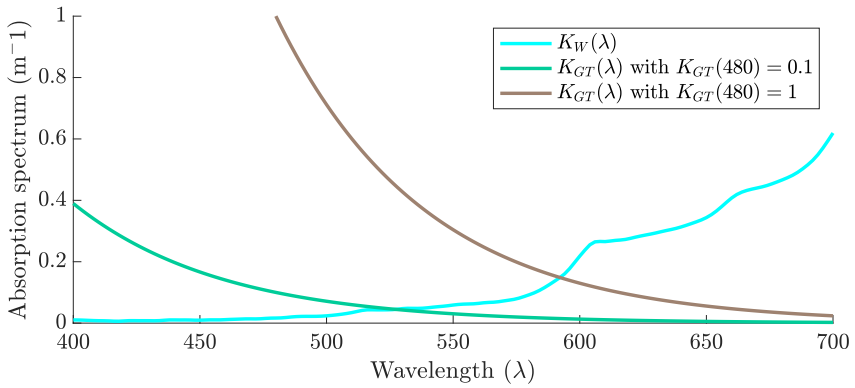

Figure 4.5: The absorption spectrum of pure water (Pope and Fry, 1997; Stomp et al., 2007b), and the absorption spectra for lakes with gilvin and tripton concentrations representative of oligotrophic or mesotrophic waters ($K_{BG}(480) = 0.1\text{m}^{-1}$), and eutrophic waters ($K_{BG}(480) = 1)\text{m}^{-1}$.

each of these variables with $S = 0.017nm^{-1}$ as in (Stomp et al., 2007b) and referenced in (Kirk, 2010). We fix our reference wavelength, λ_r, to be $480nm$. Typically, the background attenuation is larger in lakes that are highly polluted due to the high concentrations of gilvin and tripton. For this reason, we use $K_{BG}(480)$ as a proxy for the pollution level and trophic state of the lake, and vary $K_{BG}(480)$ between $0.1 - 3\text{m}^{-1}$. That is, low $K_{BG}(480)$ values correspond to oligotrophic, clear lakes whereas high $K_{BG}(480)$ values correspond to eutrophic, turbid lakes. Lastly, we consider the absorption spectra of red and green cyanobacteria species. In Figure 4.1 we see that there are significant differences in the absorption spectra between the phytoplankton allowing for niche differentiation.

4.7.2 Competition outcomes of red and green cyanobacteria

We now show the steady state outcome for when red and green cyanobacteria compete for light in lakes of various trophic states.

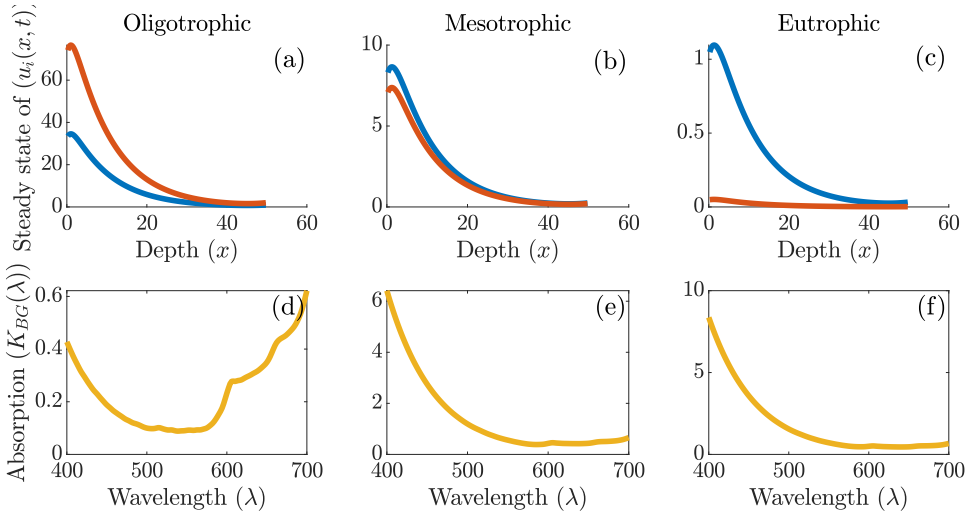

Figure 4.6: (a)-(c) show steady state outcomes of competition between green cyanobacteria, $u_1(x,t)$ (shown in blue), and red cyanobacteria, $u_2(x,t)$ (shown in red), for various amounts of gilvin and tripton that correspond to oligotrophic, mesotrophic and eutrophic states, respectively. (d)-(f) shows the background absorption for those states with $K_{BG}(480) = 0.1\text{m}^{-1}$, $K_{BG}(480) = 1.1\text{m}^{-1}$, $K_{BG}(480) = 2\text{m}^{-1}$, respectively.

In Figure 4.6 the competition outcome between green cyanobacteria (*Synechocystis* strain) and red cyanobacteria (*Synechococcus* strain) is shown.

In Figure 4.1, the green cyanobacteria absorption spectra is shown in blue and the red cyanobacteria is shown in red. Their absorption spectra are sufficiently different so that niche differentiation occurs. That is, the green cyanobacteria mainly absorbs light in the orange-red ranges, whereas the red cyanobacteria absorbs more green light. Both species absorb blue light similarly. Thus, the light availability throughout the water column plays an important role in competition outcome. In Figures 4.6(d)-(f) we see that as the gilvin and tripton concentrations increase (shifting from oligotrophic to mesotrophic to eutrophic) the background absorption's shift to absorb proportionally more blue and green light, leaving proportionally more orange and red light available. This shift in available light then modifies the competitive

outcome, where red cyanobacteria clearly dominate in the oligotrophic state whereas green cyanobacteria dominate in the eutrophic state, even though the two species coexist in both situations.

4.8 Discussion

In this chapter we explore niche differentiation along the light spectrum by extending well established reaction-diffusion equations in Section 4.2 (Jiang et al., 2019; Hsu and Lou, 2010; Du and Mei, 2011). We model competition between species allowing for various scenarios of incident light availability and absorption spectra. Our main theoretical results, found in Section 4.3, stem from the theory of monotone dynamical systems and include the existence and attractiveness of the equilibrium. These results give a condition for when the semi-trivial equilibria exist and are locally stable and as an extension provide a condition for coexistence. The condition for coexistence is made explicit and offers direct biological interpretations based on model parameters. Niche differentiation is introduced in Section 4.4 by allowing the absorption spectra ($k_i(\lambda)$) of competing species to change. We consider the case where the competing species niches are completely disjoint and provide a condition for coexistence. Furthermore we consider the case when competing species occupy the same niche and provide competitive outcomes based on transport related parameters and show that species who are able to stay closer to the surface through either advection or turbulent diffusion will competitively exclude. These results give a base to study the impacts niche differentiation will have on coexistence outcomes in Section 4.5.

We show numerically, in Section 4.5, a myriad of mechanisms in which coexistence can occur. When two specialists compete competitive advantages

given by advection or incident light can be overcome when niche differentiation is sufficient as shown in Figures 4.2. We see that competitive exclusion occurs when the overlap between the incident light and a species' absorption spectrum is large. In this case the competitive advantage is gained through the incident light as in Figure 4.2a. In addition, competitive advantage due to advection can always be overcome for sufficient niche differentiation as in Figure 4.2b. Similarly, for specialist versus generalist competition coexistence readily occurs for intermediate degrees of niche differentiation. However, if the specialist has too narrow of a niche, then the overlap between their absorption spectrum and the incident light is small which is detrimental to their growth as shown in Figure 4.3. In both competitive cases niche differentiation in the light spectrum is enough to overcome competitive exclusion, offering exciting insight towards an explanation of the paradox of the plankton.

Furthermore, to fully explore the ecological diversity and the paradox of the plankton we consider a system with N competing species. First, we show analytically that coexistence of N species is possible under sufficient niche differentiation and proper action conversion spectrum ($a_i(\lambda)$) functions. This result further explains the paradox of the plankton through niche differentiation and can furthermore offer a suggestion to the evolutionary strategies phytoplankton may take in partitioning the light spectrum and utilization of wavelengths for growth (Holtrop et al., 2021). Second, we provide numerical simulations for a five species competition scenario with an advection and incident light advantage present. Under small niche differentiation competitive exclusion occurs. However, as the niches are separated more species are able to coexist even though competitive advantages are present.

Lastly, we numerically study the competition dynamics for absorption spec-

tra and background attenuation functions that are representative of real species and ecosystems. We consider the absorption spectra of green and red cyanobacteria species and explore the competitive outcome as it depends on the nutrient status, or turbidity of the ecosystem as shown in Figure 4.6. Typically speaking, clear lakes host higher abundances of red cyanobacteria whereas green cyanobacteria out-compete in turbid, eutrophic lakes (Stomp et al., 2007b). This is consistent with our competition simulation, showing the potential usefulness of our model in understanding phytoplankton competition.

In this chapter we explored a potential explanation to the paradox of the plankton by allowing for niche differentiation in the light spectrum. To do this we made several simplifying assumptions about the biological system, such as our sufficient nutrient assumption. It is well known that phytoplankton dynamics heavily depend on nutrient dynamics (Whitton, 2012; Klausmeier, Litchman, and Levin, 2004; Reynolds, 2006). Thus, in order to fully understand phytoplankton future attempts at modelling niche differentiation should also allow for the explicit consideration of nutrient and nutrient uptake dynamics. We have also assumed that our model parameters are constant in time. This in general is not true for ecological systems, and in particular those that explicitly consider light. Light availability is periodic on the time scales of days and, in addition, periodic seasonally. In addition to light, parameters related to mortality and motility can depend on water temperature and thus change seasonally. This type of oscillatory forcing can significantly change dynamics and especially when considering transient dynamics (Hastings et al., 2018).

Even though our model can be improved in various ways, our results are strikingly biologically intuitive and are consistent with the current state of the

biological literature regarding the paradox of the plankton and niche differentiation in the light spectrum (Stomp et al., 2007b; Burson et al., 2019; Luimstra et al., 2020). Our work contributes to the deeper understanding of niche differentiation and phytoplankton competition and can be used as a foundation for future studies of phytoplankton dynamics and predictive modelling. In conclusion, our study shows that niche differentiation can promote coexistence of phytoplankton species in a robust way, thus supporting one explanation of the Hutchinson's paradox.

Chapter 5

Concluding remarks

In this thesis I studied the ecological complexity of phytoplankton dynamics by using the mathematical theories of singular perturbations, stability, bifurcations, and monotone dynamical systems. Furthermore, the complexity of phytoplankton dynamics is broken down into palatable questions pertaining to transient dynamics of phytoplankton, management strategies based on the coupled human interactions with phytoplankton, and competitive outcomes of phytoplankton species based on niche differentiation. In this concluding chapter I summarize the results, and discuss how they fit into the current state of the literature and the overarching theme of this thesis. I further discuss the limitations of the work and suggest future avenues of research.

5.1 Summary

In Chapter 2 I studied the transient dynamics of a stoichiometric cyanobacteria model with an explicit consideration of available resources. In much of the stoichiometric literature a natural separation of timescales occurs and the application of the quasi steady state approximation is seen (Peace, Poteat, and Wang, 2016; Wang et al., 2007; Wang, Kuang, and Loladze, 2008; Sterner and Elser, 2002). However, under the quasi steady state assumption transient

dynamics are easily lost, hence motivating this chapter. I considered a mechanistically derived stoichiometric cyanobacteria model that depends on light and phosphorus for growth in which the internal nutrient dynamics occur on a faster time scale than the external nutrient concentration and population dynamics. Due to the separation of timescales I was able to study both the fast and slow subsystems individually. The dynamics on the fast subsystem show a quick uptake of external nutrients, however the internal nutrient content is limited either by the initial amount of nutrient in the system or by the maximum amount of nutrient a cell can store. The dynamics on the slow scale are then restricted to one of two sub-manifolds corresponding to light limitation and nutrient limitation. The dynamics switch from light limitation to nutrient limitation after some period of time signalling the collapse of a bloom. Eventually, the dynamics will tend to a stable equilibrium point with cyanobacterial abundance much lower than the peak abundance, provided the initial external nutrient concentration is large. Although the phases of CB dynamics have been well documented (Whitton, 2012; Paerl and Otten, 2013; Merel et al., 2013), the driving mechanisms behind each phase were lacking understanding (Melina Celeste et al., 2017; Wang et al., 2007; Berger et al., 2006). This work offers an in-depth mathematical understanding of each phase, thus in general giving a good understanding of the transient dynamics of CB. In terms of studying the ecological complexity of phytoplankton in general, a comprehension of their transient dynamics builds a necessary and solid footing towards achieving the goal of this thesis.

In Chapter 3 I extended the results and model of Chapter 2 to include socio-economic dynamics that directly influence the nutrient dynamics of a lake system. I modelled the socio-economic component with a game theoretic

approach, deriving probabilities of an individual assuming environmentally favourable strategies based on costs associated with infrastructure, ostracism, social pressure, concern for CB and property value loss. In the case of a single lake model, I showed that bistability occurs between two regimes corresponding to high CB abundance with low cooperation and low CB abundance with high cooperation. I provided graphical analysis in the phase line and phase plane and discuss the socio-economic parameter values that lead to regime shifts. The bistability in the single lake case is consistent with the literature on lake pollution and eutrophication and moreover to hysteresis phenomena observed in many ecological systems (Carpenter, 2005; Suzuki and Iwasa, 2009; Keitt, Lewis, and Holt, 2001; Grover, 2003), however I have shown these classical bistability results apply to cyanobacteria as well. In the case of a network of lakes that are connected socially I also observed multiple steady states. Each steady state can considered as a regime corresponding to the following scenarios: the entire network is in a high cooperation state, the entire network is in a low cooperation state, or the network has some lakes in a high cooperation state and some in low cooperation state. To my knowledge, this tristability is a new result showing additional complexities that can arise in the interaction between phytoplankton and humans. I gained further insights into the regimes and their basins of attraction through a series of bifurcation plots and phase plane analysis. This work was pivotal in achieving the overarching goal of this thesis by explicitly considering the role humans and their contributions to eutrophication have on phytoplankton dynamics in general. An understanding of the coupled socio-economic and ecological dynamics of phytoplankton gets me one step closer to the broader understanding of the ecological complexities behind phytoplankton dynamics.

Lastly, in Chapter 4 I studied coexistence of competing phytoplankton species and explained their observed diversity. The diversity of phytoplankton species is superficially a contradiction of the competitive exclusion principle. However, upon investigation into the species specific utilization of light I was able to discern that niche differentiation occurs. Thus, in order to mathematically establish the robust coexistence of species that is readily observed in ecology, but rarely in mathematical models with limited nutrient competition (Jiang et al., 2019; Yoshiyama et al., 2009; Burson et al., 2019; Jiang, Lam, and Lou, 2021), I introduced non-uniformity of wavelength utilization and explored the dynamics of phytoplankton in unmixed ecosystems by considering a spatially explicit model. I gave conditions, through application of monotone dynamical systems theory, for competitive exclusion and coexistence and extend the results to look at the promotion of coexistence through niche differentiation numerically. I considered two key competitive scenarios of specialist vs. specialist competition and specialist vs. generalist competition. In each case niche differentiation is enough to overcome competitive exclusion where advantages are gained through advection or diffusion. I furthermore showed that niche differentiation can give rise to competitive advantages depending on the profile of available light. The results of this chapter are mostly consistent with the current state of the literature on niche differentiation (Luimstra et al., 2020; Burson et al., 2019; Stomp et al., 2007b), but offer a deeper understanding of the robustness of the coexistence regions and their dependencies on other model parameters. This work sheds light on the modelling efforts required for meaningful results of phytoplankton diversity and competition with explicit dependence on light availability and utilization. Furthermore, in the context of this thesis, these results contribute to another key aspect of the

overall understanding of the complexities involved in phytoplankton dynamics.

5.2 Discussion

Although the work in this thesis improves the overall understanding of phytoplankton dynamics some shortcomings and areas of future work should be noted. To start, in Chapters 2 and 3 many simplifications using singular perturbation theory were utilized. Although these simplifications were necessary for the analysis I performed they do take away some key aspects of the dynamics. That is, parameters of small orders are neglected in the analysis but still contribute to the ecological dynamics. Furthermore, certain model components are mechanistic in nature, but are simple and may not accurately represent the true ecological process. To circumvent this potential issue the results and modelling efforts should be supported with a more rigorous use of empirical evidence. I further note that in the case of socio-economic dynamics a serious gap exists in human choice data limiting the applicability of such models, although this gap is slowly being filled in certain ecological systems (e.g. Lim and Neary (2016) and Grêt-Regamey, Huber, and Huber (2019)). Nevertheless, these results should not be deemed inaccurate due to these simplifications and shortcomings, but rather perceived as approximations of the full system with similar qualitative behaviour.

The dependence of phytoplankton on nutrients is irrefutable and in this thesis I considered at most one nutrient to govern their dynamics. In cases of strong nutrient limitation this assumption may be reasonable, but in general phytoplankton growth synergistically depends on multiple nutrients simultaneously (Klausmeier, Litchman, and Levin, 2004; Branco et al., 2018). In my modelling efforts the assumption of single nutrient limitation (in Chapters 2

and 3), or no nutrient limitation (in Chapter 4) does not apply in general and future extensions of this work should include more possibilities for nutrient dynamics. Recent literature (Paerl and Barnard, 2020) and my speculation suggests that this consideration will mathematically yield more possibilities for coexistence if the species do not compete for nutrients equivalently and bloom formations will persist for longer periods of time if light becomes limiting. In addition, the complex internal nutrient cycles that occur naturally are not considered in this work. Typically speaking, processes of sedimentation and resuspension of nutrients within a water body can drastically alter aquatic nutrient concentrations (Paerl, 2014; Carpenter, 2005). Furthermore, human interactions and anthropogenic disturbances can perturb such natural nutrient cycles (Yan et al., 2021; Loewen et al., 2020) further complicating nutrient dynamics. Given the highly dependent nature of phytoplankton on nutrients, a clear direction for future modelling involves a more rigorous consideration of nutrient cycles.

Another key aspect that is missing from my modelling efforts is the consideration of many environmental factors, such as temperature and seasonality (White and Hastings, 2020; Giani et al., 2020). These factors have been shown to be highly influential in phytoplankton growth and species diversity. For example, species compositions and abundance are shown to change temporally and are speculated to be driven by climatic and geographical factors (Loewen, Vinebrooke, and Zurawell, 2021; Ralston and Moore, 2020). Furthermore, the majority of temperate lakes have seasons with ice cover, drastically changing the ecosystem for an extended period of time. Moving forward, considerations of seasonality are crucial and have started to be considered in the modelling literature with striking results (Zhao, Yuan, and Wang,

2020; Chen et al., 2017; Wollrab et al., 2021).

Phytoplankton are primary producers located at the base of most aquatic food webs. Their dynamics heavily influence food web dynamics and furthermore, are often coupled via producer-grazer interactions and various interactions with higher trophic levels. In this thesis I neglected the effects of grazing and trophic interactions on phytoplankton dynamics, but recent studies suggest that they are critical for a holistic understanding of phytoplankton dynamics. For example, empirical data suggests that algae dynamics strongly influence grazer dynamics (Starke et al., 2021; Bell et al., 2019; Elser et al., 2016) while several studies show the complex dynamics of producer-grazer interactions (Urabe et al., 2002; Hall, 2009; Peace and Wang, 2019; Camara, Yamapi, and Mokrani, 2019). The added component of trophic interactions in phytoplankton dynamics increases the ecological complexity, but may be necessary in order to deepen the understanding of phytoplankton dynamics in future work.

In conclusion, this thesis contributes to the scientific field of phytoplankton dynamics in a broad way by filling in the gaps in the modelling literature and expanding on the ecological understanding. I have provided detailed analysis of the transient dynamics of cyanobacteria and studied the coupled dynamics between the ecological dynamics of phytoplankton and human interaction. Furthermore, I have used a spatially explicit phytoplankton model to show that niche differentiation in the light spectrum is one potential explanation of the paradox of the plankton. This work has implications for management strategies to mitigate the prevalence of harmful algal blooms, for mathematicians and theoretical ecologists inquiring about the applications of singular perturbation theory, stability and bifurcation theory, and monotone dynami-

cal systems theory, and for expanding the modelling efforts within the framework of ecological stoichiometry. All in all, this thesis has accomplished the goal of gaining understanding of the ecological complexity of phytoplankton dynamics.

Bibliography

Andersen, Tom, James J. Elser, and Dag O. Hessen (2004). "Stoichiometry and population dynamics". *Ecology Letters* 7.9, pp. 884–900.

Beckage, Brian, Katherine Lacasse, Jonathan M. Winter, Louis J. Gross, Nina Fefferman, Forrest M. Hoffman, Sara S. Metcalf, Travis Franck, Eric Carr, Asim Zia, and Ann Kinzig (2020). "The Earth has humans, so why don't our climate models?" *Climatic Change* 163.1, pp. 181–188.

Beisner, BE, DT Haydon, and K. Cuddington (2003). "Alternative stable states in ecology". *Frontiers in Ecology and the Environment* 1.7, pp. 376–382.

Bell, Alex T.C., Dennis L. Murray, Clay Prater, and Paul C. Frost (2019). "Fear and food: Effects of predator-derived chemical cues and stoichiometric food quality on Daphnia". *Limnology and Oceanography* 64.4, pp. 1706–1715.

Berger, Stella A, Sebastian Diehl, Thomas J. Kunz, Dieter Albrecht, Amine M. Oucible, and Sylvie Ritzer (2006). "Light supply, plankton biomass, and seston stoichiometry in a gradient of lake mixing depths". *Limnology and Oceanography* 51.4, pp. 1898–1905.

Bertram, Richard and Jonathan E. Rubin (2017). "Multi-timescale systems and fast-slow analysis". *Mathematical Biosciences* 287, pp. 105–121.

Branco, Pedro, Martijn Egas, James J. Elser, and Jef Huisman (2018). "Eco-evolutionary dynamics of ecological stoichiometry in plankton communities". *American Naturalist* 192.1, E1–E20.

Burson, Amanda, Maayke Stomp, Emma Greenwell, Julia Grosse, and Jef Huisman (2018). "Competition for nutrients and light: testing advances in resource competition with a natural phytoplankton community". *Ecology* 99.5, pp. 1108–1118.

Burson, Amanda, Maayke Stomp, Lisette Mekkes, and Jef Huisman (2019). "Stable coexistence of equivalent nutrient competitors through niche differentiation in the light spectrum". *Ecology* 100.12.

Bury, Thomas M., Chris T. Bauch, and Madhur Anand (2019). "Charting pathways to climate change mitigation in a coupled socio-climate model". *PLoS Computational Biology* 15.6, e1007000.

Camara, B. I., R. Yamapi, and H Mokrani (2019). "Environmental stochastic effects on phytoplankton–zooplankton dynamics". *Nonlinear Dynamics* 96.3, pp. 2013–2029.

Carpenter, Stephen R. (2005). "Eutrophication of aquatic ecosystems: Bistability and soil phosphorus". *Proceedings of the National Academy of Sciences* 102.29, pp. 10002–10005.

Chang, Xiaoyuan, Junping Shi, and Hao Wang (2021). "Spatial modeling and dynamics of organic matter biodegradation in the absence or presence of bacterivorous grazing". *Mathematical Biosciences* 331, p. 108501.

Chen, Ming, Meng Fan, Xing Yuan, and Huaiping Zhu (2017). "Effect of seasonal changing temperature on the growth of phytoplankton". *Mathematical Biosciences and Engineering* 14.5-6, pp. 1091–1117.

Cunningham, Brady R. and Seth G. John (2017). "The effect of iron limitation on cyanobacteria major nutrient and trace element stoichiometry". *Limnology and Oceanography* 62.2, pp. 846–858.

Darvehei, Pooya, Parisa A. Bahri, and Navid R. Moheimani (2018). "Model development for the growth of microalgae: A review". *Renewable and Sustainable Energy Reviews* 97, pp. 233–258.

Diehl, Sebastian, Stella Berger, and Rainer Wöhrl (2005). "Flexible Nutrient Stoichiometry Mediates Environmental". *Ecology* 86.11, pp. 2931–2945.

Downs, Theresa M., Marc Schallenberg, and Carolyn W. Burns (2008). "Responses of lake phytoplankton to micronutrient enrichment: A study in two New Zealand lakes and an analysis of published data". *Aquatic Sciences* 70.4, pp. 347–360.

Droop, M. R. (1968). "Vitamin B12and Marine Ecology. IV. The Kinetics of Uptake, Growth and Inhibition in Monochrysis Lutheri". *Journal of the Marine Biological Association of the United Kingdom* 48.3, pp. 689–733.

Du, Yihong and Sze-Bi Hsu (2010). "On a nonlocal reaction-diffusion problem arising from the modeling of phytoplankton growth". *SIAM Journal on Mathematical Analysis* 42.3, pp. 1305–1333.

Du, Yihong and Linfeng Mei (2011). "On a nonlocal reaction-diffusion-advection equation modelling phytoplankton dynamics". *Nonlinearity* 24.1, pp. 319–349.

Elser, James J., Thomas H. Chrzanowski, Robert W. Sterner, and Kenneth H. Mills (1998). "Stoichiometric Constraints on Food-Web Dynamics: A Whole-Lake Experiment on the Canadian Shield". *Ecosystems* 1, pp. 120–136.

Elser, James J., Marcia Kyle, Jennifer Learned, Michelle L. McCrackin, Angela Peace, and Laura Steger (2016). "Life on the stoichiometric knife-edge: Effects of high and low food C: P ratio on growth, feeding, and respiration in three Daphnia species". *Inland Waters* 6.2, pp. 136–146.

Fair, Kathyrn R, Vadim A Karatayev, Madhur Anand, and Chris Bauch (2021). "Population behavioural dynamics can mediate the persistence of emerging infectious diseases". *medRxiv*.

Farahbakhsh, Isaiah, Chris T. Bauch, and Madhur Anand (2021). "Best response dynamics improve sustainability and equity outcomes in common-pool resources problems, compared to imitation dynamics". *Journal of Theoretical Biology* 509, p. 110476.

Fenichel, Neil (1979). "Geometric Singular Perturbation Theory Ordinary Differential Equations". *Journal of Differential Equations* 31, pp. 53–98.

Fransson, Niklas and Tommy Gärling (1999). "Environmental concern: Conceptual definitions, measurement methods, and research findings". *Journal of Environmental Psychology* 19.4, pp. 369–382.

Giani, Alessandra, Zofia E. Taranu, Gabriela von Rückert, and Irene Gregory-Eaves (2020). "Comparing key drivers of cyanobacteria biomass in temperate and tropical systems". *Harmful Algae* 97.

Grêt-Regamey, Adrienne, Sibyl H. Huber, and Robert Huber (2019). "Actors' diversity and the resilience of social-ecological systems to global change". *Nature Sustainability* 2.4, pp. 290–297.

Griffith, Edward J., Alfred Beeton, Jean M. Spencer, and Dee T. Mitchell (1973). *Environmental phosphorus handbook*. New York: Wiley, p. 718.

Grover, James P. (2003). "The Impact of Variable Stoichiometry on Predator-Prey Interactions: A Multinutrient Approach". *The American Naturalist* 162.1, pp. 29–43.

Hall, Spencer R. (2009). "Stoichiometrically explicit food webs: Feedbacks between resource supply, elemental constraints, and species diversity". *Annual Review of Ecology, Evolution, and Systematics* 40, pp. 503–528.

Hastings, Alan (2010). "Timescales, dynamics, and ecological understanding". *Ecology* 91.12, pp. 3471–3480.

Hastings, Alan (2016). "Timescales and the management of ecological systems". *Proceedings of the National Academy of Sciences of the United States of America* 113.51, pp. 14568–14573.

Hastings, Alan, Karen C. Abbott, Kim Cuddington, Tessa Francis, Gabriel Gellner, Ying-Cheng Lai, Andrew Morozov, Sergei Petrovskii, Katherine Scranton, and Mary Lou Zeeman (2018). "Transient phenomena in ecology". *Science* 361.6406.

Heggerud, Christopher M., Hao Wang, and Mark A. Lewis (2020). "Transient dynamics of a stoichiometric cyanobacteria model via multiple-scale analysis". *SIAM Journal on Applied Mathematics* 80.3, pp. 1223–1246.

Hek, Geertje (2010). "Geometric singular perturbation theory in biological practice". *Journal of Mathematical Biology* 60.3, pp. 347–386.

Hess, Peter (1991). *Periodic-parabolic boundary value problems and positivity*. Harlow: Longman Scientific & Technical, p. 139.

Hessen, Dag O., James J. Elser, Robert W. Sterner, and Jotaro Urabe (2013). "Ecological stoichiometry: An elementary approach using basic principles". *Limnology and Oceanography* 58.6, pp. 2219–2236.

Hodgkin, A. L. and A. F. Huxley (1952). "A quantitative description of membrane current and its application to conduction and excitation in nerve". *Journal of Physiology* 117.4, pp. 500–544.

Hofbauer, Josef and Karl Sigmund (2003). "Evolutionary game dynamics". *Bulletin of the American Mathematical Society* 40.4, pp. 479–519.

Holtrop, Tadzio, Jef Huisman, Maayke Stomp, Levi Biersteker, Jeroen Aerts, Théophile Grébert, Frédéric Partensky, Laurence Garczarek, and Hendrik Jan van der Woerd (2021). "Vibrational modes of water predict spectral niches for photosynthesis in lakes and oceans". *Nature Ecology and Evolution* 5.1, pp. 55–66.

Hsu, S. B., H. L. Smith, and Paul Waltman (1996). "Competitive exclusion and coexistence for competitive systems on ordered Banach spaces". *Transactions of the American Mathematical Society* 348.10, pp. 4083–4094.

Hsu, Sze-Bi and Yuan Lou (2010). "Single phytoplankton species growth with light and advection in a water column". *SIAM Journal on Applied Mathematics* 70.8, pp. 2942–2974.

Hsu, Sze-Bi, Junping Shi, and Feng-Bin Wang (2014). "Further studies of a reaction-diffusion system for an unstirred chemostat with internal storage". *Discrete and Continuous Dynamical Systems - Series B* 19.10, pp. 3169–3189.

Huang, Qihua, Laura Parshotam, Hao Wang, Caroline Bampfylde, and Mark A. Lewis (2013). "A model for the impact of contaminants on fish population dynamics". *Journal of Theoretical Biology* 334, pp. 71–79.

Huang, Qihua, Hao Wang, and Mark A. Lewis (2015). "The impact of environmental toxins on predator-prey dynamics". *Journal of Theoretical Biology* 378, pp. 12–30.

Huisman, Jef, Geoffrey A. Codd, Hans W. Paerl, Bas W. Ibelings, Jolanda M.H. Verspagen, and Petra M. Visser (2018). "Cyanobacterial blooms". *Nature Reviews Microbiology* 16.8, pp. 471–483.

Huisman, Jef and Franz J Weissing (1994). "Light limited growth and competition for light in well mixed aquatic environments: an elementary model". *Ecology* 75.2, pp. 507–520.

Hutchinson, G. E. (1961). "The Paradox of the Plankton". *The American Naturalist* 95.882, pp. 137–145.

Iwasa, Yoh, Yukari Suzuki-Ohno, and Hiroyuki Yokomizo (2010). "Paradox of nutrient removal in coupled socioeconomic and ecological dynamics for lake water pollution". *Theoretical Ecology* 3.2, pp. 113–122.

Iwasa, Yoh, Tomoe Uchida, and Hiroyuki Yokomizo (2007). "Nonlinear behavior of the socio-economic dynamics for lake eutrophication control". *Ecological Economics* 63.1, pp. 219–229.

Jiang, Danhua, King-Yeung Lam, and Yuan Lou (2021). "Competitive exclusion in a nonlocal reaction–diffusion–advection model of phytoplankton populations". *Nonlinear Analysis: Real World Applications* 61, p. 103350.

Jiang, Danhua, King-Yeung Lam, Yuan Lou, and Zhi-Cheng Wang (2019). "Monotonicity and global dynamics of a nonlocal two-species phytoplankton model". *SIAM Journal on Applied Mathematics* 79.2, pp. 716–742.

Kaebernick, Melanie and Brett A. Neilan (2001). "Ecological and molecular investigations of cyanotoxin production". *FEMS Microbiology Ecology* 35.1, pp. 1–9.

Kalff, Jacob. (2002). *Limnology: inland water ecosystems.* Upper Saddle River, NJ: Prentice Hall, p. 592.

Keener, James P. and James Sneyd (1998). *Mathematical Physiology.* Vol. 8. Springer-Verlag New York, p. 1067.

Keitt, Timothy H., Mark A. Lewis, and Robert D. Holt (2001). "Allee effects, invasion pinning, and species' borders". *American Naturalist* 157.2, pp. 203–216.

Kinzig, Ann P., Paul R. Ehrlich, Lee J. Alston, Kenneth Arrow, Scott Barrett, Timothy G. Buchman, Gretchen C. Daily, Bruce Levin, Simon Levin, Michael Oppenheimer, Elinor Ostrom, and Donald Saari (2013). "Social norms and global environmental challenges: The complex interaction of behaviors, values, and policy". *BioScience* 63.3, pp. 164–175.

Kirk, John T.O. (2010). *Light and photosynthesis in aquatic ecosystems.* Third. Cambridge: Cambridge University Press, pp. 1–651.

Klausmeier, Christopher A., Elena Litchman, and Simon A. Levin (2004). "Phytoplankton growth and stoichiometry under multiple nutrient limitation". *Limnology and Oceanography* 49.4, part 2, pp. 1463–1470.

Koch, Florian, Sara Beszteri, Lars Harms, and Scarlett Trimborn (2019). "The impacts of iron limitation and ocean acidification on the cellular stoichiometry, photophysiology, and transcriptome of Phaeocystis antarctica". *Limnology and Oceanography* 64.1, pp. 357–375.

Kong, Jude D., Paul Salceanu, and Hao Wang (2017). "A stoichiometric organic matter decomposition model in a chemostat culture". *Journal of Mathematical Biology* 76, pp. 1–36.

Kong, Jude D., Hao Wang, T. Siddique, J. Foght, Kathleen Semple, Zvonko Burkus, and Mark A. Lewis (2019). "Second-generation stoichiometric mathematical model to predict methane emissions from oil sands tailings". *Science of the Total Environment* 694, p. 133645.

Kuehn, Christian (2015). "Multiple time scale dynamics". *Applied Mathematical Sciences (Switzerland)*. Vol. 191. Springer, pp. 1–814.

Lacroix, Christelle, Eric W. Seabloom, and Elizabeth T. Borer (2017). "Environmental nutrient supply directly alters plant traits but indirectly determines virus growth rate". *Frontiers in Microbiology* 8, p. 2116.

Lam, King-Yeung and Daniel Munther (2016). "A remark on the global dynamics of competitive systems on ordered Banach spaces". *Proceedings of the American Mathematical Society* 144.3, pp. 1153–1159.

Larson, Chad A., Hongsheng Liu, and Sophia I. Passy (2015). "Iron supply constrains producer communities in stream ecosystems". *FEMS Microbiology Ecology* 91.5, p. 41.

Lee, Joung-Hun and Yoh Iwasa (2011). "Tourists and traditional divers in a common fishing ground". *Ecological Economics* 70, pp. 2350–2360.

Lim, Wooyoung and Philip R. Neary (2016). "An experimental investigation of stochastic adjustment dynamics". *Games and Economic Behavior* 100, pp. 208–219.

Loewen, Charlie J.G., Rolf D. Vinebrooke, and Ron W. Zurawell (2021). "Quantifying seasonal succession of phytoplankton trait-environment as-

sociations in human-altered landscapes". *Limnology and Oceanography* 66, pp. 1409–1423.

Loewen, Charlie J.G., Faye R. Wyatt, Colleen A. Mortimer, Rolf D. Vinebrooke, and Ron W. Zurawell (2020). "Multiscale drivers of phytoplankton communities in north-temperate lakes". *Ecological Applications* 30.5, e02102.

Loladze, Irakli, Yang Kuang, and James J. Elser (2000). "Stoichiometry in producer-grazer systems: Linking energy flow with element cycling". *Bulletin of Mathematical Biology* 62.6, pp. 1137–1162.

Ludwig, D, D. D. Jones, and C. S. Holling (1978). "Qualitative Analysis of Insect Outbreak Systems: The Spruce Budworm and Forest". *The Journal of Animal Ecology* 47.1, p. 315.

Luimstra, Veerle M., Jolanda M. H. Verspagen, Tianshuo Xu, J. Merijn Schuurmans, and Jef Huisman (2020). "Changes in water color shift competition between phytoplankton species with contrasting light-harvesting strategies". *Ecology* 101.3, e02951.

Martínez, Carlos, Francis Mairet, and Olivier Bernard (2018). "Theory of turbid microalgae cultures". *Journal of Theoretical Biology* 456, pp. 190–200.

Melina Celeste, Crettaz Minaglia, Rosso Lorena, Aranda Jorge Oswaldo, Go?i Sandro, Sedan Daniela, Andrinolo Dario, and Giannuzzi Leda (2017). "Mathematical modeling of Microcystis aeruginosa growth and [D-Leu 1] microcystin-LR production in culture media at different temperatures". *Harmful Algae* 67, pp. 13–25.

Merel, Sylvain, Walker David, Ruth Chicana, Shane Snyder, Estelle Baurès, and Olivier Thomas (2013). "State of knowledge and concerns on cyanobacterial blooms". *Environment International* 59, pp. 303–327.

Mitra, Aditee and Kevin J. Flynn (2005). "Predator-prey interactions: Is 'ecological stoichiometry' sufficient when good food goes bad?" *Journal of Plankton Research* 27.5, pp. 393–399.

Monod, Jacques (1949). "The Growth of Bacterial Cultures". *Annual Review of Microbiology* 3.1, pp. 371–394.

Morel, François M.M. (1987). "Kinetics of Nutrient Uptake and Growth in Phytoplankton". *Journal of Phycology* 23.1, pp. 137–150.

Nicholls, Sarah and John Crompton (2018). "A comprehensive review of the evidence of the impact of surface water quality on property values". *Sustainability* 10.2, p. 500.

North, R. L., S. J. Guildford, R. E.H. Smith, S. M. Havens, and M. R. Twiss (2007). "Evidence for phosphorus, nitrogen, and iron colimitation of phytoplankton communities in Lake Erie". *Limnology and Oceanography* 52.1, pp. 315–328.

Orr, Philip T. and Gary J. Jones (1998). "Relationship between microcystin production and cell division rates in nitrogen-limited Microcystis aeruginosa cultures". *Limnology and Oceanography* 43.7, pp. 1604–1614.

Paerl, Hans W. (2014). "Mitigating Harmful Cyanobacterial Blooms in a Human- and Climatically-Impacted World". *Life* 4.4, pp. 988–1012.

Paerl, Hans W. and Malcolm A. Barnard (2020). "Mitigating the global expansion of harmful cyanobacterial blooms: Moving targets in a human- and climatically-altered world". *Harmful Algae* 96.

Paerl, Hans W. and Timothy G. Otten (2013). "Harmful Cyanobacterial Blooms: Causes, Consequences, and Controls". *Microbial Ecology* 65.4, pp. 995–1010.

Peace, Angela, Monica D Poteat, and Hao Wang (2016). "Somatic Growth Dilution of a toxicant in a predator–prey model under stoichiometric constraints". *Journal of Theoretical Biology* 407.

Peace, Angela and Hao Wang (2019). "Compensatory Foraging in Stoichiometric Producer–Grazer Models". *Bulletin of Mathematical Biology* 81.12, pp. 4932–4950.

Peace, Angela et al. (2021). "Stoichiometric Ecotoxicology for a Multisubstance World". *BioScience* 71.2, pp. 132–147.

Pedro, Sansao A., Frank T. Ndjomatchoua, Peter Jentsch, Jean M. Tchuenche, Madhur Anand, and Chris T. Bauch (2020). "Conditions for a Second Wave of COVID-19 Due to Interactions Between Disease Dynamics and Social Processes". *Frontiers in Physics* 8, p. 574514.

Perko, Lawrence (2001). *Differential Equations and Dynamical Systems*. Third. Springer-Verlag.

Pigeon Lake Watershed Management Plan Steering Committee, (plwmp.ca) (2018). *The Pigeon Lake Draft Watershed Management Plan 2018.*

Poon, Kai-Tak, Fei Teng, Jason T. Chow, and Zhansheng Chen (2015). "Desiring to connect to nature: The effect of ostracism on ecological behavior". *Journal of Environmental Psychology* 42, pp. 116–122.

Pope, Robin M. and Edward S. Fry (1997). "Absorption spectrum (380–700 nm) of pure water II Integrating cavity measurements". *Applied Optics* 36.33, p. 8710.

Ralston, David K. and Stephanie K. Moore (2020). "Modeling harmful algal blooms in a changing climate". *Harmful Algae* 91.

Redfield, A (1934). "On the proportions of organic derivatives in sea water and their relation to the composition of plankton". *James Johnstone Memorial Volume, University Press, Liverpool*, pp. 177–192.

Reynolds, C. S. (2006). *The ecology of phytoplankton*. Cambridge University Press, pp. 1–535.

Rinaldi, S. and S. Muratori (1992). "Slow-fast limit cycles in predator-prey models". *Ecological Modelling* 61.3-4, pp. 287–308.

Rubin, Jonathan and Martin Wechselberger (2007). "Giant squid-hidden canard: The 3D geometry of the Hodgkin-Huxley model". *Biological Cybernetics* 97.1, pp. 5–32.

Satake, Akiko, Heather M. Leslie, Yoh Iwasa, and Simon A. Levin (2007). "Coupled ecological-social dynamics in a forested landscape: Spatial interactions and information flow". *Journal of Theoretical Biology* 246.4, pp. 695–707.

Shigesada, Nanako and Akira Okubo (1981). "Analysis of the self-shading effect on algal vertical distribution in natural waters". *Journal of Mathematical Biology* 12.3, pp. 311–326.

Smith, Hal L. (1995). *Monotone dynamical systems: an introduction to the theory of competitive and cooperative systems: an introduction to the theory*

of competitive and cooperative systems. No. 41. American Mathematical Society.

Smolders, A. and J.G.M. Roelofs (1993). "Sulphate-mediated iron limitation and eutrophication in aquatic ecosystems". *Aquatic Botany* 46, pp. 247–253.

Starke, Cody W.E., Catriona L.C. Jones, Wesley S. Burr, and Paul C. Frost (2021). "Interactive effects of water temperature and stoichiometric food quality on Daphnia pulicaria". *Freshwater Biology* 66.2, pp. 256–265.

Sterner, R.W and J.J Elser (2002). *Ecological Stoichiometry: The Biology of Elements from Molecules to the Biosphere*. Princeton, NJ: Princeton University Press, p. 439.

Stomp, Maayke, Jef Huisman, Lucas J Stal, and Hans CP Matthijs (2007a). "Colorful niches of phototrophic microorganisms shaped by vibrations of the water molecule". *ISME Journal* 1, pp. 271–282.

Stomp, Maayke, Jef Huisman, Lajos Vörös, Frances R. Pick, Maria Laamanen, Thomas Haverkamp, and Lucas J. Stal (2007b). "Colourful coexistence of red and green picocyanobacteria in lakes and seas". *Ecology Letters* 10, pp. 290–298.

Sun, T. Anthony and Frank M. Hilker (2020). "Analyzing the mutual feedbacks between lake pollution and human behaviour in a mathematical social-ecological model". *Ecological Complexity* 43, p. 100834.

Sun, T. Anthony and Frank M. Hilker (2021). "Comparison between best-response dynamics and replicator dynamics in a social-ecological model of lake eutrophication". *Journal of Theoretical Biology* 509.

Suzuki, Yukari and Yoh Iwasa (2009). "The coupled dynamics of human socio-economic choice and lake water system: The interaction of two sources of nonlinearity". *Ecological Research* 24, pp. 479–489.

Taranu, Zofia E., Ron W. Zurawell, Frances Pick, and Irene Gregory-Eaves (2012). "Predicting cyanobacterial dynamics in the face of global change: The importance of scale and environmental context". *Global Change Biology* 18.12, pp. 3477–3490.

Tavoni, Alessandro, Maja Schlüter, and Simon Levin (2012). "The survival of the conformist: Social pressure and renewable resource management". *Journal of Theoretical Biology* 299, pp. 152–161.

Teichreb, C (2012). *Lake and Watershed Management Options for the Control of Nuisance Blue-Green Algal Blooms in Pigeon Lake, Alberta*. Tech. rep., p. 21.

Thampi, Vivek A., Chris T. Bauch, and Madhur Anand (2019). "Socio-ecological mechanisms for persistence of native Australian grasses under pressure from nitrogen runoff and invasive species". *Ecological Modelling* 413, p. 108830.

Urabe, Jotaro, James J. Elser, Marcia Kyle, Takehito Yoshida, Tatsuki Sekino, and Zenichiro Kawabata (2002). "Herbivorous animals can mitigate unfavourable ratios of energy and material supplies by enhancing nutrient recycling". *Ecology Letters* 5.2, pp. 177–185.

Van De Waal, Dedmer B., Jolanda M.H. Verspagen, Miquel Lürling, Ellen Van Donk, Petra M. Visser, and Jef Huisman (2009). "The ecological stoichiometry of toxins produced by harmful cyanobacteria: An experimental test of the carbon-nutrient balance hypothesis". *Ecology Letters* 12.12, pp. 1326–1335.

van der Pol, Balth (1926). "LXXXVIII. On "relaxation-oscillations"". *The London, Edinburgh, and Dublin Philosophical Magazine and Journal of Science* 2.11, pp. 978–992.

Wang, Hao, Lin Jiang, and Joshua S. Weitz (2009). "Bacterivorous grazers facilitate organic matter decomposition: A stoichiometric modeling approach". *FEMS Microbiology Ecology* 69.2, pp. 170–179.

Wang, Hao, Yang Kuang, and Irakli Loladze (2008). "Dynamics of a mechanistically derived stoichiometric producer-grazer model". *Journal of Biological Dynamics* 2.3, pp. 286–296.

Wang, Hao, Hall Smith, Yang Kuang, and James J Elser (2007). "Dynamics of stoichiometric bacteria-algae interactions in the epilimnion". *SIAM Journal on Applied Mathematics* 68.2, pp. 503–522.

Wang, Ying, Jianfeng Hu, Haoran Pan, Shiyu Li, and Pierre Failler (2016). "An integrated model for marine fishery management in the Pearl River

Estuary: Linking socio-economic systems and ecosystems". *Marine Policy* 64, pp. 135–147.

Watson, Sue B., Brian Alan Whitton, Scott N. Higgins, Hans W. Paerl, Bryan W. Brooks, and John D. Wehr (2015). "Harmful Algal Blooms". *Freshwater Algae of North America: Ecology and Classification*. Elsevier, pp. 873–920.

White, Easton R. and Alan Hastings (2020). "Seasonality in ecology: Progress and prospects in theory". *Ecological Complexity* 44, p. 100867.

Whitton, Brian A. (2012). *Ecology of cyanobacteria II: Their diversity in space and time*. Springer Netherlands, pp. 1–760.

Williams, Kipling D. (2007). "Ostracism". *Annual Review of Psychology* 58, pp. 425–452.

Williams, Kipling D. and Steve A. Nida (2011). "Ostracism: Consequences and coping". *Current Directions in Psychological Science* 20.2, pp. 71–75.

Wolf, David and H. Allen Klaiber (2017). "Bloom and bust: Toxic algae's impact on nearby property values". *Ecological Economics* 135, pp. 209–221.

Wollrab, Sabine, Lyubov Izmest'yeva, Stephanie E. Hampton, Eugene A. Silow, Elena Litchman, and Christopher A. Klausmeier (2021). "Climate chage–driven regime shifts in a planktonic food web". *American Naturalist* 197.3, pp. 281–295.

Wurtsbaugh, Wayne A. and A. J. Horne (1983). "Iron in eutrophic Clear Lake, California: its importance for algal nitrogen fixation and growth (Aphanizomenon flos-aquae)." *Canadian Journal of Fisheries and Aquatic Sciences* 40.9, pp. 1419–1429.

Yan, Kai, Jian-chu Xu, Wei Gao, Ming-jiu Li, Zeng-wei Yuan, Fu-suo Zhang, and James Elser (2021). "Human perturbation on phosphorus cycles in one of China's most eutrophicated lakes". *Resources, Environment and Sustainability* 4, p. 100026.

Yoshiyama, Kohei, Jarad P. Mellard, Elena Litchman, and Christopher A. Klausmeier (2009). "Phytoplankton Competition for Nutrients and Light in a Stratified Water Column". *The American Naturalist* 174.2, pp. 190–203.

Zhang, Jimin, Jude D. Kong, Junping Shi, and Hao Wang (2021). "Phytoplankton Competition for Nutrients and Light in a Stratified Lake: A Mathematical Model Connecting Epilimnion and Hypolimnion". *Journal of Nonlinear Science* 31.2, pp. 1–42.

Zhao, Shengnan, Sanling Yuan, and Hao Wang (2020). "Threshold behavior in a stochastic algal growth model with stoichiometric constraints and seasonal variation". *Journal of Differential Equations* 268.9, pp. 5113–5139.